

# **Optimisation of CT protocols for cardiac imaging using three-dimensional printing technology**

**Kamarul Amin Abdullah**

MSc, BSc (Honours)

A thesis submitted in fulfilment of the requirements for the degree of

Doctor of Philosophy (PhD)

Faculty of Health Sciences

University of Sydney

**2018**

## **Statement of Authorship**

I, **Kamarul Amin Abdullah**, hereby declare that the work contained within this thesis is my own and has not been submitted to any other university or institution as a part or a whole requirement for any higher degree.

I, **Kamarul Amin Abdullah**, hereby declare that I was the principal researcher of all work included in this thesis, including work published with multiple authors.

In addition, ethical approval from the Human Research Ethics Committee was granted for the studies presented in this thesis.

**Kamarul Amin Abdullah**

Discipline of Medical Radiation Sciences,

Faculty of Health Sciences,

The University of Sydney,

NSW, Australia.

**Date:** 31<sup>st</sup> March 2018

## Abstract

**Objectives:** This thesis investigates the application of 3D-printing technology for optimising coronary computed tomography (CT) angiography (CCTA) protocols using iterative reconstruction (IR) algorithm as a dose optimisation strategy. The specific objectives are to: (i) design and develop a novel 3D-printed cardiac insert phantom derived from a volumetric computed tomography (CT) image datasets of the Lungman phantom; (ii) and (iii) investigate its application to evaluate the effect on CT image quality of IR algorithms and their strengths with a low tube current or voltage for dose reduction of CCTA protocols.

**Methods:** The study was conducted in three phases. In phase one, the novel 3D-printed cardiac insert phantom was designed and developed. The size and shape of this printed phantom replicated the original cardiac insert of the Lungman anthropomorphic chest phantom. The attenuation (Hounsfield Unit, HU) values of the printed phantom filling materials were compared to coronary CT angiography (CCTA) patients and Catphan® 500 images. In phase two, the printed phantom was placed within the Lungman phantom and scanned at multiple dose levels, and the datasets were reconstructed using the filtered back projection (FBP) and different IR algorithm strengths. The image quality characteristics of image noise, signal-noise ratio (SNR), and contrast-noise ratio (CNR) were measured and compared to the previous literature to determine the dose reduction potential. In the third phase, the influence of using different IR algorithm strengths with low-tube voltage for dose optimisation studies was investigated. The printed phantom and the Catphan® 500 phantoms were scanned at different tube currents and voltages. The results obtained were

then compared to the patient datasets to measure the agreement between the phantoms and patient datasets.

**Results:** In phase one, a novel 3D-printed cardiac insert phantom was developed. The measurements of CT HU values were consistent between the printed phantom, patient and Catphan® 500 images. In phase two, the results of the printed phantom showed that decreasing dose levels had significantly increased the image noise ( $p < 0.001$ ). As a result, the SNR and CNR were significantly decreased ( $p < 0.001$ ). The application of IR algorithm at various strengths had yielded a stepwise improvement of noise image quality with a dose reduction potential of up to 40%. Image noise was reduced significantly ( $p < 0.001$ ) and thus increased the SNR and CNR as compared to the FBP. In phase three, the printed phantom results showed a significant interaction between the effects of low-tube voltage and the IR algorithm strengths on image quality (all  $p < 0.001$ ) but not the CT HU values. The mean differences in image quality characteristics were small between the patient-phantom datasets. The optimised CT protocols allowed up to 57% dose reduction in CCTA protocols while maintaining the image quality.

**Conclusions:** The 3D printing technology was used to produce a novel design of cardiac insert phantom for the Lungman phantom. The 3D-printed cardiac insert phantom can be used to evaluate the effect of using IR algorithm on dose reduction and image quality. The dose optimisation assessment using the phantom-method demonstrated a combination of IR algorithm and low tube voltage could further reduce the radiation dose to the patient while maintaining the image quality. This thesis proposes and validates a new method of developing phantoms for CCTA dose optimisation studies.

## **Acknowledgements**

I would like to address my sincere thanks to my primary supervisor, Dr Peter L. Kench for all his assistance, advice, supervision, support, and trust that facilitated the timely completion of my Ph.D. study. He had given all the necessary freedom in bringing forward of my own idea especially before the beginning of my Ph.D. study. Also, I would like to acknowledge my auxiliary supervisors, Associate Professor Mark F. McEntee and Dr Warren M. Reed, for being very good mentors and reviewers especially during the development of this 3D-printed cardiac insert phantom as well as during the writing process of this thesis.

I would also like to acknowledge our main associates; (i) Dr Will Ryder, a medical physicist, who had introduced and taught me about 3D printing technology when he was still working under the Brain and Mind Centre, and also (ii) Mr Mark Dobson, Ms Jackie Behn and all staff from the Bankstown-Lidcombe Hospital for their valuable time and access to the SPECT-CT scanner.

I would also like to thanks Dr Alun Pope from the School of Education for his assistance in the statistical analyses. His feedback and suggestions on this matter had helped me to determine and perform the appropriate test and thus producing accurate results for all my studies in this thesis.

Special thanks too to the Universiti Sultan Zainal Abidin (UniSZA) and the Ministry of Higher Education Malaysia (MOHE) for providing me with the scholarship throughout my Ph.D. study. I also want to acknowledge the financial support given by the Faculty of Health Sciences, The University of Sydney which had allowed me to present my research works at international and national conferences.

I would also like to thank the “Proofreading United Services” and “Proofreading By A UK PhD” companies for their service in editing the English for this thesis and help me to acquire the standard required.

I wish to thank all my colleagues and friends from the Discipline of Medical Radiation Sciences who had always helped me since my first year until the final semester of my Ph.D. study, and also to all my fellow Malaysians who supported me and my family since we had firstly arrived in Sydney, Australia.

Finally, I dedicate this thesis to my beloved wife; Norulhafizah Mat Dahan, my lovely daughters; Nur Qaisara Aminah and Natasha Aminah, my admirable late father; Abdullah @ Abu Bakar Che Min, my caring mother; W Meriam Wan Sulaiman, my understanding parents-in-law; Mat Dahan Abd Rahman and Kelsom Ali, and my supportive brothers and sisters; Karma Amin, Karman Amin, Md Hanafiah Amin, Shahrul Amin, Karimah@Aminah, Kasyidah Aminah, and Kamaliah Aminah for all their continuous prayers, support, inspiration, encouragement and love.

## **Publications and Presentations**

Parts of the work presented in this thesis have been published, submitted for publication, formatted for publication submission or presented in the following forms:

### **Peer-reviewed journals articles**

- a) Abdullah, K.A., McEntee, M. F., Reed, W., & Kench, P. L. (2016). Radiation dose and diagnostic image quality associated with iterative reconstruction in coronary CT angiography: A systematic review. *Journal of Medical Imaging and Radiation Oncology*, 60, 459–468. doi:10.1111/1754-9485.12473. [Published]
- b) Abdullah, K.A., McEntee, M. F., Reed, W., & Kench, P. L. (2018). Development of an organ-specific insert phantom generated using a 3D printer for investigations of cardiac computed tomography protocols. *Journal of Medical Radiation Sciences*, 1-9. doi: 10.1002/jmrs.279. [Published]
- c) Abdullah, K.A., McEntee, M. F., Reed, W., & Kench, P. L. (2018). Dose reduction in computed tomography using iterative reconstruction: A phantom study examining the impact on image quality. *Journal of Computer Assisted Tomography*. [Submitted for publication]
- d) Abdullah, K.A., McEntee, M. F., Reed, W., & Kench, P. L. (2018). Reducing dose using higher iterative reconstruction strengths with low tube voltage in cardiac CT protocols: Dual-phantom and patient datasets. *Journal of Cardiovascular Computed Tomography*. [Formatted for publication submission]

### **Conference proceedings/papers/poster/e-poster**

- a) Abdullah, KA, Mark F. McEntee, Warren Reed, Peter L. Kench. Development of a 3D printed cardiac phantom. *Higher Degree Research (HDR) Bazaar, Faculty of Health Sciences*. November 2016.
- b) Abdullah, K., McEntee, M., Reed, W., Kench, P. (2017). Using 3D printed cardiac CT phantom for dose reduction and image quality. *12th Annual Scientific Meeting of Medical Imaging and Radiation Therapy (ASMMIRT)*, Perth, Western Australia.

### **Oral presentations**

- a) Abdullah, KA, Mark F. McEntee, Warren Reed, Peter L. Kench. A systematic review of radiation dose and diagnostic image quality associated with iterative reconstruction in coronary CT angiography. *The Medical Image Optimization and Perception research group (MIOPeG) seminar*. October, 2015.
- b) Abdullah, KA, Mark F. McEntee, Warren Reed, Peter L. Kench. Dose optimization in cardiac CT examination using iterative reconstruction. *Higher Degree Research (HDR) Bazaar, Faculty of Health Sciences*. November, 2015.
- c) Abdullah, KA, Mark F. McEntee, Warren Reed, Peter L. Kench. Development of a 3D printed cardiac CT phantom. *The Medical Image Optimization and Perception research group (MIOPeG) seminar*. June, 2016.
- d) Abdullah, KA, Mark F. McEntee, Warren Reed, Peter L. Kench. Measuring image quality between FBP and IR using 3D printed cardiac phantom: Progress work. *Medical Imaging Physics Research Group seminar*. July, 2017.



## Table of Content

Statement of Authorship .....	ii
Abstract.....	iii
Acknowledgements .....	v
Publications and Presentations .....	vii
Table of Content.....	x
List of Tables .....	xiii
List of Figures .....	xv
<b>CHAPTER 1 Introduction and background.....</b>	<b>1</b>
1.1 Increasing CT radiation dose.....	2
1.2 Radiation-induced cancers risk.....	4
1.3 Challenges in dose optimisation strategies .....	6
1.4 Phantom studies for dose optimisation .....	8
1.5 Main and specific objectives .....	10
1.6 Ethics approval .....	10
1.7 Thesis outlines .....	11
1.8 References .....	12
<b>CHAPTER 2 Systematic review: Dose reduction with iterative reconstruction algorithm in coronary CT angiography .....</b>	<b>24</b>
2.1 Bridging section.....	25
2.1.1 Background.....	25
2.1.2 Recent literature after publication .....	26
2.1.3 References .....	27
2.2 Manuscript.....	30
2.2.1 Abstract .....	30
2.2.2 Introduction.....	31
2.2.3 Materials and Methods .....	33
2.2.4 Results.....	37
2.2.5 Discussion.....	47

2.2.6 References.....	50
<b>CHAPTER 3 Development of a novel 3D-printed cardiac insert phantom for investigations in coronary CT angiography.....</b>	<b>56</b>
3.1 Bridging section.....	57
3.1.1 Background.....	57
3.1.2 References.....	60
3.2 Manuscript.....	64
3.2.1 Abstract.....	64
3.2.2 Introduction.....	65
3.3.3 Materials and Methods.....	67
3.3.4 Results.....	76
3.3.5 Discussion.....	79
3.3.6 References.....	82
<b>CHAPTER 4 An investigation of CT image quality using iterative reconstruction algorithm and a 3D-printed cardiac insert phantom .....</b>	<b>87</b>
4.1 Bridging section.....	88
4.1.1 Background.....	88
4.1.2 References.....	91
4.2 Manuscript.....	94
4.2.1 Abstract.....	94
4.2.2 Introduction.....	95
4.2.3 Materials and Methods.....	97
4.2.4 Results.....	101
4.2.5 Discussion.....	106
4.2.6 References.....	110
<b>CHAPTER 5 Optimisation of iterative reconstruction strengths in a low tube voltage coronary CT angiography using a 3D-printed cardiac insert phantom .....</b>	<b>120</b>
5.1 Bridging section.....	121
5.1.1 Background.....	121
5.1.2 References.....	123
5.2 Manuscript.....	126

5.2.1 Abstract .....	126
5.2.2 Introduction.....	127
5.2.3 Materials and Methods .....	129
5.2.4 Results.....	134
5.2.5 Discussion.....	139
5.2.6 References .....	142
<b>CHAPTER 6 Discussion, limitations, future investigations, and conclusions.....</b>	<b>147</b>
6.1 Discussion .....	148
6.2 Limitations.....	153
6.3 Future investigations.....	155
6.4 Conclusions .....	155
6.5 References .....	156
<b>Appendices .....</b>	<b>161</b>
Appendix 1: Ethics approval letter.....	162
Appendix 2: Site specific authorisation letter.....	164
Appendix 3: 3D-printed models and the softcopy link of the models. ....	165

## List of Tables

Table 1.1 Some of the major types of IR algorithms based on product names and vendors...	7
Table 2.1: A table shows the Boolean operators and keywords used.....	34
Table 2.2: Summary of study details of the selected citation (part 1).....	42
Table 2.3: Summary of study details of the selected citation (part 2).....	43
Table 2.4: Summary of radiation dose indicators of the selected citations.....	44
Table 2.5: Summary of image quality indicators of the selected citations. ....	45
Table 2.6: Summary of study details for radiation dose indicators. ....	46
Table 2.7: Summary of study details for diagnostic image quality indicators. ....	46
Table 3.1: The 3D printer settings applied in this study. In achieving very fine details with several ranges of printing materials or 3D printer while avoiding gaps, leaking, and overlaps; varying results could be generated. NB These settings are only applicable if a printer similar to Creatbot DM Plus Model (Mankati, Shanghai, China) and a software program similar to Simplify3D (Ohio, USA) are employed to design and to construct the phantom.....	73
Table 3.2: Mean of attenuation values (HU) obtained with FBP (FC18) for the 3D-printed cardiac insert, as compared to the patient image datasets, and Catphan® 500 at 120 kVp.	79
Table 4.1: CT acquisition parameters and reconstruction settings. Four different protocols are used; protocols A, B, C, and D. For image reconstructions, FBP and three strengths of AIDR3D are used; mild, moderate, and strong.....	98
Table 4.2: Results of image noise, SNR, and CNR at multiple dose levels using the 3D-printed cardiac insert phantom. Protocol A is the reference protocol, to demonstrate the dose reduction potential between other three protocols of B, C, and D between FBP and IR	

algorithms. Increasing the strength of IR algorithm (AIDR3D) results in more noise reduction. The strong level has the highest noise reduction while the mild has the lowest among the three IR strengths.....102

Table 4.3: The summary of the literature which compares the difference in image noise, signal-noise ratio (SNR), and contrast-noise ratio (CNR) between FBP and IR algorithms. ....104

Table 5.1: Summary of CT parameters and reconstruction settings. ....131

Table 5.3: Results of HU, image noise, SNR, and CNR of the 3D-printed cardiac insert phantom between 120 kVp and 100 kVp. ....135

Table 5.4: Results of *modulation transfer function*, MTF at 120 kVp and 100 kVp.....137

## List of Figures

Figure 1.1 The estimated number of CT scans performed annually in the (a) United States [15, 16] and (b) Australia [17].	3
Figure 2.1: Flow chart outlining the search strategy used for this systematic review.	38
Figure 2.2: The boxplot shows the comparison of effective dose between FBP and IR.	47
Figure 3.1 An example of physical phantoms is the Catphan® 500 (The Phantom Laboratory, Salem, NY). This phantom is widely used for testing the performance of CT scanners. The phantom consists of five modules to assess the image quality; (i) CTP401 for slice width, sensitometry and pixel size, (ii) CTP528 for line pair and point source spatial resolution, (iv) CTP515 for sub slice and supra slice low contrast and (v) CTP486 for image uniformity [11].	58
Figure 3.2 (a) The Lungman anthropomorphic chest phantom by Kyoto Kagaku co., Japan is placed on the CT table. (b) The removable cardiac (arrow) and lung structures contained within the Lungman phantom.	59
Figure 3.3: (a) An anthropomorphic chest phantom (Lungman N-01, Kyoto Kagaku, Co., Ltd., Kyoto, Japan). The anthropomorphic chest phantom was scanned on a multi-detector CT scanner in order to obtain the volumetric datasets of the original cardiac insert; (b) The original size and the appearance of the cardiac insert; (c) The segmentation process using 3D Slicer software program (The Slicer Community, Harvard) [17]. The cardiac insert was segmented to ensure that the modelling process could be performed to produce the heart-shaped shell; and (d) The virtual 3D model of the original cardiac insert.	70
Figure 3.4: (a) A cross-sectional diagram of the new custom-made design of 3D-printed cardiac insert phantom. The measurements of each model were determined based on the	

adjustments made so that the model could fit the size of the heart-shaped shell perfectly, as well as to be suitably positioned in the anthropomorphic chest phantom. The modelling parts of the removable inserts within the heart-shaped shell are (b) removable insert A, and (c) removable insert B..... 71

Figure 3.5: Three separate tasks were carried out to facilitate the printing tasks. (a) Insert A was divided into Parts I and II; (b) Insert B was separated into three parts (Parts I, II, and III); and (c) Heart-shaped shell was divided into Parts I and II. These separation tasks of printing parts eased the process of filling with varied density materials after the printing process. .... 72

Figure 3.6: A 3D-printed cardiac insert phantom; heart-shaped shell, insert A, and insert B, before (a-c) and after the printing process (d-f), respectively..... 77

Figure 3.7: The resulting axial CT images of (a) four inserts in Catphan® 500 phantom; (b) and (c) patient image datasets for cardiac CT; (d) original cardiac insert of anthropomorphic chest phantom; (e-f) 3D-printed cardiac insert phantom with contrast materials (CM), oil, air, water and jelly segments labelled..... 78

Figure 4.1: (a) The 3D-printed cardiac insert phantom. (b) A schematic diagram of the phantom with all filled materials. (c) The anthropomorphic chest phantom, containing the 3D-printed cardiac insert phantom, is placed on the scanner couch. (d) An axial CT image shows the contrast-enhanced region of the 3D-printed cardiac insert phantom; the centre simulates the contrast filled ascending aorta, and the varying size diameters of cylindrical demonstrate coronary arteries..... 99

Figure 4.2: For dose reduction potential analysis, a comparison of image noise, signal-noise ratio (SNR), and contrast-noise ratio (CNR) among results were obtained with our 3D-

printed cardiac insert phantom and the relevant previous literature. The literature sets the mean percentage variations published for comparison among other protocols B, C, and D. From the graph, overall protocol B results are below the mean values indicating similar image quality to reference protocol A. For protocol C and D, the image noise, SNR, and CNR results are above the mean values. ....105

Figure 4.3: CT images of the 3D-printed cardiac insert phantom at four dose levels in columns and reconstruction methods, FBP, AIDR3Dmild, AIDR3Dstandard, and AIDR3Dstrong, in rows. The insert contains contrast-material to simulate the ascending aorta and varying size of coronary arteries during cardiac CT imaging of CCTA. ....106

Figure 5.1: (a) The Catphan® 500 phantom (The Phantom Laboratory, Greenwich, NY, USA); (b) The 3D-printed cardiac insert phantom; (c) The Catphan® 500 phantom was positioned on the scanner table; and (d) The anthropomorphic chest phantom (Lungman N-01, Kyoto Kagaku, Japan), with the 3D-printed cardiac insert phantom positioned within (arrow), was placed on the scanner table. ....130

Figure 5.2: (a) To measure noise an ROI was placed within the contrast-enhanced region of the 3D-printed cardiac insert phantom simulating the ascending aorta. (b) Two similar sizes of ROIs were placed to measure CNR between the contrast material (the ascending aorta) and the oil (fat). (c) The CTP528 module of Catphan® 500 phantom was used for the evaluation of MTF (axial spatial resolution). (d) The CTP515 module of Catphan® 500 phantom was used for the evaluation of low contrast resolution. ....133

Figure 5.3: Bar graphs demonstrate significant differences in image noise (a), SNR (b), and CNR (c) (all  $P < 0.05$ ) between the 120-kVp and the 100-kVp. No significant differences of 120 kVp FBP versus 100 kVp ASIR 60% for image noise, 120 kVp ASIR 40% versus 100



kVp ASIR 60% for SNR, and 120 kVp FBP versus 100 kVp ASIR 40% for CNR. The 120-kVp series reconstructed with ASIR 60% provided the lowest image noise and highest SNR and CNR ( $P < 0.05$ ), whereas 100-kVp series reconstructed with FBP showed the highest image noise and lowest SNR and CNR.....136

Figure 5.4: Results of low contrast resolution using CTP515 module of Catphan® 500. ...138

Figure 5.5: Bland-Altman plot. Differences in measured a) image noise, b) signal-noise ratio (SNR), and c) contrast-noise ratio (CNR) between the 3D-printed cardiac insert phantom and patient. Dotted lines delineate limits of agreement between two datasets. ....139

# **CHAPTER 1 Introduction and background**

The first chapter presents an overview of the research topic, the problem addressed by the research presented in this thesis, the objectives and specific aims of the work, an outline of the research process, and the overview of the thesis chapters.

## **1.1 Increasing CT radiation dose**

Computed Tomography (CT) imaging system has been recognised as an accurate, rapid, and convenient diagnostic tool [1-3]. However, since its introduction, the rapid increase of radiation dose received from CT examinations to the population has become a particular concern among health professionals [4, 5]. In the United Kingdom, for example, according to a multi-center survey, the radiation dose of CT examinations to the population is around 68% of the dose from medical exposure compare to 40% over a decade, from 1998 to 2008 [6]. The recent report of the National Council on Radiation Protection and Measurements (NCRP) has stated that the contribution of CT examinations to the radiation dose of United States population is 24% and has increased by 10% per year since 1993 [7]. In Australia, the radiation dose from CT examinations has increased by 36% from 2006 to 2012 [8]. Thus, the increasing of CT radiation dose is a global trend [9-12] and CT examinations are now considered to be the largest contributor to the population dose [13].

The primary cause of the increasing CT radiation dose to the population is due to the rapid increase in the number of CT scanners available and scans being requested. In the United States and Japan, for example, according to a survey conducted in 1996 [14] the number of CT scanners per 1 million population was 26 in the United States and 64 in Japan, respectively. Furthermore, it is estimated that more than 62 million CT scans are currently requested each year in the United States, as compared with about 3 million in 1980 [15, 16]. In Australia, the number of CT scanners have also increased with the annual growth rate ranging from 0.6 to 2.1 million over the last 15 years (1994-2009), with an average increase of 8.5% per year [17] (see Figure 1.1).

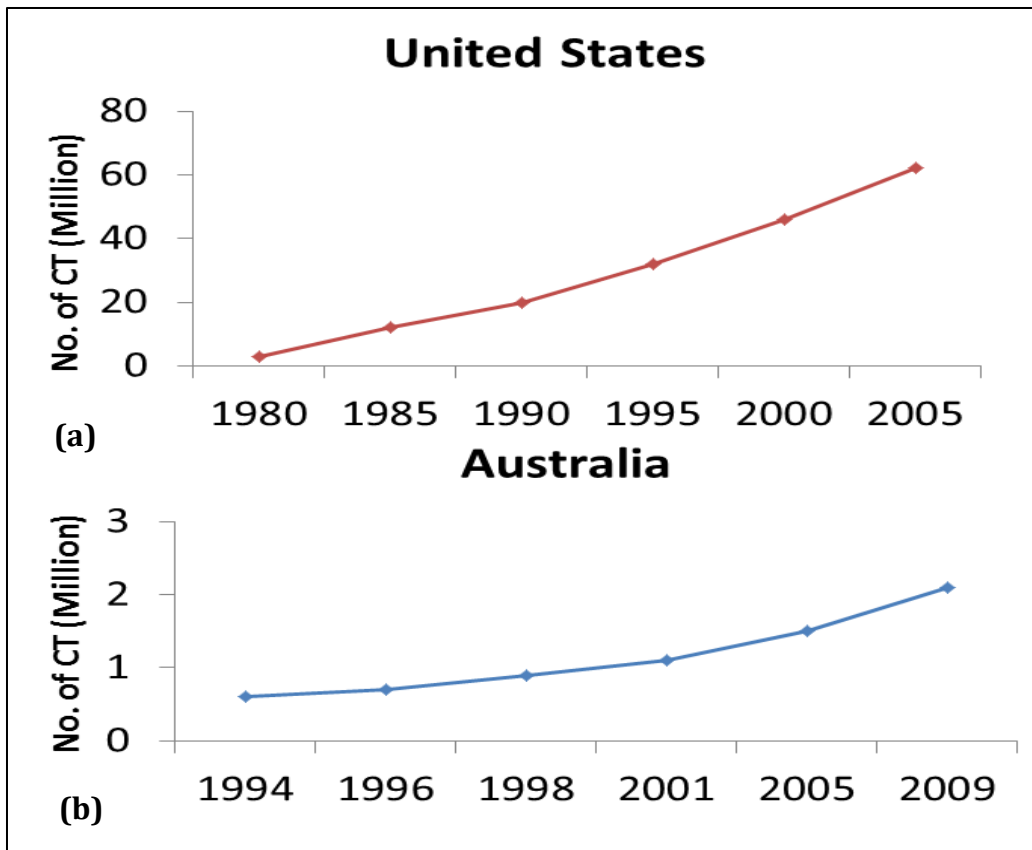


Figure 1.1 The estimated number of CT scans performed annually in the (a) United States [15, 16] and (b) Australia [17].

CT radiation dose has also increased due to the recent technological developments that gives major improvement to the diagnostic applications and accuracy of the CT systems [18]. This is demonstrated by the increase of CT radiation dose reported after the installation of multi-slice CT (MSCT) scanners due to the increase in the number of detectors and field of view. A national survey in the United Kingdom for 2003, for example, has reported that the mean dose for adult patients of MSCT scanners was found to be 10% higher than the single-slice CT (SSCT) scanner [19]. Another study by Huda and Mergo [20] has reported that an increase dose of 30% and 150% for CT head and body, respectively, was found for MSCT scanners when compared to SSCT scanners. In Australia, a single

centre study reported that the mean of dose length product (DLP) for routine CT examinations, i.e., head, chest, abdominal and lumbar spine, has increased by 11-70% from SSCT to 16-slices MDCT scanners [21].

In recent years, the availability of cardiac CT services has resulted in radiologists and cardiologists using CT scanners to investigate cardiac disease [22]. Coronary CT angiography (CCTA), for example, is one of the cardiac CT services that has experienced tremendous growth [23-25]. Previously, the evaluation of the coronary artery disease (CAD) with CT scanners was limited due to the technical difficulties associated with imaging small coronary structures in a moving organ. However, the recent advances in CT scanners and electrocardiographic (ECG)-gating methods have resulted in the improved temporal and spatial resolution required to make CCTA clinically feasible [26, 27]. Currently, the cardiovascular imaging, including CCTA, accounts for nearly one-third of diagnostic imaging services [28, 29]. Therefore, given the relatively safe, less invasive procedure, and more recent advances of CT scanners available, thus, the number of CCTA scans being requested is also increased and consequently, increasing the radiation dose.

## **1.2 Radiation-induced cancers risk**

As mentioned in the earlier section, CT examinations are by far the most common source of medical radiation exposure of many developed countries. The large number of patients receiving radiation exposure from CT examinations has raised serious concerns about the patient safety, especially to the risk of radiation-induced cancers [30, 31]. Radiation-induced cancer risk occurs when the DNA has been damaged by the hydroxyl radicals as a result of the x-ray interactions with the water molecules [32]. In normal

circumstances, the damage caused by radiation-induced can be repaired by various systems within the cell, but DNA double-strand breaks are less easily repaired. Consequently, the damage occasionally can lead to induction of point mutations, chromosomal translocations, and gene fusions, all of which are linked to the induction of cancer [33]. In a typical CT examination, the organ being studied typically receives a radiation dose in the range of 15 mSv for an adult with an average of two to three CT scans per study. At this dose level, as reviewed elsewhere [34], the risk for radiation-induced cancer is most likely to occur although relatively small.

CCTA is also associated with radiation-induced cancer risk due to the radiation dose incidence on the lung and female breast organs during the scanning. The estimation of the cancer risk is usually based on the measured organ dose and/or effective dose which can be reported according to the age, sex, and countries [35, 36]. A study by Einstein et al. [37], for example, has reported that with the organ dose that ranged from 42 to 91 mSv for the lungs and 50 to 80 mSv for the female breast, the cancer risk estimates are 0.7% for a 20-year-old woman and 0.03% for an 80-year-old man. A study by Huang et al. [31], which used effective dose, has reported that with 3.7 mSv of prospective ECG-gating CCTA, the cancer risk estimates are 0.014% and 0.035% for English, 0.013% and 0.036% for US, and 0.017% and 0.060% for Hong Kong males and females, respectively. Consequently, these estimates of cancer risk from the literature suggest that the use CCTA is associated with a non-negligible lifetime-attributable risk of cancer.

### **1.3 Challenges in dose optimisation strategies**

In conjunction with the concerns about increasing CT dose associated with the risk of radiation-induced cancers and to adhere to the "as low as reasonably achievable (ALARA)" principle, various dose optimisation strategies have been developed. For CCTA, the most common strategies [38-40] used are tube current reduction, low tube voltage, high-pitch protocol, scan coverage limitation, bismuth shielding, ECG-controlled tube current modulation, prospective ECG-gating method, and iterative reconstruction (IR) algorithm. Of these, IR algorithm has become a particular interest among researchers due to its ability to reduce noise at low exposure factors and thus, reducing dose while maintaining the image quality [41-43]. Currently, filtered back projection (FBP) is the most widely used of image reconstruction algorithm to reconstruct the data into CT images due to its robust and fast algorithm. However, FBP inherently increasing the image noise and producing artifacts at low exposure factors [44-46], and consequently, IR algorithm is used.

Since the introduction of the first IR algorithm in 2008 [47], multiple studies have shown the potential of such algorithms to maintain or improve the image quality and to allow for dose reduction while maintaining the image quality [41, 48, 49]. Along with these studies, different types of IR algorithms have also been introduced by the vendors to promote their solutions to reduce the dose in CT examinations. Although all types of IR algorithms perform iterative image corrections at some point in the CT image reconstruction process, there are considerable technical differences between one IR algorithm to another which the details mechanism are usually undisclosed. Furthermore, some vendors even offer more than one type of IR algorithm in their product range. Consequently, in an attempt to optimise the CT protocols using different IR algorithms, the

results of dose reduction is always varied and makes them difficult to be compared. A summary of the different types of IR algorithms with respect to their vendors is outlined in the Table 1.1.

Table 1.1 Some of the major types of IR algorithms based on product names and vendors.

<b>Algorithm</b>	<b>Acronym</b>	<b>Vendor</b>
ASIR [50]	Adaptive Statistical Iterative Reconstruction	GE Healthcare, Milwaukee, MI
Veo [51]	Product name, not acronym	GE Healthcare, Milwaukee, MI
iDOSE <sup>4</sup> [52]	Product name, not acronym	Philips Medical Systems, Best, Netherlands
IMR [53]	Iterative Model Reconstruction	Philips Medical Systems, Best, Netherlands
IRIS [54]	Iterative Reconstruction in Image Space	Siemens Healthcare, Forchheim, Germany
SAFIRE [55]	Sinogram Affirmed Iterative Reconstruction	Siemens Healthcare, Forchheim, Germany
AIDR 3D [56]	Adaptive Iterative Dose Reduction 3D	Toshiba Medical Systems, Tokyo, Japan

Each IR algorithm has taken unique approaches to noise reduction based on the distinct strength levels or settings [49, 57]. These strength levels are usually being selected after the data acquisitions and during the reconstruction process. In general, the selection of the IR algorithm strength levels influences the noise characteristics and image artifacts [44, 58]. As a result, the selection of the preferred IR strength levels is a specific clinical task germane to the individual preferences for image quality. For example, an individual may prefer a higher IR strength levels for the detection of low-contrast structures, whereas



a lower levels may be chosen to aim at improving spatial resolution or decreasing artifacts, rather than noise reduction. In early generation of IR algorithms, overuse of the noise reduction can be associated with an “over smoothing” of the images, which leads to a blotchy appearances [59, 60]. In the recent generation of IR algorithms, these effects have been reduced and the techniques have been improved to allow for a more effective artifacts reduction [43, 53, 61]. However, a practical consideration is still required prior to the selection of IR strength levels in order to produce image quality comparable to the traditional FBP techniques.

#### **1.4 Phantom studies for dose optimisation**

Phantom-based dose optimisation methodology is appropriate for CCTA studies because the use of patient datasets is problematic due to the potential of increased radiation dose and difficulties in recruiting a large cohort of patients who have known or suspected CAD [49, 62]. Phantoms designed to assess the effect of IR algorithm on the image quality are available in various types and shapes. The Catphan series (The Phantom Laboratories, Salem, NY) and American College of Radiology (ACR) phantoms are the most commonly used in the CCTA dose optimisation studies [47, 63-65]. These phantoms are preferred due to their comprehensive and sophisticated features to perform various testing including areas of sensitometry, contrast, resolution, geometry, and positioning. However, these phantoms cannot replicate accurately the CCTA images due to their uniform shape and size and consequently, a more realistic phantom is desired.

The ‘Lungman’ anthropomorphic chest phantom (Kyoto Kagaku co., Japan) has a body size of an adult patient and a cardiac insert phantom to simulate the heart organ [66].

The surrounding structures such as bones, lungs, muscles, and soft tissues have similar properties and image appearances to the real patient. However, the cardiac insert phantom in the Lungman phantom does not have appropriate heart features to simulate the CCTA images but only a homogenous and single material. Consequently, the lack of CCTA image features can be addressed by replacing the current cardiac insert with a newly designed cardiac insert phantom that can provide appropriate CCTA image appearances similar to the real human heart.

Image noise, which mainly depends on the number of photons reaching the detector, is one of the principal determinants of image quality [1, 67-70]. It can be measured by placing the region of interest (ROI) in the vascular contrast-enhanced structures such as in the aorta or the left ventricle wall [71]. Despite the image noise, image interpretability is also influenced by the degree of vascular enhancement. Previous studies [72-76] have suggested that attenuation values of 300-400 HU in the aorta are required for the image interpretation of the small vessels in CCTA. Therefore, it is important when designing a new cardiac insert phantom to include these features to enable the evaluation of image quality for the CCTA dose optimisation studies.

The use of 3D printing technology in phantom development studies is increasing dramatically [62, 77-80]. Many biomedical researchers have already explored its potential to produce phantoms that could replicate the appropriate features for different types of anatomical regions [81-83]. However, the application of a 3D-printed cardiac insert phantom of a Lungman phantom for dose optimisation studies is unique. Consequently, evidence to demonstrate the application of this 3D-printed cardiac insert phantom for CCTA dose optimisation is lacking.

## **1.5 Main and specific objectives**

This thesis investigates the application of 3D-printing technology for optimising CCTA protocols using IR algorithm as a dose optimisation strategy.

The specific objectives for each study conducted (as outlined in the chapters three, four and five respectively) for this thesis are to: -

1. develop a novel design of 3D-printed cardiac insert phantom derived from volumetric CT image datasets of anthropomorphic chest phantom for the investigations of CCTA protocols.
2. investigate the use of a 3D-printed cardiac insert phantom in the evaluation of an IR algorithm and its different strength levels for dose reduction potential in CCTA protocols.
3. evaluate the optimal IR algorithm strengths for a low tube voltage CCTA protocols using a phantom-based methodology and validate using patient image noise characteristics.

## **1.6 Ethics approval**

Ethics approval was obtained from the South Western Sydney Local Health District (SWSLHD) Research and Ethics Committee for Low and Negligible Risk Research to access patient image datasets (Appendix 1). The hospital's 'site-specific authorisation' letter is provided in Appendix 2.

## 1.7 Thesis outlines

This thesis is arranged into six chapters inclusive of the published, accepted, submitted, and in-preparation articles. Each chapter is presented as individual sections associated with the references. The outlines of the thesis are described in the next preceding paragraphs.

Chapter 2 examines the primary literatures reporting on the dose reduction potential achieved using the IR algorithm compared to the FBP while maintaining the image quality. This chapter also focuses on assessing the current changes of dose reduction potential among different types of IR algorithm available by all major CT vendors based on the studies retrieved from seven online databases. Part of this chapter has been published in the *Journal of Medical Imaging and Radiation Oncology (JMRO)* 2016; 60:459-68. doi: 10.1111/1754-9485.12473.

Chapter 3 explains the methodological aspects of developing a physical cardiac insert phantom using the 3D printing technology. The chapter outlines the process of fabricating physical models from the volumetric CT image datasets and the printing process of the physical cardiac insert phantom. The attenuation properties of the anatomical structures of this novel cardiac insert phantom are also outlined. Part of this chapter has been published in the *Journal of Medical Radiation Sciences (JMRS)* 2018; xx:1-9. doi: 10.1002/jmrs.279.

Chapter 4 explores the utility of the 3D-printed cardiac insert phantom to evaluate the impact of IR algorithm and its selectable strengths for dose reduction in CCTA while maintaining the image quality. This chapter compares the experimental results obtained

with the findings in previous literature. Part of this chapter has been submitted to the *Journal of Computer Assisted Tomography (JCAT)* and currently under review.

Chapter 5 investigates the application of the 3D printed cardiac insert phantom for assessing CCTA dose reduction potential using different IR algorithm strengths and tube voltage. The 3D-printed cardiac insert and Catphan® 500 (The Phantom Laboratory, Salem, NY) phantoms are used to measure the impact of the different CCTA protocols. Patient datasets are used to confirm and validate the results obtained. Part of this chapter is currently in final preparation and will be submitted to the *Journal of Cardiovascular Computed Tomography (JCCT)*.

Chapter 6 summarises the findings and discusses the implications and contribution of the research project. The limitations of the research project and the recommendations for future studies are also outlined.

## **1.8 References**

- [1] L. W. Goldman, "Principles of CT: radiation dose and image quality," *J Nucl Med Technol*, vol. 35, no. 4, pp. 213-25; quiz 226-8, Dec 2007.
- [2] H. Shi, A. J. Aschoff, H.-J. Brambs, and M. H. Hoffmann, "Multislice CT imaging of anomalous coronary arteries," *European radiology*, vol. 14, no. 12, pp. 2172-2181, 2004.
- [3] J. D. Mathews *et al.*, "Cancer risk in 680,000 people exposed to computed tomography scans in childhood or adolescence: data linkage study of 11 million Australians," *BMJ*, vol. 346, p. f2360, May 21 2013.

- [4] F. A. Mettler, P. W. Wiest, J. A. Locken, and C. A. Kelsey, "CT scanning: patterns of use and dose," *Journal of Radiological Protection*, vol. 20, no. 4, p. 353, 2000.
- [5] K. Matthews and P. C. Brennan, "The application of diagnostic reference levels: General principles and an Irish perspective," *Radiography*, vol. 15, no. 2, pp. 171-178, 2009/05/01/ 2009.
- [6] E. Dougeni, K. Faulkner, and G. Panayiotakis, "A review of patient dose and optimisation methods in adult and paediatric CT scanning," *Eur J Radiol*, vol. 81, no. 4, pp. e665-83, Apr 2012.
- [7] D. A. Schauer and O. W. Linton, "NCRP Report No. 160, Ionizing Radiation Exposure of the Population of The United States, Medical Exposure - Are We Doing Less With More, and Is There A Role for Health Physicists," *Health Physics*, vol. 97, no. 1, pp. 1-5, 2009.
- [8] D. A. Gibson, R. E. Moorin, J. Semmens, and D. A. J. Holman, "The disproportionate risk burden of CT scanning on females and younger adults in Australia: a retrospective cohort study," *Australian and New Zealand journal of public health*, vol. 38, no. 5, pp. 441-448, 2014.
- [9] A. Kaul, B. Bauer, J. Bernhardt, D. Nosske, and R. Veit, "Effective doses to members of the public from the diagnostic application of ionizing radiation in Germany," *European Radiology*, vol. 7, no. 7, pp. 1127-1132, 1997.
- [10] O. W. Linton, J. F. A. Mettler, P. National Council on Radiation, and Measurements, "National conference on dose reduction in CT, with an emphasis on pediatric patients," *AJR. American journal of roentgenology*, vol. 181, no. 2, p. 321, 2003.

- [11] P. Scanff, J. Donadieu, P. Pirard, and B. Aubert, "Population exposure to ionizing radiation from medical examinations in France," *British Journal of Radiology*, vol. 81, no. 963, pp. 204-213, 2008.
- [12] W. B. Shrimpton PC, "The Increasing Importance of X Ray Computed Tomography as a Source of Medical Exposure," *Radiation Protection Dosimetry*, 1995.
- [13] D. M. Yeh, H. Y. Tsai, Y. S. Tyan, Y. C. Chang, L. K. Pan, and T. R. Chen, "The Population Effective Dose of Medical Computed Tomography Examinations in Taiwan for 2013," *PLoS One*, vol. 11, no. 10, p. e0165526, 2016.
- [14] U. N. S. C. o. t. E. o. A. Radiation, "Sources and effects of ionizing radiation. UNSCEAR 2000 report to the General Assembly, with scientific annexes. Volume I: Sources," 2000.
- [15] I. IMV, "CT Market Summary Report," *Des Plaines, IL: IMV Medical Information Division*, 2006.
- [16] D. J. Brenner and E. J. Hall "Computed Tomography — An Increasing Source of Radiation Exposure," *New England Journal of Medicine*, vol. 357, no. 22, pp. 2277-2284, 2007.
- [17] Z. Brady, T. M. Cain, and P. N. Johnston, "Paediatric CT imaging trends in Australia," *J Med Imaging Radiat Oncol*, vol. 55, no. 2, pp. 132-42, Apr 2011.
- [18] P. Dawson, "Patient dose in multislice CT: why is it increasing and does it matter?," *The British journal of radiology*, vol. 77 Spec No 1, p. S10, 2004.
- [19] P. C. Shrimpton, M. C. Hillier, M. A. Lewis, and M. Dunn, "National survey of doses from CT in the UK: 2003," *The British journal of radiology*, vol. 79, no. 948, p. 968, 2006.

- [20] W. Huda and P. J. Mergo, "How will the introduction of multi-slice CT affect patient doses?," in *International Conference on Radiation Protection in Medicine* Vienna, 2001: IAEA.
- [21] H. J. C. P., "Patient doses in multi-slice CT and the importance of optimisation," *Australasian Physical & Engineering Sciences in Medicine* vol. 28, no. 2, 2005.
- [22] A. M. den Harder *et al.*, "New horizons in cardiac CT," *Clin Radiol*, vol. 71, no. 8, pp. 758-67, Aug 2016.
- [23] S. Achenbach *et al.*, "Coronary computed tomography angiography with a consistent dose below 1 mSv using prospectively electrocardiogram-triggered high-pitch spiral acquisition," *Eur Heart J*, vol. 31, no. 3, pp. 340-6, Feb 2010.
- [24] T. G. Flohr, U. J. Schoepf, and B. M. Ohnesorge, "Chasing the heart: new developments for cardiac CT," *Journal of thoracic imaging*, vol. 22, no. 1, pp. 4-16, 2007.
- [25] A. J. Foy, S. S. Dhruva, B. Peterson, J. M. Mandrola, D. J. Morgan, and R. F. Redberg, "Coronary Computed Tomography Angiography vs Functional Stress Testing for Patients With Suspected Coronary Artery Disease: A Systematic Review and Meta-analysis," *JAMA Intern Med*, Oct 02 2017.
- [26] H. T. Abada, C. Larchez, B. Daoud, A. Sigal-Cinqualbre, and J. F. Paul, "MDCT of the coronary arteries: feasibility of low-dose CT with ECG-pulsed tube current modulation to reduce radiation dose," *AJR Am J Roentgenol*, vol. 186, no. 6 Suppl 2, pp. S387-90, Jun 2006.
- [27] F. Cademartiri, G. Luccichenti, R. Marano, and P. Pavone, "Techniques for the optimisation of coronary artery opacification in non-invasive angiography with a 16-row multislice computed tomography," vol. 107, ed. Italy, 2004, pp. 24-24.



- [28] D. C. Levin, V. M. Rao, L. Parker, A. J. Frangos, and J. H. Sunshine, "Recent trends in utilization of cardiovascular imaging: how important are they for radiology?," *Journal of the American College of Radiology*, vol. 2, no. 9, pp. 736-739, 2005.
- [29] M. W. Itagaki, R. D. Suh, and J. G. Goldin, "Cardiac CT research: exponential growth," *Radiology*, vol. 252, no. 2, pp. 468-476, 2009.
- [30] D. J. Brenner and E. J. Hall, "Cancer Risks from CT Scans: Now We Have Data, What Next?," *Radiology*, vol. 265, no. 2, pp. 330-331, 2012/11/01 2012.
- [31] B. Huang, J. Li, M. W. M. Law, J. Zhang, Y. Shen, and P. L. Khong, "Radiation dose and cancer risk in retrospectively and prospectively ECG-gated coronary angiography using 64-slice multidetector CT," *The British Journal of Radiology*, vol. 83, no. 986, pp. 152-158, 2010.
- [32] K. Rothkamm and M. Löbrich, "Evidence for a lack of DNA double-strand break repair in human cells exposed to very low x-ray doses," *Proceedings of the National Academy of Sciences*, vol. 100, no. 9, pp. 5057-5062, 2003.
- [33] F. Mitelman, B. Johansson, and F. Mertens, "The impact of translocations and gene fusions on cancer causation," *Nature Reviews Cancer*, vol. 7, no. 4, p. 233, 2007.
- [34] D. J. Brenner *et al.*, "Cancer risks attributable to low doses of ionizing radiation: assessing what we really know," *Proceedings of the National Academy of Sciences*, vol. 100, no. 24, pp. 13761-13766, 2003.
- [35] D. J. Brenner, C. D. Elliston, E. J. Hall, and W. E. Berdon, "Estimated risks of radiation-induced fatal cancer from pediatric CT," *American journal of roentgenology*, vol. 176, no. 2, pp. 289-296, 2001.

- [36] A. Sodickson *et al.*, "Recurrent CT, cumulative radiation exposure, and associated radiation-induced cancer risks from CT of adults," *Radiology*, vol. 251, no. 1, pp. 175-184, 2009.
- [37] A. J. Einstein, M. J. Henzlova, and S. Rajagopalan, "Estimating risk of cancer associated with radiation exposure from 64-slice computed tomography coronary angiography," *JAMA*, vol. 298, no. 3, pp. 317-323, 2007.
- [38] J. E. Costello, N. D. Cecava, J. E. Tucker, and J. L. Bau, "CT Radiation Dose: Current Controversies and Dose Reduction Strategies," *American Journal of Roentgenology*, vol. 201, no. 6, pp. 1283-1290, 2013.
- [39] J. P. Earls and J. Leipsic, "Cardiac Computed Tomography Technology and Dose-reduction Strategies," *Radiologic Clinics of North America*, vol. 48, no. 4, pp. 657-+, 2010.
- [40] M. K. Kalra *et al.*, "Strategies for CT Radiation Dose Optimization," *Radiology*, vol. 230, no. 3, pp. 619-628, 2004/03/01 2004.
- [41] P. M. Almeida, "Improving iterative image reconstruction for X-ray CT," *Comput Biol Med*, vol. 43, no. 8, p. 1062, Sep 2013.
- [42] M. Beister, D. Kolditz, and W. A. Kalender, "Iterative reconstruction methods in X-ray CT," *Phys Med*, vol. 28, no. 2, pp. 94-108, Apr 2012.
- [43] L. L. Geyer *et al.*, "State of the Art: Iterative CT Reconstruction Techniques," *Radiology*, vol. 276, no. 2, pp. 338-356, 2015.
- [44] B. Chen, J. C. Ramirez Giraldo, J. Solomon, and E. Samei, "Evaluating iterative reconstruction performance in computed tomography," *Med Phys*, vol. 41, no. 12, p. 121913, Dec 2014.

- [45] S. Gordic *et al.*, "Optimizing radiation dose by using advanced modelled iterative reconstruction in high-pitch coronary CT angiography," *Eur Radiol*, vol. 26, no. 2, pp. 459-68, Feb 2016.
- [46] J. Greffier, A. Fernandez, F. Macri, C. Freitag, L. Metge, and J. P. Beregi, "Which dose for what image? Iterative reconstruction for CT scan," *Diagn Interv Imaging*, vol. 94, no. 11, pp. 1117-21, Nov 2013.
- [47] A. K. Hara, R. G. Paden, A. C. Silva, J. L. Kujak, H. J. Lawder, and W. Pavlicek, "Iterative reconstruction technique for reducing body radiation dose at CT: feasibility study," *AJR Am J Roentgenol*, vol. 193, no. 3, pp. 764-71, Sep 2009.
- [48] A. Aslam, U. Khokhar, M. Cortegiano, M. Poon, and S. Voros, "Adaptive Iterative Dose Reduction Is Associated with Significant Reduction in Total and Computed Tomography Coronary Angiography Radiation Exposure and Improved Image Quality, Compared to Traditional Filtered Backprojection on 320-Multidetector Computed Tomography," *Journal of the American College of Cardiology*, vol. 61, no. 10, 2013.
- [49] M. L. Aurumskjold, K. Ydstrom, A. Tingberg, and M. Soderberg, "Improvements to image quality using hybrid and model-based iterative reconstructions: a phantom study," *Acta Radiol*, vol. 58, no. 1, pp. 53-61, Jan 2017.
- [50] D. C. Benz *et al.*, "Adaptive Statistical Iterative Reconstruction-V: Impact on Image Quality in Ultralow-Dose Coronary Computed Tomography Angiography," *J Comput Assist Tomogr*, vol. 40, no. 6, pp. 958-963, Nov/Dec 2016.

- [51] M. J. Willeminck *et al.*, "Computed tomography radiation dose reduction: Effect of different iterative reconstruction algorithms on image quality," *Journal of Computer Assisted Tomography*, vol. 00, no. 00, pp. 1-9, 2014.
- [52] Y. Funama *et al.*, "Combination of a low-tube-voltage technique with hybrid iterative reconstruction (iDose) algorithm at coronary computed tomographic angiography," *J Comput Assist Tomogr*, vol. 35, no. 4, pp. 480-5, Jul-Aug 2011.
- [53] E. J. Halpern, E. L. Gingold, H. White, and K. Read, "Evaluation of coronary artery image quality with knowledge-based iterative model reconstruction," *Acad Radiol*, vol. 21, no. 6, pp. 805-11, Jun 2014.
- [54] M. S. Bittencourt *et al.*, "Iterative reconstruction in image space (IRIS) in cardiac computed tomography: initial experience," *Int J Cardiovasc Imaging*, vol. 27, no. 7, pp. 1081-7, Oct 2011.
- [55] B. K. Han, K. L. Grant, R. Garberich, M. Sedlmair, J. Lindberg, and J. R. Lesser, "Assessment of an iterative reconstruction algorithm (SAFIRE) on image quality in pediatric cardiac CT datasets," *J Cardiovasc Comput Tomogr*, vol. 6, no. 3, pp. 200-4, May-Jun 2012.
- [56] E. Angel, "AIDR 3D Iterative Reconstruction: Integrated, Automated and Adaptive Dose Reduction," *White Paper*, pp. 1-10, 2012.
- [57] A. D. Hardie, R. M. Nelson, R. Egbert, W. J. Rieter, and S. V. Tipnis, "What is the preferred strength setting of the sinogram-affirmed iterative reconstruction algorithm in abdominal CT imaging?," *Radiol Phys Technol*, vol. 8, no. 1, pp. 60-3, Jan 2015.

- [58] C. von Falck *et al.*, "Influence of sinogram affirmed iterative reconstruction of CT data on image noise characteristics and low-contrast detectability: an objective approach," *PLoS One*, vol. 8, no. 2, p. e56875, 2013.
- [59] J. Leipsic *et al.*, "Adaptive statistical iterative reconstruction: assessment of image noise and image quality in coronary CT angiography," *AJR Am J Roentgenol*, vol. 195, no. 3, pp. 649-54, Sep 2010.
- [60] F. Mueck *et al.*, "Upgrade to iterative image reconstruction (IR) in abdominal MDCT imaging: a clinical study for detailed parameter optimization beyond vendor recommendations using the adaptive statistical iterative reconstruction environment (ASIR)," in *RöFo-Fortschritte auf dem Gebiet der Röntgenstrahlen und der bildgebenden Verfahren*, 2012, vol. 184, no. 03, pp. 229-238: © Georg Thieme Verlag KG.
- [61] E. Maeda *et al.*, "The feasibility of Forward-projected model-based Iterative Reconstruction SoluTion (FIRST) for coronary 320-row computed tomography angiography: A pilot study," *Journal of Cardiovascular Computed Tomography*, vol. 11, no. 1, pp. 40-45, 2017.
- [62] J. Solomon and E. Samei, "Quantum noise properties of CT images with anatomical textured backgrounds across reconstruction algorithms: FBP and SAFIRE," *Med Phys*, vol. 41, no. 9, p. 091908, Sep 2014.
- [63] S. Guariglia, G. Meliaddò, E. Zivelonghi, L. Pinali, S. Montemezzi, and C. Cavedon, "Dose reduction and image quality in CT examinations using an iterative reconstruction algorithm: a phantom study," *Biomedical Physics & Engineering Express*, vol. 1, no. 4, 2015.

- [64] S. D. Kordolaimi, I. Saradeas, A. Ploussi, I. Pantos, S. Argentos, and E. P. Efstathopoulos, "Introduction of an effective method for the optimization of CT protocols using iterative reconstruction algorithms: comparison with patient data," *AJR Am J Roentgenol*, vol. 203, no. 4, pp. W434-9, Oct 2014.
- [65] F. Zarb, M. F. McEntee, and L. Rainford, "CT Radiation Dose and Image Quality Optimization Using a Porcine Model," *Radiologic technology*, vol. 85, no. 2, pp. 127-36, 2013.
- [66] S. Rodriguez Perez, N. W. Marshall, L. Struelens, and H. Bosmans, "Characterization and validation of the thorax phantom Lungman for dose assessment in chest radiography optimization studies," *J Med Imaging (Bellingham)*, vol. 5, no. 1, p. 013504, Jan 2018.
- [67] L. Yu *et al.*, "Radiation dose reduction in computed tomography: techniques and future perspective," *Imaging Med*, vol. 1, no. 1, pp. 65-84, Oct 2009.
- [68] O. Ghekiere *et al.*, "Image quality in coronary CT angiography: challenges and technical solutions," *Br J Radiol*, vol. 90, no. 1072, p. 20160567, 2017.
- [69] O. S. Grosser *et al.*, "Improvement of image quality and dose management in CT fluoroscopy by iterative 3D image reconstruction," *European Radiology*, vol. 27, no. 9, pp. 3625-3634, 2017.
- [70] Y. Xu, W. He, H. Chen, Z. Hu, J. Li, and T. Zhang, "Impact of the adaptive statistical iterative reconstruction technique on image quality in ultra-low-dose CT," *Clin Radiol*, vol. 68, no. 9, pp. 902-8, Sep 2013.

- [71] J. Ripsweden *et al.*, "Impact on image quality and radiation exposure in coronary CT angiography: 100 kVp versus 120 kVp," *Acta Radiol*, vol. 51, no. 8, pp. 903-9, Oct 2010.
- [72] F. Tatsugami *et al.*, "A new technique for noise reduction at coronary CT angiography with multi-phase data-averaging and non-rigid image registration," (in eng), *Eur Radiol*, vol. 25, no. 1, pp. 41-8, 2015.
- [73] S. Leschka *et al.*, "Low kilovoltage cardiac dual-source CT: attenuation, noise, and radiation dose," (in eng), *Eur Radiol*, vol. 18, no. 9, pp. 1809-17, 2008.
- [74] F. Tatsugami *et al.*, "The effect of adaptive iterative dose reduction on image quality in 320-detector row CT coronary angiography," *British Journal of Radiology*, vol. 85, no. 1016, pp. e378-e382, 2012.
- [75] S. Achenbach *et al.*, "Comparative assessment of image quality for coronary CT angiography with iobitridol and two contrast agents with higher iodine concentrations: iopromide and iomeprol. A multicentre randomized double-blind trial," *Eur Radiol*, vol. 27, no. 2, pp. 821-830, Feb 2017.
- [76] E. Y. Kim, D. W. Yeh, Y. H. Choe, W. J. Lee, and H. K. Lim, "Image quality and attenuation values of multidetector CT coronary angiography using high iodine-concentration contrast material: a comparison of the use of iopromide 370 and iomeprol 400," *Acta Radiol*, vol. 51, no. 9, pp. 982-9, Nov 2010.
- [77] A.-K. Carton, P. Bakic, C. Ullberg, H. Derand, and A. D. A. Maidment, "Development of a physical 3D anthropomorphic breast phantom," *Medical Physics*, vol. 38, no. 2, pp. 891-6, 2011.

- [78] J. I. Gear, C. Long, D. Rushforth, S. J. Chittenden, C. Cummings, and G. D. Flux, "Development of patient-specific molecular imaging phantoms using a 3D printer," *Med Phys*, vol. 41, no. 8, p. 082502, Aug 2014.
- [79] S. Leng *et al.*, "Anatomic modeling using 3D printing: quality assurance and optimization," *3D Printing in Medicine*, vol. 3, no. 1, 2017.
- [80] B. R. Whiting, C. Hoeschen, J. Solomon, F. Bochud, and E. Samei, "Design of anthropomorphic textured phantoms for CT performance evaluation," presented at the Medical Imaging 2014: Physics of Medical Imaging, 2014.
- [81] J. I. Gear *et al.*, "Abdo-Man: a 3D-printed anthropomorphic phantom for validating quantitative SIRT," *EJNMMI Phys*, vol. 3, no. 1, p. 17, Dec 2016.
- [82] T. Boltz, W. Pavlicek, M. Renno, and A. Jensen, "An anthropomorphic beating heart phantom for cardiac X-ray CT imaging evaluation," *Journal of Applied Clinical Medical Physics*, vol. 11, no. 1, pp. 1-12, 2010.
- [83] J. C. Aidan, D. Shahmirzadi, X. L. Ronny, J. D. Barry, E. K. Elisa, and M. M. Tim, "3D-Printed Tissue-Mimicking Phantoms for Medical Imaging and Computational Validation Applications," *3D Printing and Additive Manufacturing*, vol. 1, no. 1, pp. 14-23, 2014.



## **CHAPTER 2 Systematic review: Dose reduction with iterative reconstruction algorithm in coronary CT angiography**

Part of this chapter has been published in *Journal of Medical Imaging and Radiation Oncology*, 60 (2016) 459–468, doi:10.1111/1754-9485.12473.

## 2.1 Bridging section

### 2.1.1 Background

As described in the previous chapter, a number of dose optimisation strategies have been introduced in CCTA to reduce the patient dose to as low as reasonably achievable (ALARA) [1-3]. However, the radiation dose remains an important issue for CCTA due to the increasing number of CT examinations over the past few years, and consequently the associated radiation-induced cancer risks [4, 5]. IR algorithm is not considered a new technique as it was first proposed several decades ago [6]. However, IR algorithm was not practical for CT clinical practice due to its long processing time, owing to the lack of computational power at that time, and the algorithms complexity [6, 7]. With the recent advancements in the computer processing, IR algorithm has become feasible for routine CT clinical practice [8]. Over the past years, many new generations and types of IR algorithm have been introduced by the CT vendors, leading to a surge in the number of publications. Consequently, there is a need to further investigate the IR algorithm in keeping with the regular changes and updates by the CT vendors.

Different types of IR algorithm are available to provide solutions for increasing image noise at low exposure factors. Each IR algorithm has its own noise reduction algorithms which are usually undisclosed by the CT vendors due to business competition. As a result, each IR algorithm will produce different levels of noise reduction resulting in a wide range in dose reduction potential. For example, the iDose (Philips Medical Systems, Best, Netherlands) IR algorithm has been reported to have achieved up to 63% dose reduction while maintaining the image quality [9] whereas the ASIR (*Adaptive statistical iterative reconstruction*, GE Healthcare, Waukesha, WI) was reported to be 27% [10].

Therefore, a thorough systematic review of IR algorithm is needed to present the average ranges of dose reduction potential from all major CT vendors.

The findings of systematic review have revealed that the average ranges of dose reduction using IR algorithm is varied from 30-41%. All the selected studies had shown no statistical difference of image quality characteristics between the FBP and a lower dose CT protocol using the IR algorithm. Consequently, these results are used as the benchmark for dose reduction potential using IR algorithm and the first step to guide the CCTA dose optimisation studies in this thesis.

### **2.1.2 Recent literature after publication**

Several new studies have been published since the publication of this systematic review. After the re-introduction of IR algorithm into CT systems in 2008 [6, 8], the investigation on the effect of IR algorithm on dose reduction potential and image quality is still being explored actively by many researchers. A study by Cha et al. [11] in 2018, for example, continued to evaluate the effect between FBP and IR algorithm (iDose<sup>4</sup>, Philips Medical Systems, Best, Netherlands) on dose reduction potential while maintaining the image quality. Along with the recent updates by the CT vendors, new IR algorithm of iterative model reconstruction (*IMR*) algorithm has also been included in this study. The authors reported that compared with iDose<sup>4</sup> and FBP, IMR provided higher quality images with less radiation exposure in CCTA. Similarly, a study by Maeda et al. [12] which compared *AIDR3D* with the new IR algorithm of *FIRST* (Forward-projected model-based Iterative Reconstruction SoluTion, Toshiba Medical Systems, Tokyo, Japan) showed that

similar image quality was found between both IR algorithms when 28% radiation dose has been reduced.

Two recent systematic reviews [13, 14] were found which also investigated the effect of FBP and IR on dose reduction potential and image quality in CCTA. Both studies reported that IR algorithm can reduce radiation dose to the patient while maintaining the image quality, similar results to the systematic review shown in this chapter. The review by Armstrong et al. [13] did not provide any specific amount or range of dose reduction but Den Harder et al. [14] reported that IR algorithm allows for effective dose up to 48% with preserved objective and subjective image quality. However, there were some limitations to their methodology. With respect to the literature search, both studies have not included 2008 in their initial search strategy and only a small number of literature databases were used therefore, some relevant articles were excluded. Consequently, the review by Armstrong et al. [13] only included three studies while Den Harder et al. [14] included 10.

### 2.1.3 References

- [1] D. Ketelsen *et al.*, "High-pitch computed tomography coronary angiography-a new dose-saving algorithm: estimation of radiation exposure," *Radiol Res Pract*, vol. 2012, p. 724129, 2012.
- [2] A. Moscariello *et al.*, "Coronary CT angiography: image quality, diagnostic accuracy, and potential for radiation dose reduction using a novel iterative image reconstruction technique-comparison with traditional filtered back projection," *Eur Radiol*, vol. 21, no. 10, pp. 2130-8, Oct 2011.

- [3] Z. Sun, G. H. Choo, and K. H. Ng, "Coronary CT angiography: Current status and continuing challenges," *British Journal of Radiology*, vol. 85, no. 1013, pp. 495-510, 2012.
- [4] A. H. Mahnken, G. Mühlenbruch, R. W. Günther, and J. E. Wildberger, "Cardiac CT: coronary arteries and beyond," *European Radiology*, vol. 17, no. 4, pp. 994-1008, 2007.
- [5] H. W. Goo, "State-of-the-Art CT Imaging Techniques for Congenital Heart Disease," *Korean Journal of Radiology*, vol. 11, no. 1, pp. 4-18, 2010.
- [6] M. Beister, D. Kolditz, and W. A. Kalender, "Iterative reconstruction methods in X-ray CT," *Phys Med*, vol. 28, no. 2, pp. 94-108, Apr 2012.
- [7] C. Chartrand-Lefebvre, O. Prosmanne, M. Belair, and E. Therasse, "Radiation dose reduction in computed tomography: implementation of an iterative image reconstruction method," *Can Assoc Radiol J*, vol. 64, no. 4, p. 386, Nov 2013.
- [8] K. A. Abdullah, M. F. McEntee, W. Reed, and P. L. Kench, "Radiation dose and diagnostic image quality associated with iterative reconstruction in coronary CT angiography: A systematic review," *J Med Imaging Radiat Oncol*, vol. 60, no. 4, pp. 459-68, Aug 2016.
- [9] Y. Hou, J. Zheng, Y. Wang, M. Yu, M. Vembar, and Q. Guo, "Optimizing radiation dose levels in prospectively electrocardiogram-triggered coronary computed tomography angiography using iterative reconstruction techniques: a phantom and patient study," *PLoS One*, vol. 8, no. 2, p. e56295, 2013.
- [10] O. Tumor, K. Soon, F. Brown, and M. Mykytowycz, "New scanning technique using Adaptive Statistical Iterative Reconstruction (ASIR) significantly reduced the

- radiation dose of cardiac CT," *J Med Imaging Radiat Oncol*, vol. 57, no. 3, pp. 292-6, Jun 2013.
- [11] M. J. Cha, J. S. Seo, D. S. Yoo, and S. Chong, "Knowledge-based iterative model reconstruction in coronary computed tomography angiography: comparison with hybrid iterative reconstruction and filtered back projection," *Acta Radiol*, vol. 59, no. 3, pp. 280-286, Mar 2018.
- [12] E. Maeda *et al.*, "The feasibility of Forward-projected model-based Iterative Reconstruction SoluTion (FIRST) for coronary 320-row computed tomography angiography: A pilot study," *Journal of Cardiovascular Computed Tomography*, vol. 11, no. 1, pp. 40-45, 2017.
- [13] I. Armstrong, M. Trevor, and M. Widdowfield, "Maintaining image quality and reducing dose in prospectively-triggered CT coronary angiography: A systematic review of the use of iterative reconstruction," *Radiography*, vol. 22, no. 1, pp. 84-92, 2016.
- [14] A. M. Den Harder *et al.*, "Dose reduction with iterative reconstruction for coronary CT angiography: a systematic review and meta-analysis," *Br J Radiol*, vol. 89, no. 1058, p. 20150068, 2016.

## 2.2 Manuscript

This section is written in a manuscript version as submitted to *Journal of Medical Imaging and Radiation Oncology*, 60 (2016) 459–468, doi:10.1111/1754-9485.12473.

**Title:** Radiation dose and diagnostic image quality associated with iterative reconstruction in coronary CT angiography: A systematic review

**Authors:** Kamarul Amin Abdullah<sup>1,2</sup>, Mark F McEntee<sup>1</sup>, Warren Reed<sup>1</sup>, Peter L Kench<sup>1</sup>

**Affiliations:** 1. Discipline of Medical Radiation Sciences, Faculty of Health Sciences, The University of Sydney, New South Wales, Australia.

2. Centre of Medical Imaging, Faculty of Health Sciences, Universiti Sultan Zainal Abidin, Terengganu, Malaysia.

### 2.2.1 Abstract

**Objective:** To evaluate the radiation dose reduction achieved using IR algorithm compared to FBP in CCTA and assess the impact on diagnostic image quality.

**Methods:** A systematic search of seven electronic databases was performed to identify all studies using a developed keywords strategy. A total of 14 studies met the criteria and were included in a review analysis.

**Results:** The results showed that there was a significant reduction in radiation dose when using IR algorithm compared to FBP ( $P < 0.05$ ). The mean and standard deviation difference of  $CTDI_{vol}$  and DLP were  $14.70 \pm 6.87$  mGy and  $186 \pm 120$  mGy.cm respectively. The mean  $\pm$  SD difference of  $E_D$  was  $2.9 \pm 1.7$  mSv with the range from 1.0 to 5.0 mSv. The assessment of

diagnostic image quality showed no significant difference ( $P>0.05$ ). The mean  $\pm$  SD difference of image noise, signal-noise ratio (SNR) and contrast-noise ratio (CNR) were  $1.05 \pm 1.29$  HU,  $0.88 \pm 0.56$  and  $0.63 \pm 1.83$  respectively. The mean  $\pm$  SD percentages of overall image quality scores were  $71.79 \pm 12.29\%$  (FBP) and  $67.31 \pm 22.96\%$  (IR algorithm). The mean  $\pm$  SD percentages of coronary segment analysis were  $95.43 \pm 2.57\%$  (FBP) and  $97.19 \pm 2.62\%$  (IR algorithm).

**Conclusion:** This review analysis shows that CCTA with the use of IR algorithm leads to a significant reduction in radiation dose as compared to the use of FBP. Diagnostic image quality of IR algorithm at reduced dose (30–41%) is comparable to FBP at standard dose in the diagnosis of CAD.

**Key words:** coronary artery disease, coronary CT angiography, dose reduction, filtered back projection, iterative reconstruction

### 2.2.2 Introduction

A minimally invasive tool for screening patients with suspected coronary artery disease (CAD) is highly desirable, to exclude those with or without significant stenosis. In most developed countries, coronary CT angiography (CCTA) has been shown to be a reliable method for the exclusion of CAD and is now recommended for routine use in clinical practice [1, 2]. CCTA has become a more powerful diagnostic imaging tool than conventional coronary angiography, which tends to underestimate the significance of stenosis and thus, limits performance [3]. However, CCTA has the disadvantage of a high radiation dose to the patient and the potential risk of cancer over a lifetime period [3, 4].



In recent years, several approaches have been taken to optimise radiation dose in CCTA such as tube current reduction, low tube voltage, tube current modulation, and prospective ECG-gating [5, 6]. A newer approach that has recently become commercially available from CT vendors is to optimise the CT image reconstruction. Currently, the most widely used reconstruction technique is FBP, which uses an analytic reconstruction algorithm that assumes all acquired projection data are noise free [7]. In FBP, image characteristics will be updated by filtering the acquired projection data and projecting back into image space to reconstruct the overall image [8]. This reconstruction technique is fast and robust but may lead to noisy images, which limits the amount of dose reduction achievable by simply reducing exposure factors during acquisition.

IR algorithm, a statistical method and an alternative technique to FBP, has been introduced to allow imaging at lower radiation dose with comparable image noise to FBP [9, 10]. As a result, dose reduction may be achieved while maintaining diagnostic image quality. IR algorithm can reduce image noise by performing repeated iterative reconstruction cycles and comparing the images reconstructed from acquired projection data to a modelled projection. With every cycle or iteration, the reconstructed image is updated to selectively identify and subtract image noise [11]. Thus, the final images will have similar or superior diagnostic image quality to that using FBP despite a significant reduction in acquisition exposure factors.

While IR algorithm is a particularly useful technique, it has been historically impractical owing to the heavy computational burden, poor convergence speed and additional time requirements [12]. As a result, CT vendors have developed a hybrid FBP and IR algorithms that is feasible for clinical use. Each vendor has a proprietary IR

algorithm that shows promise of minimising the relationship between image noise and radiation dose. Generally, in this technique, FBP is utilised to obtain the initial reconstructed image, which is used as a starting point for IR algorithm [13]. The FBP is blended with IR algorithm at different strengths to optimise the reconstruction technique. Consequently, the technique will have the less computational burden and faster speed. However, differences in IR algorithm implementation by each vendor have caused a wide variation in outcomes regarding overall radiation dose reduction.

Over the past years, much research has been performed on the use of IR algorithm for CT examinations. However, only a few studies have investigated the use of IR algorithm during CCTA. Conclusions from the application of IR algorithm in other CT examinations may not apply to CCTA as different diagnostic image quality criteria are used. Therefore, the purpose of this systematic literature search is to evaluate the potential for radiation dose reduction using IR algorithm for CCTA and also the impact on diagnostic image quality of IR algorithm compared to FBP.

### **2.2.3 Materials and Methods**

#### *2.2.3.1 Search strategy*

The literature search was carried out using a Preferred Reporting Items for Systematic Reviews and Meta-Analysis (PRISMA) strategy [14] and the following seven databases: MEDLINE; Web of Science; EMBASE; CINAHL; Science Direct; IEEE Xplore; and SPIE Digital Library. The search was limited to items published between 2008 and 2015 as the first commercial IR algorithm for clinical use was released in late 2008 [15]. The search

was limited to include all the studies that had been published in the English language and were performed on human subjects. The search terms used are shown in Table 2.1.

Table 2.1: A table shows the Boolean operators and keywords used.

Radiation dose		Image quality
CT dose/s		CT image/s
CT dosage		Digital image/s
CT radiation dose/s	OR	CT image quality
CT dosimetry		CT diagnostic image quality
MSCT dose		Image noise
MDCT dose		CT image noise
AND		
Multidetector CT		Image reconstruction
Multislice CT		CT image reconstruction
Dual source CT		Iterative reconstruction
CT coronary angiography/m		CT iterative reconstruction
coronary CT angiography/m	OR	CT iterative algorithm
MSCT coronary angiography		CT iterative image
MDCT coronary angiography		Filtered back projection
DSCT coronary angiography		Conventional back projection
†CT, Computed Tomography, ‡MSCT, Multi-slice Computed Tomography, §MDCT, Multi-detector Computed Tomography,		

### 2.2.3.2 Criteria for selection

All studies were selected based on the inclusion and exclusion criteria developed using a Population, Intervention or Exposure (PECO), Comparison, Outcomes (PICO) methodology [16]. Studies that compared the radiation dose and diagnostic image quality between IR algorithm and FBP in adult patients (>18 years old) who underwent CCTA for

investigation of CAD using a multi-slice/detector or a dual-source CT scanners were included.

Studies excluded were those that used phantoms, animals or both phantoms and humans as they did not specifically analyse the detection and classification of coronary arteries. Case reports, summaries or reviews were also excluded due to insufficient information about the background of the study, methodology and statistical data analysis (e.g. mean, median and standard deviation). Finally, studies that specifically recruited obese patients were excluded, this reduced the impact of patient weight as a biasing factor on the dose.

#### *2.2.3.3 Quality assessment*

The quality assessment was carried out by two reviewers using a customised table based on the *Quality Assessment Tool for Quantitative Studies* developed by the Effective Public Health Practice Project (EPHPP) [17]. A table was created to assess the risk of bias, identify any poor quality or irrelevant citations; assess the reproducibility of the scanning parameters and reconstruction protocols; and evaluate the study design conducted to meet the criteria of selection.

#### *2.2.3.4 Data extraction*

The following data were extracted from each study: first author name; type of IR; total number of patients; patient age and gender; method of ECG-gating (retrospective or prospective); the size of detector collimation; gantry rotation time; and exposure factors (kVp, mA).

Radiation dose was assessed using CT dose index volume ( $CTDI_{vol}$ ), dose-length-product (DLP) and effective dose ( $E_D$ ). These descriptors facilitate radiation dose comparisons between different CT protocols and procedures [18]. The  $CTDI_{vol}$  and DLP can evaluate the radiation quantity of the specific CT examination performed, while  $E_D$  estimates the potential radiation risk from a specific CT examination [19]. The  $E_D$  was calculated as the DLP times standard conversion factor for CT chest of  $0.014 \text{ mSv/mGy/cm}^{-1}$  [20]. This method was selected as most of the included studies used this conversion factor. If studies used a different conversion factor, the  $E_D$  was recalculated using the above method to allow comparison.

The measures of diagnostic image quality were divided into the quantitative and qualitative assessment. The measures for quantitative assessment were the image noise, the signal-noise ratio (SNR) and the contrast-noise ratio (CNR), whereas for qualitative assessment were multi-point Likert-type scale and coronary segments analysis. Most studies implement a 5-point Likert-type scale from 1 (poor) to 5 (excellent). However, some studies used a 3- or 4-point scale, therefore, all scores were converted into percentages, for example, 3/5 would be 60%, 2/3 would be 66%. The coronary segment analysis involved measures of interpretable vessels in accordance with the coronary artery model of American Heart Association (AHA) [21]. Only vessels with a minimum diameter of 1.5 mm were included. The descriptors of radiation dose and diagnostic image quality for both FBP and IR algorithm were recorded regarding mean  $\pm$  standard deviation, range or percentage values wherever available. The analysis of coronary segments was presented as a percentage to enable comparison between FBP and IR algorithm.

### *2.2.3.5 Statistical analysis*

Data were entered into SPSS software (version 21, IBM Corp., New York) for analysis. Results were presented as a mean and standard deviation. The values of radiation dose and diagnostic image quality descriptors were combined across studies using the one sample test. Statistical hypotheses (2-tailed) were tested at the 5% level of significance (p-value <0.05).

## **2.2.4 Results**

### *2.2.4.1 Search result*

The flow chart for identifying relevant studies is shown in Figure 2.1. The preliminary electronic databases search returned a total of 1,293 citations. Removal of duplication resulted in 721 citations being identified as relevant to the review. Of these, 547 citations were not related to FBP and IR algorithm. A further 94 citations were removed as they did not report radiation dose or diagnostic image quality. The remaining 80 citations were assessed using the inclusion and exclusion criteria of the PICO (Population, Intervention, Comparison, Outcomes) methodology [16]. This resulted in 16 citations to be included in the review. Two further citations were excluded as they did not present sufficient data to enable evaluation of radiation dose.

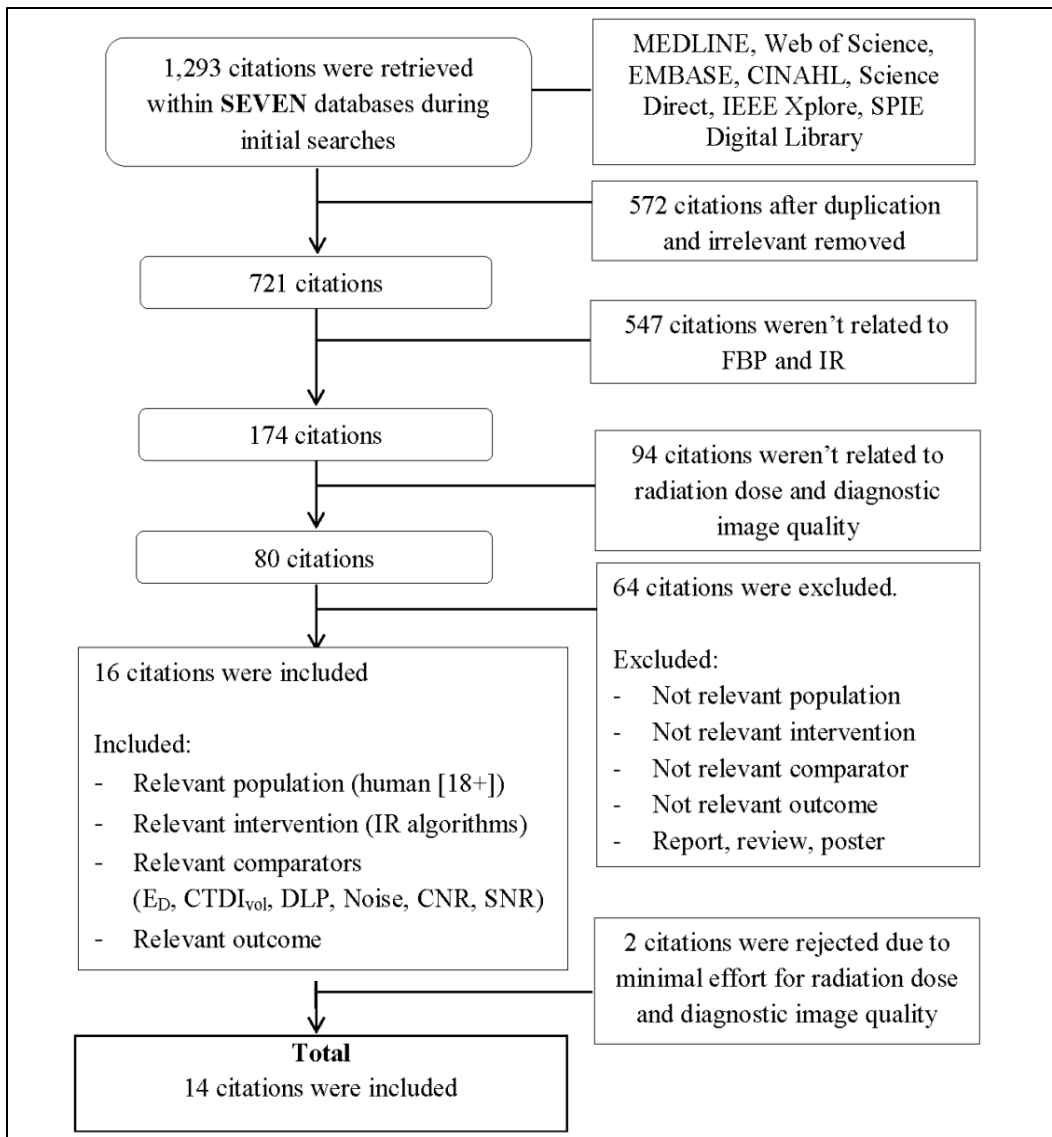


Figure 2.1: Flow chart outlining the search strategy used for this systematic review.

#### 2.2.4.2 Characteristics of selected studies

The summary of study details of the selected citation are shown in Table 2.2 and 2.3. The 14 studies recruited a total sample size of 3,428 patients [3, 22-34]. The ratio of male to female was 1,664 to 1,706 patients; but one study did not provide the ratio values between gender [34].

Research design varied among studies mainly due to differing generations and manufacturers of CT scanners being used. The scanning parameters and protocols were determined depending on variations of CT scanners. These include the electrocardiogram (ECG)-gating method used, detector collimation size, gantry rotation time, tube voltage and tube current. A total of seven studies used prospective ECG-gating [3, 23, 25, 27, 30, 31, 33], two studies used retrospective [26, 28], and four studies used both types [22, 24, 32, 34]. One study did not provide the type of ECG gating used [29]. There were four studies that used a similar size of detector collimation of 64 x 0.625 millimetres (mm), [23, 24, 26, 34] two studies that used 128 x 0.625 mm [32, 33], three studies that used 320 x 0.5 mm [3, 30, 31], and two studies of dual source scanner that used 32 x 0.625 mm [25, 28], and one study of dual source scanner that used 64 x 0.25 mm [22]. Another two studies did not provide the size of detector collimation [27, 29]. The range of gantry rotation time was 270-350 milliseconds (ms) ranging across 11 studies since three did not provide these values [27, 29, 34]. The minimum tube voltage for all studies was 80 kVp, and the maximum was 135 kVp with seven studies using between 100 and 120 kVp [23-25, 27, 28, 33, 34]. The mean  $\pm$  SD of tube current for FBP and IR algorithm across five studies was  $481.32 \pm 331.26$  and  $327.56 \pm 189.06$  respectively indicating approximately 68% reduction of tube current used [3, 31-33, 35]. Nine studies did not provide values for tube current [22-27, 29, 30]. Three studies were performed on each of the following IR algorithm; *adaptive statistical iterative reconstruction* (ASIR, GE Healthcare, Milwaukee, WI, USA) [23, 24, 26]; *sinogram affirmed iterative reconstruction* (SAFIRE, Siemens Healthcare, Erlangen, Germany) [22, 25, 27]; *adaptive iterative dose reduction* (AIDR, Toshiba Medical Systems Co Ltd., Otowara, Japan) [3, 30, 31]; iDose (Philips Healthcare, Best, the Netherlands) [32-34];



and two studies were performed with *iterative reconstruction in image space* (IRIS, Siemens Healthcare) [28, 29].

#### 2.2.4.3 Radiation dose

Dose indicators of  $CTDI_{vol}$ , DLP, and  $E_D$  were extracted from studies where available (Tables 2.4 and 2.6). Six studies did not provide  $CTDI_{vol}$  [23, 24, 26, 30-32].  $CTDI_{vol}$  for FBP ranged from 16.20 to 60.30 milligray (mGy) while for IR algorithm was from 11.30 to 36.90 mGy. The mean of  $CTDI_{vol}$  for FBP is significantly higher than IR algorithm with a difference in the mean  $\pm$  standard deviation (SD) of  $14.70 \pm 6.87$  mGy ( $P = 0.029$ ).

DLP values corresponded with  $CTDI_{vol}$  as they are derived from multiplying  $CTDI_{vol}$  with the scan length (centimetres, cm). Four studies did not report the DLP [23, 24, 26, 31]. The DLP for FBP is significantly higher ( $426 \pm 226$  mGy.cm) than IR algorithm ( $241 \pm 106$  mGy.cm) with a difference in the mean  $\pm$  SD of  $186 \pm 120$  mGy.cm ( $P = 0.019$ ).

The  $E_D$  for FBP and IR algorithm was reported in 10 studies [3, 22, 25, 27-30, 32-34]. For FBP, the  $E_D$  ranged from 3.3 to 12.1 millisievert (mSv) (mean  $\pm$  SD:  $6.0 \pm 3.2$  mSv) and for IR algorithm, ranged from 2.3 to 7.1 mSv (mean  $\pm$  SD:  $3.1 \pm 1.5$ ). The  $E_D$  for FBP is significantly higher (mean  $\pm$  SD:  $6.0 \pm 3.2$  mSv) than IR algorithm (mean  $\pm$  SD:  $3.1 \pm 1.5$ ) with a  $P$ -value  $<0.05$  ( $P = 0.023$ ). Radiation dose reduction associated with the use of IR algorithm compared to FBP varies widely, ranging from 1.0 to 5.0 mSv with mean  $\pm$  SD difference of  $2.9 \pm 1.7$  mSv (Figure 2.2).

#### 2.2.4.4 Diagnostic image quality

Diagnostic image quality was compared between FBP and IR algorithm across all studies (Tables 2.5 and 2.7). For FBP, the range of image noise was 18.70-39.00 Hounsfield units (HU) (one study did not report) [23] and 13.70-41.00 HU for IR algorithm. Although there was a reduction of the tube current for IR algorithm, there was no significant difference ( $P = 0.743$ ) in the measurement of mean  $\pm$  SD image noise ( $28.67 \pm 8.36$  HU) when compared to FBP ( $29.72 \pm 7.07$  HU).

Likewise, no studies reported statistically significant differences in mean SNR and CNR for FBP and IR algorithm, although seven studies did not provide either one or both of the values [3, 22, 23, 26, 29, 32, 33]. The mean  $\pm$  SD signal-noise ratio for FBP and IR algorithm was  $15.27 \pm 4.79$  and  $14.39 \pm 5.35$  while for CNR was  $15.67 \pm 8.37$  and  $16.30 \pm 6.54$ , respectively.

A total of nine studies used a Likert-scale point system to demonstrate overall image quality [22, 25, 26, 28-30, 33, 34, 36]. Six studies were conducted with a 5-point Likert-scale [22, 26, 28-30, 34], and another three studies used 4-point [3, 25, 33]. The five points of classifications were poor, fair, moderate, good and excellent image quality while four points classification has poor, fair, good and excellent image quality. The result of analysis showed no significant differences in overall image quality between FBP and IR algorithm with  $P = 0.711$  ( $P > 0.05$ ). Eight studies included analysis of the number of assessable and non-assessable coronary segments [23-25, 27, 30-33]. A mean  $\pm$  SD of  $95.43 \pm 2.57\%$  (FBP) and  $97.19 \pm 2.62\%$  (IR algorithm) were found to be assessable with a very small number of non-assessable segments reported in this review. Once again, no statistically significant

difference image quality was reported between FBP and IR algorithm with  $P = 0.196$  ( $P > 0.05$ ).

Table 2.2: Summary of study details of the selected citation (part 1).

Author	Type of IR	Patients (M: F)	Mean age (years $\pm$ SD)	ECG-gating
Leipsic et al. [23]	ASIR	574 (121:453)	56 $\pm$ 13 (FBP) 57 $\pm$ 13 (IR)	prospective
Shen, J. et al. [26]	ASIR	338 (169:169)	59.3 $\pm$ 9.4 (FBP) 58.8 $\pm$ 8.8 (IR)	retrospective
Tumur, O. et al. [24]	ASIR	347 (169:178)	52 $\pm$ 11 (FBP) 56 $\pm$ 13 (IR)	both
Moscariello, A. et al. [22]	SAFIRE	65 (48:17)	59.3 $\pm$ 7.7 (FBP & IR)	both
Wang, R. et al. [25]	SAFIRE	78 (45:33)	52.8 $\pm$ 10.6 (FBP) 53.7 $\pm$ 7.5 (IR)	prospective
Yin, Wei-Hua et al. [27]	SAFIRE	231 (139:92)	54.8 $\pm$ 10.1 (FBP & IR)	prospective
Park, E.A. et al. [28]	IRIS	162 (78:84)	61.3 $\pm$ 9.9 (FBP & IR)	retrospective
Renker M. et al. [29]	IRIS	24 (12:12)	56.9 $\pm$ 7.3 (FBP) 57.8 $\pm$ 8.0 (IR)	NS
Di Cesare, E. et al. [30]	AIDR	200 (138:62)	66.9 $\pm$ 7.5 (FBP) 65.2 $\pm$ 9.5 (IR)	prospective
Tomizawa N. et al. [31]	AIDR	100 (61:39)	68.8 $\pm$ 9.5 (FBP) 65.6 $\pm$ 9.6 (IR)	prospective
Williams, M. C. et al. [3]	AIDR	942 (445:497)	58 $\pm$ NS (FBP) 58 $\pm$ NS (IR)	prospective
Carrascosa, P. et al. [32]	iDose	200 (165:35)	55.6 $\pm$ 9.1 (FBP) 56.0 $\pm$ 10.1 (IR)	both
Hou, Y. et al. [33]	iDose	109 (74:35)	55 $\pm$ 13 (FBP) 56 $\pm$ 12 (IR)	prospective
Kordolaimi S.D. et al. [34]	iDose	58 (NS)	51.9 $\pm$ 15.5 (FBP) 55.7 $\pm$ 8.9 (IR)	both

NS, Not stated; FBP, Filtered back projection; IR, Iterative reconstruction; ASIR, Adaptive statistical iterative reconstruction; SAFIRE, Sinogram affirmed iterative reconstruction; IRIS, Iterative reconstruction in image space; AIDR, Adaptive iterative for dose reduction; iDose; Iterative reconstruction; ECG-gating, Electrocardiogram-gated.

Table 2.3: Summary of study details of the selected citation (part 2).

Author	Detector collimation (mm)	Gantry rotation time (ms)	Tube voltage (kVp)	Tube Current (mA)
Leipsic et al. [23]	64 × 0.625	350	100-120	275-800 (FBP & IR)
Shen, J. et al. [26]	64 × 0.625	350	120	418-598 (FBP) 255-379 (IR)
Tumur, O. et al. [24]	64 × 0.625	350	100-120	600-711 (FBP) 450-600 (IR)
Moscariello, A. et al. [22]	2 × 64 × 0.625	280	80-120	341 ± 30 (FBP & IR)
Wang, R. et al. [25]	2 × 32 × 0.625	330	100-120	354-430 (FBP) 286-370 (IR)
Yin, Wei-Hua et al. [27]	NS	NS	100-120	NS
Park, E.A. et al. [28]	2 × 32 × 0.625	330	100-120	200-380
Renker M. et al. [29]	NS	NS	80-120	320-350
Di Cesare, E. et al. [30]	320 × 0.5	350	100-135	300-510
Tomizawa N. et al. [31]	320 × 0.5	350	120	483 ± 93 (FBP) 289 ± 74 (IR)
Williams, M. C. et al. [3]	320 × 0.5	350	100-135	538 ± NS (FBP) 426 ± NS (IR)
Carrascosa, P. et al. [32]	128 × 0.625	270	100-120	203 ± 15.4 (FBP) 195.7 ± 26.8 (IR)
Hou, Y. et al. [33]	128 × 0.625	270	120	1000 (FBP) 600 (IR)
Kordolaimi S.D. et al. [34]	64 × 0.625	NS	100-120	182 ± 27.5 (FBP) 127.1 ± 29.1 (IR)

NS, Not stated; FBP, Filtered back projection; IR, Iterative reconstruction; ASIR, Adaptive statistical iterative reconstruction; SAFIRE, Sinogram affirmed iterative reconstruction; IRIS, Iterative reconstruction in image space; AIDR, Adaptive iterative for dose reduction; iDose; Iterative reconstruction; kVp, kilovoltage peak; mA, miliamperage.

Table 2.4: Summary of radiation dose indicators of the selected citations.

Author	Image Reconstruction	CTDI <sub>vol</sub> (mGy)	DLP (mGy x cm)	Effective dose, E <sub>D</sub> (mSv)
Leipsic et al. [23]	FBP	11.68-25.87	167-370	2.3-5.2
	IR	9.5-17.59	134-248	1.9-3.5
Shen, J. et al. [26]	FBP	13.3-20.1	176-269	2.5-3.8
	IR	8.1-13.4	108-167	1.5-2.3
Tumur, O. et al. [24]	FBP	39.02-64.42	277-599.4	3.88-8.39
	IR	27.88-46.73	202.5-430	2.84-6.02
Moscariello, A. et al. [22]	FBP	32.1 ± 20.3	459.8 ± 303.7	6.4 ± 4.3
	IR	16.05 ± 10.15	229.9 ± 151.8	3.2 ± 2.1
Wang, R. et al. [25]	FBP	47.73 ± 9.40	630.41 ± 124.39	8.83 ± 1.74
	IR	23.37 ± 4.74	315.33 ± 59.19	4.41 ± 0.83
Yin, Wei-Hua et al. [27]	FBP	27.5 ± 8.2	251.7 ± 80.7	3.5 ± 1.1
	IR	17.9 ± 6.6	163.7 ± 72.5	2.3 ± 1.0
Park, E.A. et al. [28]	FBP	24.7 ± 8.8	399.2 ± 156.6	6.0 ± 3.0
	IR	15.0 ± 3.7	242.1 ± 65.7	3.6 ± 1.3
Renker M. et al. [29]	FBP	41.8 ± 17.8	685.6 ± 278.8	9.6 ± 3.9
	IR	19.7 ± 9.4	266.9 ± 160.0	3.7 ± 2.2
Di Cesare, E. et al. [30]	FBP	NS	238.6 ± 57.1	3.34 ± 0.8
	IR	NS	182.14 ± 71.43	2.55 ± 1
Tomizawa N. et al. [31]	FBP	22.87-60	311-816	4.35-11.4
	IR	10.38-34.92	137-461	1.92-6.45
Williams, M. C. et al. [3]	FBP	20.6 ± NS	274 ± NS	3.84 ± NS
	IR	13.1 ± NS	168 ± NS	2.35 ± NS
Carrascosa, P. et al. [32]	FBP	NS	242.86 ± 171.4	3.4 ± 2.4
	IR	NS	171.43 ± 50	2.4 ± 0.7
Hou, Y. et al. [33]	FBP	60.3 ± 4.7	858.3 ± 109.1	12.1 ± 1.5
	IR	36.9 ± 3.5	504.4 ± 67.4	7.1 ± 0.9
Kordolaimi S.D. et al. [34]	FBP	16.2 ± 3.0	224.0 ± 73.3	3.3 ± 1.1
	IR	11.3 ± 3.2	164.5 ± 55.2	2.4 ± 0.8

NS, Not stated; FBP, Filtered back projection; IR, Iterative reconstruction; CTDI<sub>vol</sub>, Computed Tomography dose index volume; DLP, Dose-length product.

Table 2.5: Summary of image quality indicators of the selected citations.

Author	Image Recons- truction	Image Noise (HU)	Signal-noise ratio (SNR)	Contrast- noise ratio (CNR)	Qualitative assessment
Leipsic et al. [23]	FBP	NS	NS	NS	96.1%
	IR	6-10	-2 to -3	NS	97.1%
Shen, J. et al. [26]	FBP	35.00-35.03	$11.6 \pm 2.1$	NS	$3.13 \pm 0.34$
	IR	34.99-35.02	$10.9 \pm 1.9$	NS	$3.09 \pm 0.29$
Tumur, O. et al. [24]	FBP	$37.63 \pm 18.79$	$11.0 \pm 3.63$	$8.33 \pm 3.08$	93.7%
	IR	$39.93 \pm 10.22$	$10.47 \pm 3.29$	$7.95 \pm 2.68$	98.2%
Moscariello, A. et al. [22]	FBP	$24.7 \pm 7.4$	NS	NS	4(4-5)
	IR	$20.7 \pm 7$	NS	NS	4(4-5)
Wang, R. et al. [25]	FBP	$26.53 \pm 5.16$	$13.44 \pm 3.75$	$19.70 \pm 4.86$	92.7%
	IR	$27.64 \pm 3.90$	$15.58 \pm 3.15$	$20.82 \pm 4.71$	93.9%
Yin, Wei-Hua et al. [27]	FBP	$18.7 \pm 3.8$	$22.5 \pm 5.4$	$17.5 \pm 5.5$	98.6%
	IR	$13.7 \pm 2.7$	$30.5 \pm 7.4$	$23.7 \pm 7.5$	98.7%
Park, E.A. et al. [28]	FBP	$24.8 \pm 4.0$	$22.7 \pm 4.6$	$16.1 \pm 4.0$	$4.12 \pm 0.62$
	IR	$22.0 \pm 4.5$	$25.8 \pm 4.4$	$18.3 \pm 4.2$	$4.49 \pm 0.60$
Renker M. et al. [29]	FBP	$24.9 \pm 6.0$	NS	NS	4(4-5)
	IR	$26.0 \pm 7.5$	NS	NS	5(4-5)
Di Cesare, E. et al. [30]	FBP	$30.6 \pm 5.4$	$13.9 \pm 3.1$	$16.2 \pm 3.5$	95%
	IR	$27.6 \pm 3.9$	$17.7 \pm 3.5$	$20.6 \pm 3.6$	99.9%
Tomizawa N. et al. [31]	FBP	$22.1 \pm 4.3$	$18.9 \pm 4.6$	$22.1 \pm 4.9$	98%
	IR	$23.0 \pm 4.0$	$19.9 \pm 4.5$	$23.0 \pm 4.7$	98%
Williams, M. C. et al. [3]	FBP	$32 \pm NS$	NS	$12 \pm NS$	3.3(3.2, 3.4)
	IR	$41 \pm NS$	NS	$11 \pm NS$	3.1(3.0, 3.2)
Carrascosa, P. et al. [32]	FBP	$37.8 \pm 1.4$	$12.2 \pm 1.4$	NS	$91.7 \pm 4.0\%$
	IR	$38.2 \pm 2.4$	$12.1 \pm 1.4$	NS	$92.5 \pm 2.8\%$
Hou, Y. et al. [33]	FBP	$39 \pm 10$	NS	$12 \pm 4$	97.6%
	IR	$33 \pm 6$	NS	$15 \pm 3$	99.2%
Kordolaimi S.D. et al. [34]	FBP	NS	NS	NS	96.1%
	IR	6-10	-2 to -3	NS	97.1%

NS, Not stated; FBP, Filtered back projection; IR, Iterative reconstruction; HU; Hounsfield units.

Table 2.6: Summary of study details for radiation dose indicators.

Radiation Dose		FBP	IR	P-value (sig.)
CTDI <sub>vol</sub> (mGy)	N(*)	8(6*)	8(6*)	0.029 (sig.)
	Minimum	16.20	11.30	
	Maximum	60.30	36.90	
	Mean ± SD	33.87 ± 14.97	19.17 ± 8.10	
DLP (mGy.cm)	N(*)	10(4*)	10(4*)	0.019 (sig.)
	Minimum	224.00	163.70	
	Maximum	858.30	504.40	
	Mean ± SD	426.45 ± 226.29	240.84 ± 106.02	
E <sub>D</sub> (mSv)	N(*)	10(4*)	10(4*)	0.023 (sig.)
	Minimum	3.30	2.30	
	Maximum	12.10	7.10	
	Mean ± SD	6.03 ± 3.17	3.14 ± 1.49	

FBP, Filtered back projection; IR, Iterative reconstruction; (\*), no. of studies did not provide values.

Table 2.7: Summary of study details for diagnostic image quality indicators.

Diag. Image Quality		FBP	IR	P-value (sig.)
Image noise	N(*)	12(2*)	12(2*)	0.743 (no sig.)
	Minimum	18.70	13.70	
	Maximum	39.00	41.00	
	Mean ± SD	29.72 ± 7.06	28.67 ± 8.36	
Signal-noise ratio (SNR)	N(*)	9(5*)	10(4*)	0.485 (no sig.)
	Minimum	11.00	1.00	
	Maximum	22.70	30.50	
	Mean ± SD	15.27 ± 4.79	15.67 ± 8.37	
Contrast-noise ratio (CNR)	N(*)	9(5*)	9(5*)	0.509 (no sig.)
	Minimum	5.60	6.30	
	Maximum	22.10	23.70	
	Mean ± SD	14.39 ± 5.35	16.30 ± 6.54	
Overall image quality	N(*)	5(9*)	5(9*)	0.711 (no sig.)
	Minimum	62.20	87.75	
	Maximum	34.40	89.80	
	Mean ± SD	71.79 ± 12.29	67.31 ± 22.96	
Coronary segment analysis	N(*)	8(6*)	8(6*)	0.196 (no sig.)
	Minimum	91.70	92.50	
	Maximum	98.60	99.90	
	Mean ± SD	95.43 ± 2.57	97.19 ± 2.62	

FBP, Filtered back projection; IR, Iterative reconstruction; (\*), no. of studies did not provide values.

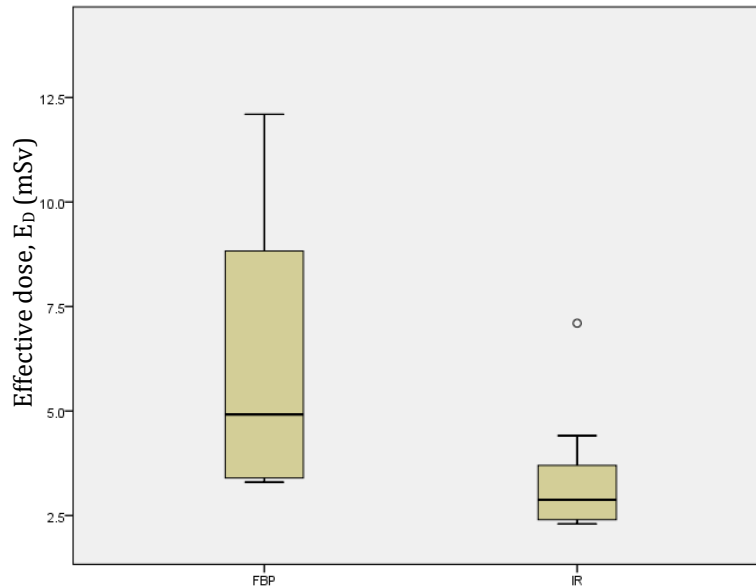


Figure 2.2: The boxplot shows the comparison of effective dose between FBP and IR.

### 2.2.5 Discussion

This systematic review presented an evaluation of the radiation dose reduction in CCTA achieved using IR algorithm in comparison to FBP. It also evaluated the impact on diagnostic image quality with relation to CAD based on the currently available literature.

Despite the development of many dose reduction strategies for CCTA, little attention has been given to IR algorithm, since studies have mainly focused on data acquisition rather than image reconstruction. This review showed that IR algorithm permits the use of lower exposure factors which provides a reduction in patient radiation dose by reducing the image noise during image reconstruction. Many types of IR algorithm have been introduced by CT vendors; these may lead to changes in radiation dose and diagnostic image quality. The results of our analysis showed that all types of IR algorithms significantly reduce radiation dose with no significant difference in diagnostic image quality between FBP and IR algorithm.



This review analysis also revealed that reported radiation dose reduction using IR algorithm varied widely across included studies. This can be described by looking at the radiation dose indicators used in the analysis such as  $CTDI_{vol}$ , DLP, and  $E_D$ . These indicators showed that most selected studies had a wider range than in the current literature. For example, the DLP range across selected studies is from 164 to 504 mGy.cm (varied by a factor of 3.1) while in the current literature is from 129 to 337 mGy.cm (varied by a factor of 2.6) [18]. This indicates that although IR algorithm has significantly reduced radiation dose, there exists a wide range of reported dose reductions. Thus, IR algorithm used in combination with other dose-saving strategies to further reduce radiation dose could be achieved.

Three identified studies have demonstrated that IR algorithm associated with other radiation dose-saving techniques, such as low tube voltage technique and prospective ECG-gating can achieve a 25–76% radiation dose reduction in CCTA [37-39]. These results were consistent with our analysis of different types of IR algorithm reported have also been combined with other dose-saving techniques. Our analysis showed that in five studies comparing 100 and 120 kVp protocols, a reduction in radiation dose from 27% to 50% while maintaining diagnostic image quality was achieved. The effective dose of lower than five mSv was reported in 80% of the studies performed with prospective ECG-gating which is comparable to a 4.7 mSv mean effective dose reported by other previous studies [40].

All studies included in this review used either quantitative or qualitative (or both) diagnostic image quality assessment. No studies had shown any statistical difference between the FBP and IR algorithm. This indicates that although the tube current was decreased, as a result of using IR algorithm, the diagnostic image quality never dropped

below the acceptable range and was similar to the FBP. However, diagnostic image quality indicators used (image noise, SNR, CNR, overall image quality and coronary segment analysis) in this review analysis may not determine the potential of radiation dose reduction. Diagnostic image quality may still deteriorate regarding spatial resolution and artefacts [41]. Therefore, both should also be included as important end-points of IR algorithm performance particularly for assessment of diagnostic accuracy in CAD.

There were some limitations with this review. Firstly, the diagnostic efficacy of detecting CAD at lower doses was not evaluated. Consequently, the results of data analysis should be used to provide an overview of the radiation dose reduction reported by literature, not the impact on diagnosis. However, it is complicated to investigate diagnostic efficacy as this can be influenced by different types of CT scanners and other radiation dose reduction strategies. Another limitation is the lack of comparison between low-dose FBP-only, routine FBP-only and low-dose IR algorithm. Naturally, the image noise would increase with low dose FBP-only, but this might not have a significant impact on diagnostic image quality for CCTA.

In summary, this review demonstrates that using IR algorithm with CCTA leads to a significant reduction of radiation dose compared to FBP. The diagnostic image quality of IR algorithm at a reduced dose (30–41%) is comparable to FBP at standard dose in the diagnosis of CAD.

## 2.2.6 References

- [1] F. G. Meinel, R. R. Bayer, 2nd, P. L. Zwerner, C. N. De Cecco, U. J. Schoepf, and F. Bamberg, "Coronary computed tomographic angiography in clinical practice: state of the art," *Radiol Clin North Am*, vol. 53, no. 2, pp. 287-96, Mar 2015.
- [2] M. Task Force *et al.*, "2013 ESC guidelines on the management of stable coronary artery disease: the Task Force on the management of stable coronary artery disease of the European Society of Cardiology," *Eur Heart J*, vol. 34, no. 38, pp. 2949-3003, Oct 2013.
- [3] M. C. Williams *et al.*, "Iterative reconstruction and individualized automatic tube current selection reduce radiation dose while maintaining image quality in 320-multidetector computed tomography coronary angiography," *Clin Radiol*, vol. 68, no. 11, pp. e570-7, Nov 2013.
- [4] Z. Sun, G. H. Choo, and K. H. Ng, "Coronary CT angiography: Current status and continuing challenges," *British Journal of Radiology*, vol. 85, no. 1013, pp. 495-510, 2012.
- [5] T. Klink, V. Obmann, J. Heverhagen, A. Stork, G. Adam, and P. Begemann, "Reducing CT radiation dose with iterative reconstruction algorithms: the influence of scan and reconstruction parameters on image quality and CTDIvol," *Eur J Radiol*, vol. 83, no. 9, pp. 1645-54, Sep 2014.
- [6] J. Shen *et al.*, "Noise-based tube current reduction method with iterative reconstruction for reduction of radiation exposure in coronary CT angiography," *Eur J Radiol*, vol. 82, no. 2, pp. 349-55, Feb 2013.

- [7] D. Fleischmann and F. E. Boas, "Computed tomography--old ideas and new technology," *Eur Radiol*, vol. 21, no. 3, pp. 510-7, Mar 2011.
- [8] X. Pan, E. Y. Sidky, and M. Vannier, "Why do commercial CT scanners still employ traditional, filtered back-projection for image reconstruction?," *Inverse Problems*, vol. 25, no. 12, 2009.
- [9] Y. Funama *et al.*, "Combination of a low-tube-voltage technique with hybrid iterative reconstruction (iDose) algorithm at coronary computed tomographic angiography," *J Comput Assist Tomogr*, vol. 35, no. 4, pp. 480-5, Jul-Aug 2011.
- [10] A. Gervaise *et al.*, "CT image quality improvement using Adaptive Iterative Dose Reduction with wide-volume acquisition on 320-detector CT," *Eur Radiol*, vol. 22, no. 2, pp. 295-301, Feb 2012.
- [11] M. Beister, D. Kolditz, and W. A. Kalender, "Iterative reconstruction methods in X-ray CT," *Phys Med*, vol. 28, no. 2, pp. 94-108, Apr 2012.
- [12] M. J. Willeminck *et al.*, "Iterative reconstruction techniques for computed tomography Part 1: technical principles," *Eur Radiol*, vol. 23, no. 6, pp. 1623-31, Jun 2013.
- [13] C. Naoum, P. Blanke, and J. Leipsic, "Iterative reconstruction in cardiac CT," *J Cardiovasc Comput Tomogr*, vol. 9, no. 4, pp. 255-63, Jul-Aug 2015.
- [14] D. Moher, A. Liberati, J. Tetzlaff, and D. G. Altman, "Preferred reporting items for systematic reviews and meta-analyses: The PRISMA statement," *British Medical Journal*, vol. 339, 2009.
- [15] J. Leipsic, B. G. Heilbron, and C. Hague, "Iterative reconstruction for coronary CT angiography: finding its way," *Int J Cardiovasc Imaging*, vol. 28, no. 3, pp. 613-20, Mar 2012.

- [16] M. National Collaborating Centre for and Tools, "Defining your question: PICO and PS," ed, 2012, pp. 1-3.
- [17] M. National Collaborating Centre for and Tools, "Quality assessment tool for quantitative studies," ed, 2010, pp. Hamilton, ON: McMaster University-Hamilton, ON: McMaster University.
- [18] Z. Sun, "Coronary CT angiography with prospective ECG-triggering: An effective alternative to invasive coronary angiography," *Cardiovascular Diagnosis and Therapy*, vol. 2, no. 1, pp. 28-37, 2012.
- [19] A. Sabarudin and Z. Sun, "Radiation dose measurements in coronary CT angiography," *World Journal of Cardiology*, vol. 5, no. 12, pp. 459-464, 2013.
- [20] J. Hausleiter *et al.*, "Estimated radiation dose associated with cardiac CT angiography," *Journal of the American Medical Association*, vol. 301, pp. 500-507, 2009.
- [21] W. G. Austen, "A reporting system on patients evaluated for coronary artery disease," *Circulation*, vol. 51, pp. 5-40, 1975.
- [22] A. Moscariello *et al.*, "Coronary CT angiography: image quality, diagnostic accuracy, and potential for radiation dose reduction using a novel iterative image reconstruction technique-comparison with traditional filtered back projection," *Eur Radiol*, vol. 21, no. 10, pp. 2130-8, Oct 2011.
- [23] J. Leipsic *et al.*, "Estimated radiation dose reduction using adaptive statistical iterative reconstruction in coronary CT angiography: the ERASIR study," *AJR Am J Roentgenol*, vol. 195, no. 3, pp. 655-60, Sep 2010.

- [24] O. Tumur, K. Soon, F. Brown, and M. Mykytowycz, "New scanning technique using Adaptive Statistical Iterative Reconstruction (ASIR) significantly reduced the radiation dose of cardiac CT," *J Med Imaging Radiat Oncol*, vol. 57, no. 3, pp. 292-6, Jun 2013.
- [25] R. Wang *et al.*, "Image quality and radiation dose of low dose coronary CT angiography in obese patients: sinogram affirmed iterative reconstruction versus filtered back projection," *Eur J Radiol*, vol. 81, no. 11, pp. 3141-5, Nov 2012.
- [26] J. Shen *et al.*, "Prospective ECG-triggered coronary CT angiography: clinical value of noise-based tube current reduction method with iterative reconstruction," *PLoS One*, vol. 8, no. 5, p. e65025, 2013.
- [27] W. H. Yin *et al.*, "Effect of reduced x-ray tube voltage, low iodine concentration contrast medium, and sinogram-affirmed iterative reconstruction on image quality and radiation dose at coronary CT angiography: results of the prospective multicenter REALISE trial," *J Cardiovasc Comput Tomogr*, vol. 9, no. 3, pp. 215-24, May-Jun 2015.
- [28] E. A. Park *et al.*, "Iterative reconstruction of dual-source coronary CT angiography: assessment of image quality and radiation dose," *Int J Cardiovasc Imaging*, vol. 28, no. 7, pp. 1775-86, Oct 2012.
- [29] M. Renker *et al.*, "Iterative image reconstruction techniques: Applications for cardiac CT," *J Cardiovasc Comput Tomogr*, vol. 5, no. 4, pp. 225-30, Jul-Aug 2011.
- [30] E. Di Cesare *et al.*, "Assessment of dose exposure and image quality in coronary angiography performed by 640-slice CT: a comparison between adaptive iterative

- and filtered back-projection algorithm by propensity analysis," *Radiol Med*, vol. 119, no. 8, pp. 642-9, Aug 2014.
- [31] N. Tomizawa, T. Nojo, M. Akahane, R. Torigoe, S. Kiryu, and K. Ohtomo, "AdaptiveIterative Dose Reduction in coronary CT angiography using 320-row CT: assessment of radiation dose reduction and image quality," *J Cardiovasc Comput Tomogr*, vol. 6, no. 5, pp. 318-24, Sep-Oct 2012.
- [32] P. Carrascosa, G. A. Rodriguez-Granillo, C. Capunay, and A. Deviggiano, "Low-dose CT coronary angiography using iterative reconstruction with a 256-slice CT scanner," *World J Cardiol*, vol. 5, no. 10, pp. 382-6, Oct 26 2013.
- [33] Y. Hou, X. Liu, S. Xv, W. Guo, and Q. Guo, "Comparisons of image quality and radiation dose between iterative reconstruction and filtered back projection reconstruction algorithms in 256-MDCT coronary angiography," *AJR Am J Roentgenol*, vol. 199, no. 3, pp. 588-94, Sep 2012.
- [34] S. D. Kordolaimi *et al.*, "Effect of iDose4 iterative reconstruction algorithm on image quality and radiation exposure in prospective and retrospective electrocardiographically gated coronary computed tomographic angiography," *Journal of computer assisted tomography*, vol. 38, no. 6, pp. 1-7, 2014.
- [35] S. D. Kordolaimi *et al.*, "Radiation dose and image noise evaluation in coronary computed tomography angiography (CCTA) using an iterative reconstruction algorithm," (in English), *Hellenic Journal of Cardiology*, vol. 55, no. 3, pp. 184-90, 2014.

- [36] F. Tatsugami *et al.*, "The effect of adaptive iterative dose reduction on image quality in 320-detector row CT coronary angiography," *British Journal of Radiology*, vol. 85, no. 1016, pp. e378-e382, 2012.
- [37] Y. Hou, J. Zheng, Y. Wang, M. Yu, M. Vembar, and Q. Guo, "Optimizing radiation dose levels in prospectively electrocardiogram-triggered coronary computed tomography angiography using iterative reconstruction techniques: a phantom and patient study," *PLoS One*, vol. 8, no. 2, p. e56295, 2013.
- [38] T. Nakaura *et al.*, "Low contrast- and low radiation dose protocol for cardiac CT of thin adults at 256-row CT: usefulness of low tube voltage scans and the hybrid iterative reconstruction algorithm," *Int J Cardiovasc Imaging*, vol. 29, no. 4, pp. 913-23, Apr 2013.
- [39] S. Oda, G. Weissman, M. Vembar, and W. G. Weigold, "Iterative model reconstruction: improved image quality of low-tube-voltage prospective ECG-gated coronary CT angiography images at 256-slice CT," *Eur J Radiol*, vol. 83, no. 8, pp. 1408-15, Aug 2014.
- [40] C. Hlaiheli *et al.*, "Dose and image quality comparison between prospectively gated axial and retrospectively gated helical coronary CT angiography," *Br J Radiol*, vol. 84, no. 997, pp. 51-7, Jan 2011.
- [41] K. D. Toennies, "Digital Image Acquisition," in *Guide to Medical Image Analysis*, 2012, pp. 21-82.



# **CHAPTER 3 Development of a novel 3D-printed cardiac insert phantom for investigations in coronary CT angiography**

Part of this chapter has been published by the *Journal of Medical Radiation Sciences* (2018)

1-9, doi: 10.1002/jmrs.279.

### **3.1 Bridging section**

This section aims to highlight the need to develop a novel design of 3D-printed cardiac insert phantom derived from volumetric CT image datasets of an anthropomorphic chest phantom for the investigations of CCTA protocols.

#### **3.1.1 Background**

Imaging phantoms are tools that can be used to optimise CT protocols without exposing the patients or animals to unnecessary radiation risk [1]. These phantoms are inert objects that can be scanned repeatedly. They can be used for calibration, research and teaching but usually, they are used to investigate various scanning parameter combinations [2, 3]. For CCTA studies, the Catphan<sup>®</sup> (The Phantom Laboratory, Salem, NY) [4-6] and American College of Radiology (ACR) [7, 8] phantoms have been commonly used for dose optimisation investigations. These phantoms are constructed of separate modules that allow an image quality assessment for specific criteria (see Figure 3.1). However, they are a symmetrical shape and not similar to the human habitus or physical anatomy. Geometric factors, such as patient size, shape, and subject contrast, can influence the image quality assessment especially during dose optimisation studies [9, 10]. Therefore, phantoms that are similar to the human body with associated organs are preferred to ensure accurate and comparable results.

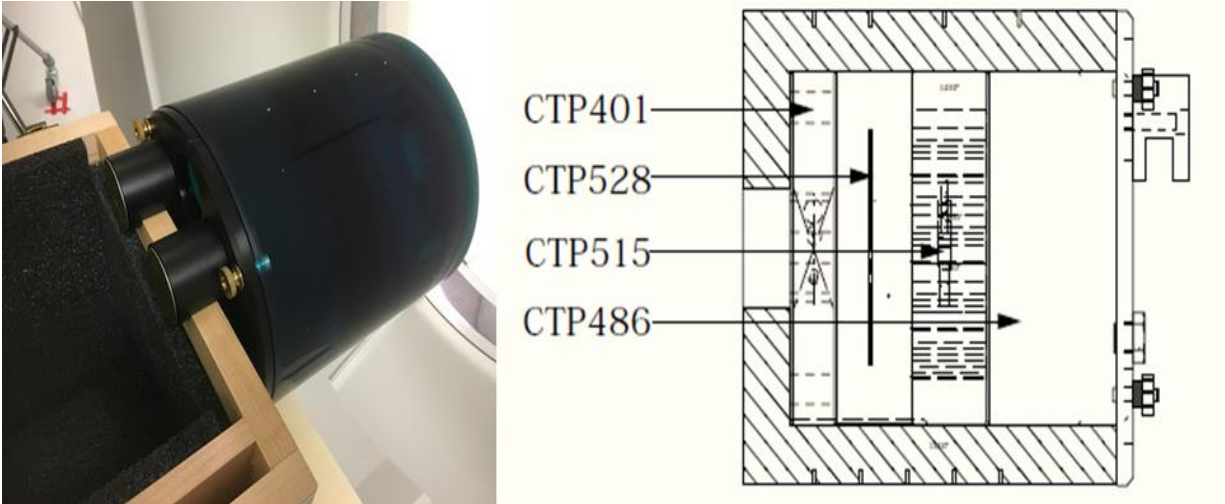


Figure 3.1 An example of physical phantoms is the Catphan® 500 (The Phantom Laboratory, Salem, NY). This phantom is widely used for testing the performance of CT scanners. The phantom consists of five modules to assess the image quality; (i) CTP401 for slice width, sensitometry and pixel size, (ii) CTP528 for line pair and point source spatial resolution, (iv) CTP515 for sub slice and supra slice low contrast and (v) CTP486 for image uniformity [11].

Anthropomorphic phantoms are also widely used in many CT dose optimisation studies [12-14]. The anthropomorphic phantoms are designed to closely resemble the patient body size, anatomy features and photon absorption. The Lungman phantom, by Kyoto Kagaku company [15], for example, has been designed to resemble chest region of normal adult patient with various body equivalent materials such as bones, lungs, muscles, and soft tissue (see Figure 3.2). The provided cardiac insert phantom is constructed from a single homogenous single material which lacks sufficient anatomical structures for CCTA image quality assessment, e.g. the contrast-enhanced regions of main arteries and other small vessels. The internal structures of the phantom, such as heart and lungs, are removable and can be replaced by other phantom inserts. Therefore, modifications of the cardiac insert design for CCTA dose optimisation studies are desirable.

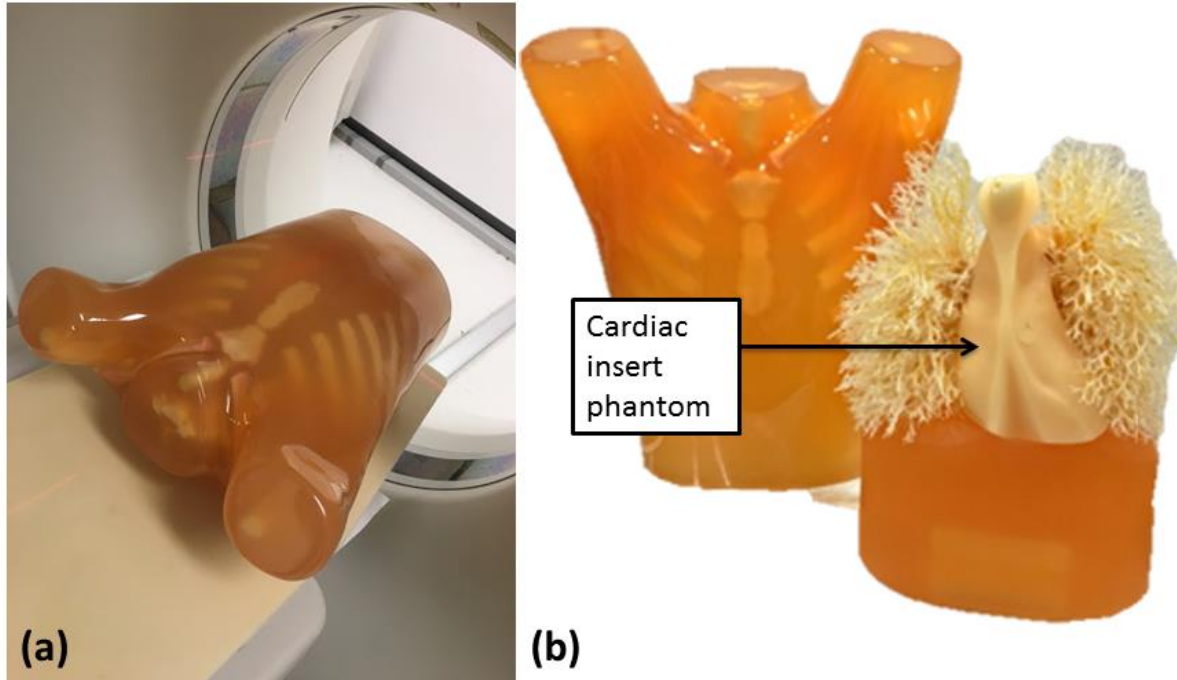


Figure 3.2 (a) The Lungman anthropomorphic chest phantom by Kyoto Kagaku co., Japan is placed on the CT table. (b) The removable cardiac (arrow) and lung structures contained within the Lungman phantom.

The cardiac insert phantom of the Lungman phantom has been used in many previous and recent investigations [16-18]. The shape and attenuation features of the Lungman phantom ensure realistic conditions during scanning the patient's body. Developing a new CCTA cardiac insert for the Lungman phantom requires technology that can duplicate the original heart size and shape so that it can be accurately positioned into the chest cavity. Consequently, 3D printing technology has been applied. This 3D printing technology is a promising technique used to rapidly fabricate a high quality and cost-effective physical models [19, 20]. In the recent years, the use of 3D printing technology has rapidly grown in medicine [21]. This technology has been used to produce various anatomical models such as personalised artificial parts, implants, medical devices, organ-specific models, and bioprinting tissues [20, 22-26]. However, the role of 3D printing

technology in developing CT phantoms in dose optimisation studies is relatively new and not well-explored. Consequently, this 3D printing technology was used in this study to produce a new cardiac insert for the Lungman phantom for performing the CCTA dose optimisation studies.

A new 3D-printed cardiac insert phantom was designed with the same shape and size as the original Lungman cardiac insert and contained different attenuating materials relevant for CCTA image quality assessment. The new 3D printed cardiac insert was positioned into the Lungman phantom and scanned using a standard CCTA protocols. The resultant images were compared to the patient and Catphan® 500 phantom images. HU values of the attenuating materials within the new 3D-printed cardiac insert phantom were comparable to tissues in the patient image datasets and materials in the Catphan® 500 phantom.

### 3.1.2 References

- [1] M. F. Bieniosek, B. J. Lee, and C. S. Levin, "Technical Note: Characterization of custom 3D printed multimodality imaging phantoms," *Med Phys*, vol. 42, no. 10, pp. 5913-8, Oct 2015.
- [2] J. Solomon and E. Samei, "Quantum noise properties of CT images with anatomical textured backgrounds across reconstruction algorithms: FBP and SAFIRE," *Med Phys*, vol. 41, no. 9, p. 091908, Sep 2014.
- [3] M. Zankl *et al.*, "The construction of computer tomographic phantoms and their application in radiology and radiation protection," *Radiation and environmental Biophysics*, vol. 27, no. 2, pp. 153-164, 1988.

- [4] M. L. Aurumskjold, K. Ydstrom, A. Tingberg, and M. Soderberg, "Improvements to image quality using hybrid and model-based iterative reconstructions: a phantom study," *Acta Radiol*, vol. 58, no. 1, pp. 53-61, Jan 2017.
- [5] T. Flohr, K. Stierstorfer, R. Raupach, S. Ulzheimer, and H. Bruder, "Performance evaluation of a 64-slice CT system with z-flying focal spot," *RöFo*, vol. 176, no. 12, pp. 1803-1810, 2004.
- [6] T. Klink, V. Obmann, J. Heverhagen, A. Stork, G. Adam, and P. Begemann, "Reducing CT radiation dose with iterative reconstruction algorithms: the influence of scan and reconstruction parameters on image quality and CTDIvol," *Eur J Radiol*, vol. 83, no. 9, pp. 1645-54, Sep 2014.
- [7] B. Chen *et al.*, "An anthropomorphic breast model for breast imaging simulation and optimization," *Acad Radiol*, vol. 18, no. 5, pp. 536-46, May 2011.
- [8] A. K. Hara, R. G. Paden, A. C. Silva, J. L. Kujak, H. J. Lawder, and W. Pavlicek, "Iterative reconstruction technique for reducing body radiation dose at CT: feasibility study," *AJR Am J Roentgenol*, vol. 193, no. 3, pp. 764-71, Sep 2009.
- [9] M. J. Siegel, B. Schmidt, D. Bradley, C. Suess, and C. Hildebolt, "Radiation dose and image quality in pediatric CT: effect of technical factors and phantom size and shape," *Radiology*, vol. 233, no. 2, pp. 515-522, 2004.
- [10] W. A. Kalender, P. Deak, M. Kellermeier, M. van Straten, and S. V. Vollmar, "Application-and patient size-dependent optimization of x-ray spectra for CT," *Medical physics*, vol. 36, no. 3, pp. 993-1007, 2009.
- [11] T. P. Laboratory, "Catphan 500 and 600 manual " *The Phantom Laboratory*, 2006.

- [12] J. Vassileva, "A phantom for dose-image quality optimization in chest radiography," *The British journal of radiology*, vol. 75, no. 898, pp. 837-842, 2002.
- [13] D. Pina, S. Duarte, T. G. Netto, C. Trad, M. Brochi, and S. de Oliveira, "Optimization of standard patient radiographic images for chest, skull and pelvis exams in conventional x-ray equipment," *Physics in Medicine & Biology*, vol. 49, no. 14, p. N215, 2004.
- [14] W. Ma *et al.*, "Anthropomorphic chest phantom imaging—the potential for dose creep in computed radiography," *Radiography*, vol. 19, no. 3, pp. 207-211, 2013.
- [15] M. Jadidi, A. Sundin, P. Aspelin, M. Båth, and S. Nyrén, "Evaluation of a new system for chest tomosynthesis: aspects of image quality of different protocols determined using an anthropomorphic phantom," *The British journal of radiology*, vol. 88, no. 1053, p. 20150057, 2015.
- [16] S. R. Pérez, N. W. Marshall, L. Struelens, and H. Bosmans, "Characterization and validation of the thorax phantom Lungman for dose assessment in chest radiography optimization studies," *Journal of Medical Imaging*, vol. 5, no. 1, p. 013504, 2018.
- [17] J. D. Thompson *et al.*, "A phantom-based JAFROC observer study of two CT reconstruction methods: the search for optimisation of lesion detection and effective dose," in *Medical Imaging 2015: Image Perception, Observer Performance, and Technology Assessment*, 2015, vol. 9416, p. 94160B: International Society for Optics and Photonics.
- [18] Y. Ohno *et al.*, "Comparative evaluation of newly developed model-based and commercially available hybrid-type iterative reconstruction methods and filter back

- projection method in terms of accuracy of computer-aided volumetry (CADv) for low-dose CT protocols in phantom study," *European journal of radiology*, vol. 85, no. 8, pp. 1375-1382, 2016.
- [19] R. Bogue, "3D printing: the dawn of a new era in manufacturing?," *Assembly Automation*, vol. 33, no. 4, pp. 307-311, 2013.
- [20] A. A. Giannopoulos, D. Mitsouras, S. J. Yoo, P. P. Liu, Y. S. Chatzizisis, and F. J. Rybicki, "Applications of 3D printing in cardiovascular diseases," *Nat Rev Cardiol*, vol. 13, no. 12, pp. 701-718, Dec 2016.
- [21] G. B. Kim *et al.*, "Three-Dimensional Printing: Basic Principles and Applications in Medicine and Radiology," *Korean J Radiol*, vol. 17, no. 2, pp. 182-97, Mar-Apr 2016.
- [22] F. Adams *et al.*, "Soft 3D-Printed Phantom of the Human Kidney with Collecting System," *Ann Biomed Eng*, vol. 45, no. 4, pp. 963-972, Apr 2017.
- [23] L. C. Ebert, M. J. Thali, and S. Ross, "Getting in touch--3D printing in forensic imaging," *Forensic Sci Int*, vol. 211, no. 1-3, pp. e1-6, Sep 10 2011.
- [24] S. Leng *et al.*, "Anatomic modeling using 3D printing: quality assurance and optimization," *3D Printing in Medicine*, vol. 3, no. 1, 2017.
- [25] M. H. Michalski, J. S. Ross, and M. Practice, "The shape of things to come: 3D printing in medicine," *American Medical Association*, vol. 312, no. 21, pp. 2213-2214, 2014.
- [26] M. Vukicevic, B. Mosadegh, J. K. Min, and S. H. Little, "Cardiac 3D Printing and its Future Directions," *JACC Cardiovasc Imaging*, vol. 10, no. 2, pp. 171-184, Feb 2017.



## 3.2 Manuscript

This section is written in a manuscript version as submitted to the *Journal of Medical Radiation Sciences*, (2018) 1-9, doi: 10.1002/jmrs.279.

**Title:** Development of a novel 3D-printed cardiac insert phantom for investigations in coronary CT angiography protocols

**Authors:** Kamarul Amin Abdullah<sup>1,2</sup>, Mark F McEntee<sup>1</sup>, Warren Reed<sup>1</sup>, Peter L Kench<sup>1</sup>

**Affiliations:** 1. Discipline of Medical Radiation Sciences, Faculty of Health Sciences, The University of Sydney, New South Wales, Australia.

2. Centre of Medical Imaging, Faculty of Health Sciences, Universiti Sultan Zainal Abidin, Terengganu, Malaysia.

### 3.2.1 Abstract

**Introduction:** An ideal organ-specific insert phantom should be able to simulate the anatomical features with appropriate appearances in the resultant CT images. This study investigated a 3D printing technology to develop a novel and cost-effective cardiac insert phantom derived from volumetric CT image datasets of anthropomorphic chest phantom.

**Methods:** Cardiac insert volumes were segmented from CT image datasets, derived from an anthropomorphic chest phantom of Lungman N-01 (Kyoto Kagaku, Japan). These segmented datasets were converted to a virtual 3D-isosurface of heart-shaped shell, while two other removable inserts were included using computer-aided design (CAD) software program. This newly designed cardiac insert phantom was later printed by using a fused

deposition modelling (FDM) process via a Creatbot DM Plus 3D printer. Then, several selected filling materials, such as contrast media, oil, water and jelly, were loaded into designated spaces in the 3D-printed phantom. The 3D-printed cardiac insert phantom was positioned within the anthropomorphic chest phantom and thirty repeated CT acquisitions performed using a multi-detector scanner at 120-kVp tube potential. Attenuation (Hounsfield Unit, HU) values were measured and compared to the image datasets of real-patient and Catphan® 500 phantom.

**Results:** The output of the 3D-printed cardiac insert phantom was a solid acrylic plastic material, which was strong, light in weight, and cost-effective. HU values of the filling materials were comparable to the image datasets of real-patient and Catphan® 500 phantom.

**Conclusions:** A novel and cost-effective cardiac insert phantom for anthropomorphic chest phantom was developed using volumetric CT image datasets with a 3D printer. Hence, this suggested the printing methodology could be applied to generate other phantoms for CT imaging studies.

**Key words:** 3D printing, cardiac insert phantom, rapid prototyping, computed tomography, computer aided design (CAD)

### 3.2.2 Introduction

Over the past few years, there has been increased use of 3D printing technology for rapid prototyping of high quality printed objects [1]. Since its introduction, 3D printing technology has been successfully applied in numerous areas, such as engineering, industry, art, education, and medicine [2, 3]. In medicine, 3D printing technology has been used for a

variety of purposes, e.g. assisting surgical planning [4], guiding interventional procedures [5], manufacturing radiology components [6], printing personalised artificial parts [7], and recently, developing phantoms [8-11].

Phantoms have been widely applied in medical imaging, especially in CT systems, commonly for both quantitative and qualitative assessments of image quality. Many prior studies [12-14] have highlighted the advantages of using phantoms, especially when the investigations involve multiple radiation exposures with different acquisitions settings. One of the most common phantoms used for the investigations of CT protocols is the anthropomorphic chest phantom (Lungman N-01, Kyoto Kagaku, Japan). This phantom has properties that are very similar to the anatomical features of an adult chest region, e.g. the lungs, bones, and muscles. However, the cardiac insert of this phantom has single, homogenous material that is not appropriate to simulate CT images, especially for cardiac CT. An ideal cardiac insert should be able at least to simulate the heart features with appropriate appearances in the resultant CT images.

Recently, many recent phantom studies [8-11, 15, 16] have employed the 3D printing technology to construct their phantoms. For example, Solomon et al., [16] asserted that this technology could be applied to generate anthropomorphic texture phantoms that are feasible to assess the quality of CT images. Another was by Leng et al., [15] which used 3D printing technology to generate a comprehensive quality assurance phantom. However, the major drivers are the limitations of available commercial phantoms which are often costly and not customisable. This 3D printing technology allows researchers to design and construct physical phantoms and organ inserts based on their preferences at a lower cost than any commercially available physical phantoms. Additionally, the successful and

validated 3D-printed physical phantoms can be reproduced by any other accessible 3D printers.

Therefore, it is indeed possible to fabricate 3D-printed phantoms with specific characteristics to suit various imaging investigations, particularly in CT systems. In this study, the investigation of 3D printing technology offers an alternative to produce a novel and cost-effective cardiac insert phantom containing a contrast-enhanced region directly from volumetric CT image datasets of anthropomorphic chest phantom. The printing methodology used in this study could be generally applied to generate other phantoms for CT imaging studies.

### **3.3.3 Materials and Methods**

The following three steps were taken to develop the new cardiac insert phantom:-

1. **Step one** involved obtaining acquisitions of volumetric datasets from a multi-detector CT scanner.
2. **Step two** involved delineating the regions of interest (ROI) from the surrounding structures, which resulted in segmented image datasets. This step also included the optimization procedure, such as smoothing and wrapping.
3. **Step three** involved printing the new physical phantom and removing unnecessary supporting structures so as to produce a final clean physical 3D-printed cardiac insert phantom.

The phantom was printed using a 3D printer of Creatbot DM Plus Model (Mankati, Shanghai, China). This 3D printer uses a fused deposition modelling (FDM) technique to develop the phantom. This FDM technique is similar to inkjet printing but a filament is used

instead of ink. *Acrylonitrile butadiene styrene* (ABS) filament passes through a moving heated extruder to print ~0.25 mm layer of material onto the build tray. Next, a cooling fan solidifies the ABS material creating a traced layer onto the tray. The process was then repeated for each layer until completed. Additional support materials were also printed on the layers to prevent the structures from collapsing.

The proceeding sections elaborate on the (a) designs of the 3D-printed cardiac insert phantom, (b) process of printing the physical models, (c) after-printing process, and (d) measurement of attenuation (HU) values.

### *3.3.3.1 Phantom design*

The 3D-printed cardiac insert phantom was made of two main assemblies, (i) the heart-shaped shell and (ii) the removable inserts:-

(i) The heart-shaped shell design was derived from the volumetric CT image datasets of an anthropomorphic chest phantom (Lungman N-01, Japan; see Figure 3.1 (a-b)). The cardiac insert was scanned on a multi-detector CT scanner (Alexion, Toshiba Medical Systems Co Ltd., Otowara, Japan) using a 120-kVp tube potential and a fixed 200 mA tube current. The reconstructed image datasets were transferred to a segmentation software program (3D Slicer, The Slicer Community, Harvard) [17] to delineate and outline structures from the carina to the apex of the heart phantom, see Figure 3.1 (c-d). Next, the segmented image datasets were exported to generate a virtual 3D-isosurface of the cardiac insert using Rhinoceros 3D (McNeel, Seattle, WA, USA) and Autodesk 123D Design (Autodesk Inc., San Rafael, CA, USA) software. To remove any defect, smoothing and surface rendering methods were performed on the 3D-surface mesh. The mesh of the cardiac insert

was then saved in a binary *stereolithography* (STL) file format before it was exported to the 3D printer for printing. The heart-shaped shell was designed to ensure it could be suitably positioned in the anthropomorphic chest phantom for CT scanning.

(ii) The removable inserts were designed to have similar structures as coronary arteries or ascending aorta (A) and ventricular anatomy (B) and fit within the heart-shaped shell. Insert A was designed with varying diameters of cylindrical structures in order to resemble the different sizes of contrast-enhanced regions of the coronary arteries and ascending aorta placed on both sides of the insert to represent the right and left sides of the heart. The diameters of the coronary arteries and the ascending aorta were set from 1.5 to 5.0 mm and 30 mm, respectively. A minimum diameter of 1.5 mm is the smallest diameter detectable as in accordance to the American Heart Association (AHA) Guidelines [18]. The dimensional size of these two removable inserts was further adjusted so that they fitted and could be suitably positioned in the heart-shaped shell. Figure 3.2 (a-c) shows the cross-sectional diagram and the virtual 3D-isosurface of the removable inserts A and B.

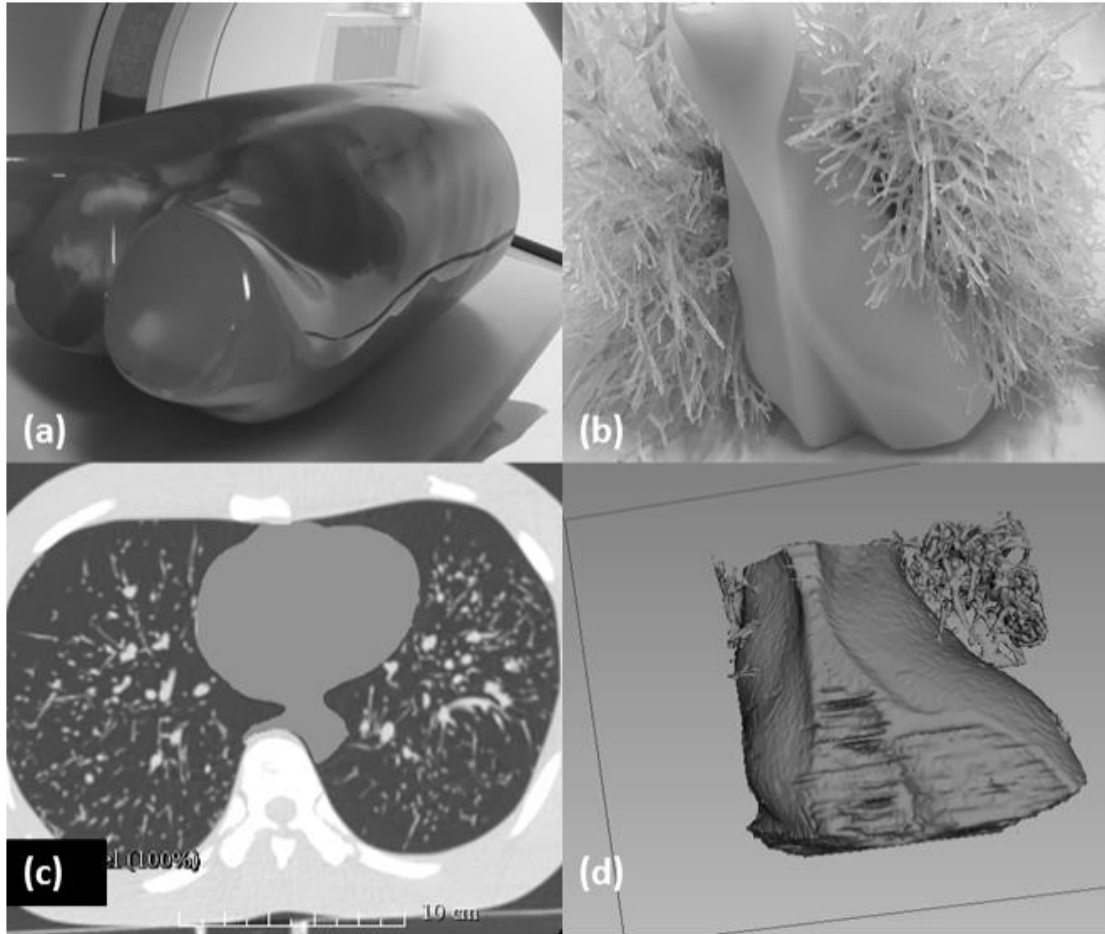


Figure 3.3: (a) An anthropomorphic chest phantom (Lungman N-01, Kyoto Kagaku, Co., Ltd., Kyoto, Japan). The anthropomorphic chest phantom was scanned on a multi-detector CT scanner in order to obtain the volumetric datasets of the original cardiac insert; (b) The original size and the appearance of the cardiac insert; (c) The segmentation process using 3D Slicer software program (The Slicer Community, Harvard) [17]. The cardiac insert was segmented to ensure that the modelling process could be performed to produce the heart-shaped shell; and (d) The virtual 3D model of the original cardiac insert.

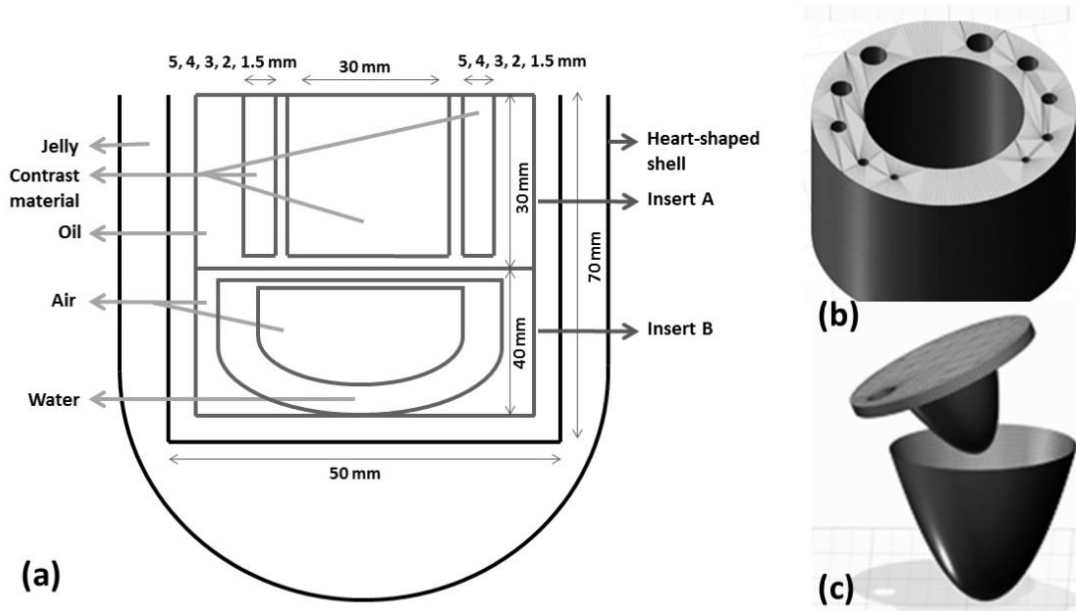


Figure 3.4: (a) A cross-sectional diagram of the new custom-made design of 3D-printed cardiac insert phantom. The measurements of each model were determined based on the adjustments made so that the model could fit the size of the heart-shaped shell perfectly, as well as to be suitably positioned in the anthropomorphic chest phantom. The modelling parts of the removable inserts within the heart-shaped shell are (b) removable insert A, and (c) removable insert B.

### 3.3.3.2 Printing process

Three printing tasks had been employed to facilitate the printing process, which were: (i) Insert A; (ii) Insert B; and (iii) Heart-shaped shell. Insert A was printed by segregating it into Parts I and II. Part I refers to the cylindrical structures, while Part II denotes the base layer (Figure 3.3a). Meanwhile, Insert B was divided into three parts (Parts I, II, and III). Part I refers to the top layer, while Part II denotes the ventricle-shape, and Part III reflects the outermost cylinder shape in which to insert both the removable inserts (Figure 3.3b). As for the heart-shaped shell, it was separated into Parts I and II, where Part I is for the shell where the removable inserts could be placed, whereas Part II is the top layer (Figure 3.3c). Such division of printing parts or assemblies allowed easy filling for the varied density materials, especially after the printing process. The printer settings



used during the 3D printing process were configured based on the Simplify3D (Ohio, USA) software program, as shown in Table 3.1.

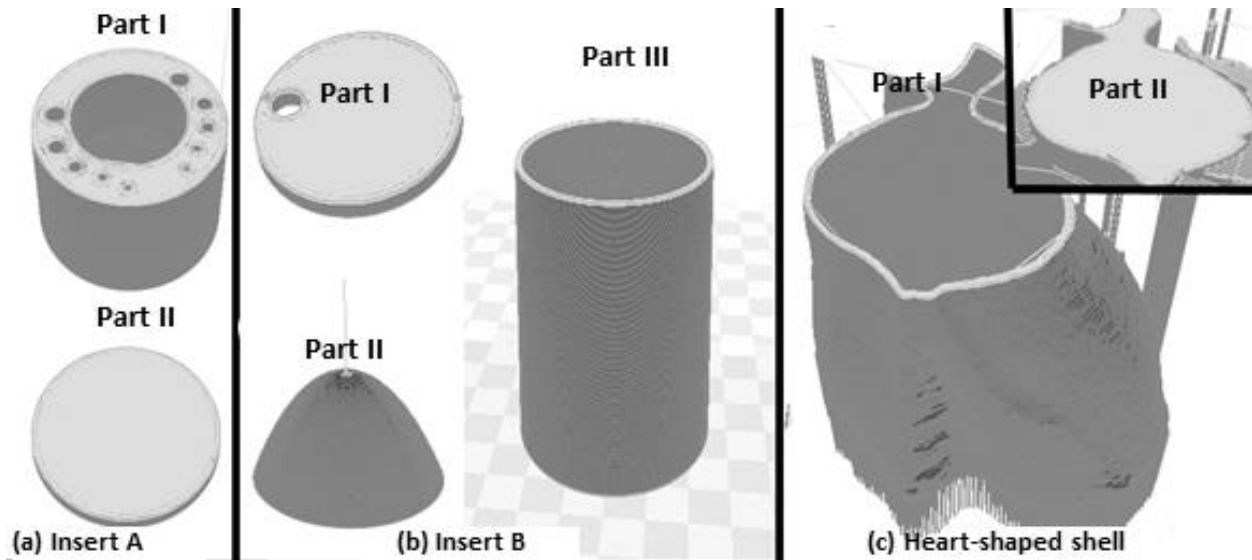


Figure 3.5: Three separate tasks were carried out to facilitate the printing tasks. (a) Insert A was divided into Parts I and II; (b) Insert B was separated into three parts (Parts I, II, and III); and (c) Heart-shaped shell was divided into Parts I and II. These separation tasks of printing parts eased the process of filling with varied density materials after the printing process.

Table 3.1: The 3D printer settings applied in this study. In achieving very fine details with several ranges of printing materials or 3D printer while avoiding gaps, leaking, and overlaps; varying results could be generated. NB These settings are only applicable if a printer similar to Creatbot DM Plus Model (Mankati, Shanghai, China) and a software program similar to Simplify3D (Ohio, USA) are employed to design and to construct the phantom.

<b>Settings</b>	<b>Selection</b>
i. Extruder	Nozzle diameter: 0.40 mm, Extrusion multiplier: 1.00,
Toolhead	Extrusion width: Auto, Retraction distance: 1.00 mm, Retraction speed: 1800.0 mm/min
ii. Layer	Primary layer height: 0.25 mm, Top/bottom solid layers: 5, Outline/perimeter shells: 5, Outline direction: Inside-out, First layer height: 90%, First layer width: 100%, First layer speed: 50%
iii. Additions: Raft	Raft layers: 1, Raft offset from part: 2.00 mm, Separation distance: 1.50 mm, Raft infill: 100%
iv. Infill	Internal fill pattern: Grid, External fill pattern: Concentric, Interior fill percentage: 10%, Outline overlap: 50%, Minimum infill length: 5.00 mm, Print sparse infill every: 1 layer, Infill angle offsets: 45/-45 degrees
v. Support: Generate support material	Support infill percentage: 25%, Dense support layers: 5 Dense infill percentage: 50%, Print support every layer Support type: Normal, Support pillar resolution: 4.00 mm

---

vi.	Temperature	Extruder: 240 degrees Celsius Heated Bed/Platform: 230 degrees Celsius
vii.	Cooling	Fan speed: 60%
viii.	G-code	Tick all boxes: 5D firmware, allow zeroing of extrusion distance, firmware supports “sticky” parameters, update machine definition (Cartesian robot), update firmware configuration (Rep/Rap)
ix.	Script	G28; home all axes
x.	Others	Default printing speed: 1800.0 mm/min, Outline under speed: 50%  Solid infill under speed: 80%, X/Y axis movement speed: 4800.0 mm/min  Z axis movement speed: 1000.0 mm/min  Filament diameter: 1.7500 mm

---

### 3.3.3.3 After-printing process

Additional support materials, e.g. rafts and pillars, were removed from the 3D-printed cardiac insert phantom. Next, the external surface of heart-shaped shell and removable inserts (Inserts A and B) was covered with *acrylonitrile butadiene styrene* (ABS) liquid to prevent leakage of the materials. This ABS liquid was produced by soaking the ABS filaments into acetone for approximately 30-45 minutes. All the removable inserts were

glued together after the process of filling the phantom with materials of different densities was completed. The heart-shaped shell that supported the two inserts was then filled with jelly to simulate the myocardium. Insert A was filled with oil, while the surrounding tube-like structures were filled with Ultravist-370 (Schering Health Care Ltd, Burgess Hill, UK) iodinated contrast media to resemble the contrast-enhanced vessels. The iodine concentration was adjusted to simulate cardiac CT imaging of coronary CT angiography at 100-120 kVp, 25-30 HU per milligram of iodine per millilitre [19]. Insert B was filled with water material and separately with air material, where the latter simulated the trachea.

#### *3.3.3.4 Attenuation properties*

The average attenuation (Hounsfield Unit, HU) values were measured to verify the properties of the phantom for cardiac CT imaging. All measurements were performed at the CT scanner workstation. The 3D-printed cardiac insert phantom was positioned in the anthropomorphic chest phantom and imaged thirty times with a multi-detector CT scanner (Alexion, Toshiba Medical Systems). The acquisitions of the phantom were performed at 120-kVp tube potential, scan FOV 250 mm and 0.75-second rotation time. The tube current was set at 200 mA and dose modulation was turned off. The projection image datasets were reconstructed by applying only FBP and FC18 reconstruction kernel with a 1.0-mm slice thickness and an axial FOV of 160-mm. The average attenuation values (Hounsfield Unit, HU) values were measured by placing the region of interest (ROI) over each material (contrast media, air, oil, and jelly) reconstructed axial images of the cardiac phantom, the relevant anatomy (ascending aorta, air, fat, and muscle) of patient image datasets and also the air and LDPE inserts of Catphan® 500 phantom (The Phantom Laboratory, Salem NY,

USA). Both patient and Catphan® 500 phantom datasets were scanned at similar acquisition protocols.

### 3.3.4 Results

The physical models and the axial CT images of the completed 3D-printed cardiac insert phantom are illustrated in Figure 3.4 and Figure 3.5, respectively. The total printing time was 12.1 hours and phantom preparation time, e.g. removing support materials, covering surfaces with *acrylonitrile butadiene styrene* (ABS) liquid, assembling all parts, and filling the phantom with materials was 10.2 hours. The cost of the phantom production was approximately US\$70, which covered the costs of the ABS filament and the internal materials used. However, the cost of the 3D printer was excluded due to institute ownership.

The mean attenuation values (HU) for circular ROI placed over varied materials within 3D-printed cardiac insert phantom, real-patient image datasets, and Catphan® 500 are tabulated in Table 3.2 for FBP image reconstruction algorithms. As a result, the measured values confirmed that the materials used in the 3D-printed cardiac insert phantom are comparable with those obtained from the real-patient image datasets and the standard CT image quality phantom Catphan® 500 phantom (Air and LDPE inserts).

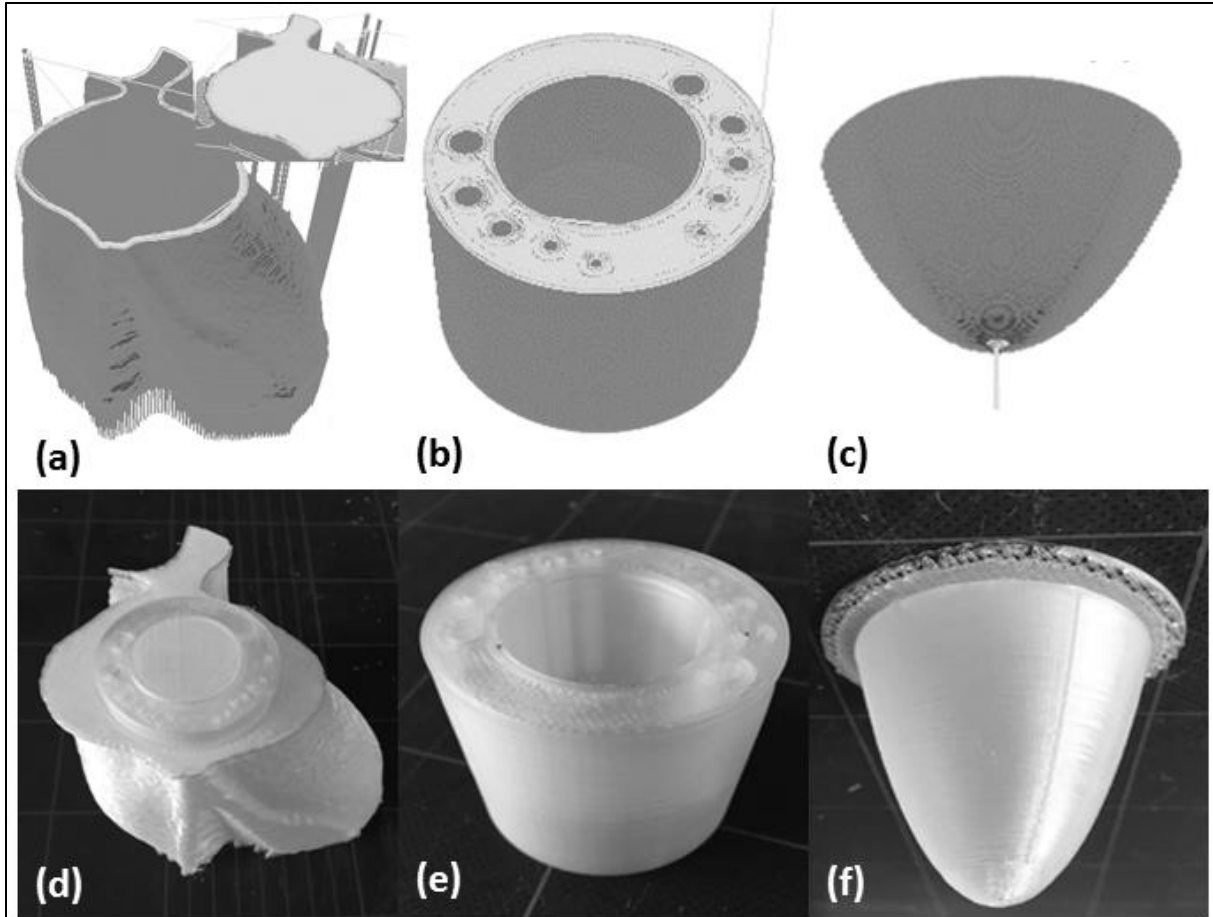


Figure 3.6: A 3D-printed cardiac insert phantom; heart-shaped shell, insert A, and insert B, before (a-c) and after the printing process (d-f), respectively.

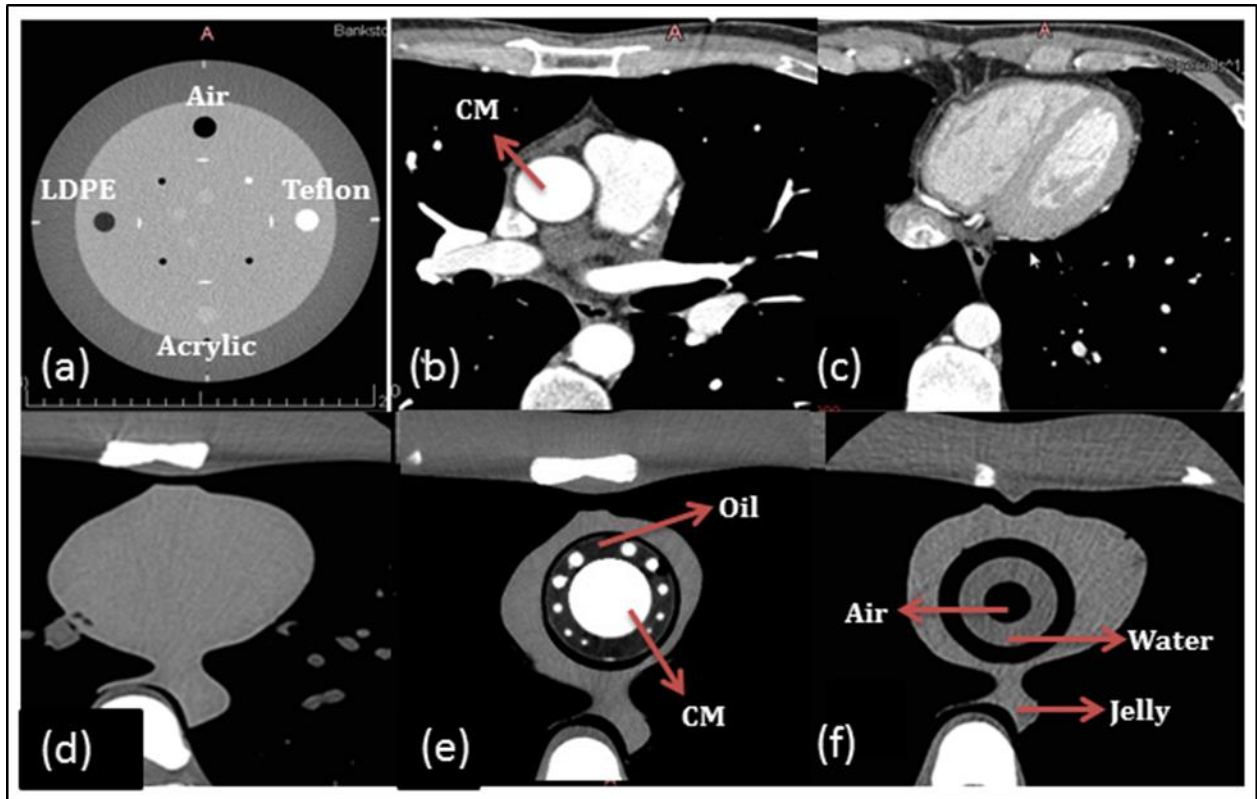


Figure 3.7: The resulting axial CT images of (a) four inserts in Catphan® 500 phantom; (b) and (c) patient image datasets for cardiac CT; (d) original cardiac insert of anthropomorphic chest phantom; (e-f) 3D-printed cardiac insert phantom with contrast materials (CM), oil, air, water and jelly segments labelled.

Table 3.2: Mean of attenuation values (HU) obtained with FBP (FC18) for the 3D-printed cardiac insert, as compared to the patient image datasets, and Catphan® 500 at 120 kVp.

<b>HU values</b>	<b>Contrast material</b>	<b>Air</b>	<b>Oil / Fat</b>	<b>Jelly / Muscle</b>
3D-printed cardiac insert	354.3	-894.1	-92.4	25.9
Patient image datasets	327.0	-847.5	-90.0	17.6
Catphan® 500	n/a	-968.9	-83.0	n/a

n/a: not available

### 3.3.5 Discussion

This paper presents a novel design of a 3D-printed cardiac insert phantom for an anthropomorphic chest phantom, including the associated 3D printing methodology. This phantom was comprised of a contrast-enhanced region to enable the investigation of the impact of various settings upon cardiac CT protocols. In a prior work [20], the use of this new cardiac insert phantom had been demonstrated to determine the impact of various image reconstruction algorithms on image quality and dose reduction potential. The results were consistent with past studies [21-23] as the image datasets reconstructed with iterative reconstruction algorithm exhibited more noise reduction, hence resulting in higher image quality, when compared to the FBP.

To ascertain image quality, researchers [24-27] measured image noise by placing the ROI within a specific anatomical contrast-enhanced region to ascertain image quality. For cardiac CT imaging of CCTA, the ROI is usually placed within the ascending aorta [24-26]. In clinical case, this anatomical region refers to the time-to-peak enhancement of the



contrast media, which has been often applied to test the adequacy of the contrast path, and therefore, overall contrast enhancement level as well as diagnostic image quality [28]. For the 3D-printed cardiac insert phantom, a cylindrical contrast-enhanced region was designed with similar diameter to the average ascending aorta (~30mm). The large size of this cylindrical contrast-enhanced region allowed for the measurement of image noise.

Despite image noise, most clinical-based studies [29-31] also employed the detectability of coronary arteries to determine the subjective image quality that resulted from varying protocols. For instance, Carrascosa et al. [30], determined the overall image quality score based on coronary artery visualization. As for the present cardiac insert phantom, the varying size of cylindrical contrast-enhanced regions represented this purpose. Hence, the edges and the detectability of these cylindrical contrast-enhanced regions over various protocols applied could be used to determine the overall subjective image quality.

Another advantage of this new insert phantom is the removable inserts. This new feature allowed the researchers to further customize the design or the filling materials used to suit their purposes. Additionally, this design was successfully developed by using a computer-aided design software program, hence making it possible for other researchers to redesign and reproduce new physical phantom models. In fact, numerous other open sources software programs are also available on the internet for users to download and use to build their phantom designs.

The primary challenge of 3D printing technology had been seeking the most apt printing methodology, which is inclusive of selecting suitable printing materials, determining the correct temperature settings of the extruders, and choosing the most

appropriate printer protocols [32]. From this work of developing the present phantom, deciding on the appropriate temperature for the extruder to lay the printing materials on the platform had been an intricate issue. Another problem that was experienced had been during the printing process of the removable inserts due to the surface intricacy and the size of subtle diameters.

The new insert phantom offers a good alternative to researchers who need to produce custom phantoms relatively quickly and cost-effectively. Sophisticated phantom production demands the use of the latest three-dimensional printer technology that allows a greater variety of filament materials and the ability to customize phantoms with the desired geometrical features. There are several limitations related to the 3D printer used. First, the new insert phantom resembled a static physical model of a dynamic organ meaning the various changes that take place during the cardiac cycle were not displayed in the projection images. Different printing materials moved by electrical motors could offer a sequence of mechanical events similar to heartbeats. Second, more advanced 3D printing technology can produce physical models with highly intricate surfaces and sides. This advanced technology could be extended to produce a phantom from the real-patient volumetric CT datasets.

This 3D-printed cardiac insert phantom was also comparable with the HU values obtained from the real-patient image datasets and the Catphan® 500 phantom. Hence, it was likely that for all the filling materials, the resulting image quality assessments did display similar results upon using the real-patients or Catphan® 500 phantom. Nonetheless, in any case, additional investigations, e.g. resolutions and detectability, using other tools are indeed necessary to ensure that the image quality assessments are accurate.

In conclusion, this study demonstrates that a novel 3D-printed cardiac insert phantom can be produced from volumetric CT images. This new insert phantom could be reproduced by investigators who need a relatively cost- and time-effective method of producing customized CT phantoms. Further advances in this 3D printing technology promise to offer more flexibility in design, and this could become a more routine method in producing phantoms in future.

### 3.3.6 References

- [1] W. Oropallo and L. A. Piegl, "Ten challenges in 3D printing," *Engineering with Computers*, vol. 32, no. 1, pp. 135-148, 2015.
- [2] S. Leng *et al.*, "Construction of realistic phantoms from patient images and a commercial three-dimensional printer," *J Med Imaging (Bellingham)*, vol. 3, no. 3, p. 033501, Jul 2016.
- [3] M. H. Michalski, J. S. Ross, and M. Practice, "The shape of things to come: 3D printing in medicine," *American Medical Association*, vol. 312, no. 21, pp. 2213-2214, 2014.
- [4] A. A. Giannopoulos, D. Mitsouras, S. J. Yoo, P. P. Liu, Y. S. Chatzizisis, and F. J. Rybicki, "Applications of 3D printing in cardiovascular diseases," *Nat Rev Cardiol*, vol. 13, no. 12, pp. 701-718, Dec 2016.
- [5] L. C. Ebert, M. J. Thali, and S. Ross, "Getting in touch--3D printing in forensic imaging," *Forensic Sci Int*, vol. 211, no. 1-3, pp. e1-6, Sep 10 2011.
- [6] B. W. Miller *et al.*, "3D printing in X-ray and Gamma-Ray Imaging: A novel method for fabricating high-density imaging apertures," *Nucl Instrum Methods Phys Res A*, vol. 659, no. 1, pp. 262-268, Dec 10 2011.

- [7] A. Goyanes, U. Det-Amornrat, J. Wang, A. W. Basit, and S. Gaisford, "3D scanning and 3D printing as innovative technologies for fabricating personalized topical drug delivery systems," *J Control Release*, vol. 234, pp. 41-8, Jul 28 2016.
- [8] B. R. Whiting, C. Hoeschen, J. Solomon, F. Bochud, and E. Samei, "Design of anthropomorphic textured phantoms for CT performance evaluation," presented at the Medical Imaging 2014: Physics of Medical Imaging, 2014.
- [9] S. Leng, L. Yu, T. Vrieze, J. Kuhlmann, B. Chen, and C. H. McCollough, "Construction of Realistic Liver Phantoms from Patient Images using 3D Printer and Its Application in CT Image Quality Assessment," *Proc SPIE Int Soc Opt Eng*, vol. 2015, 2015.
- [10] J. Madamesila, P. McGeachy, J. E. Villarreal Barajas, and R. Khan, "Characterizing 3D printing in the fabrication of variable density phantoms for quality assurance of radiotherapy," *Phys Med*, vol. 32, no. 1, pp. 242-7, Jan 2016.
- [11] M. J. Kim *et al.*, "Characterization of 3D printing techniques: Toward patient specific quality assurance spine-shaped phantom for stereotactic body radiation therapy," *PLoS One*, vol. 12, no. 5, p. e0176227, 2017.
- [12] M. L. Aurumskjold, K. Ydstrom, A. Tingberg, and M. Soderberg, "Improvements to image quality using hybrid and model-based iterative reconstructions: a phantom study," *Acta Radiol*, vol. 58, no. 1, pp. 53-61, Jan 2017.
- [13] J. H. Baek, W. Lee, K. H. Chang, J. W. Chung, and J. H. Park, "Optimization of the scan protocol for the reduction of diaphragmatic motion artifacts depicted on CT angiography: a phantom study simulating pediatric patients with free breathing," *Korean J Radiol*, vol. 10, no. 3, pp. 260-8, May-Jun 2009.

- [14] C. Ghetti, O. Ortenzia, and G. Serreli, "CT iterative reconstruction in image space: a phantom study," *Phys Med*, vol. 28, no. 2, pp. 161-5, Apr 2012.
- [15] S. Leng *et al.*, "Anatomic modeling using 3D printing: quality assurance and optimization," *3D Printing in Medicine*, vol. 3, no. 1, 2017.
- [16] J. Solomon and E. Samei, "Quantum noise properties of CT images with anatomical textured backgrounds across reconstruction algorithms: FBP and SAFIRE," *Med Phys*, vol. 41, no. 9, p. 091908, Sep 2014.
- [17] A. Fedorov *et al.*, "3D Slicer as an image computing platform for the Quantitative Imaging Network," *Magn Reson Imaging*, vol. 30, no. 9, pp. 1323-41, Nov 2012.
- [18] W. G. Austen, "A reporting system on patients evaluated for coronary artery disease," *Circulation*, vol. 51, pp. 5-40, 1975.
- [19] K. T. Bae, "Intravenous Contrast Medium Administration and Scan Timing at CT: Considerations and Approaches," *Radiology*, vol. 256, no. 1, pp. 32-61, 2010.
- [20] K. A. Abdullah, M. F. McEntee, W. Reed, and P. L. Kench, "Using 3D printed cardiac CT phantom for dose reduction and diagnostic image quality assessment," in *12th Annual Scientific Meeting of Medical Imaging and Radiation Therapy (ASMMIRT)*, Perth, Western Australia, 2017.
- [21] K. A. Abdullah, M. F. McEntee, W. Reed, and P. L. Kench, "Radiation dose and diagnostic image quality associated with iterative reconstruction in coronary CT angiography: A systematic review," *J Med Imaging Radiat Oncol*, vol. 60, no. 4, pp. 459-68, Aug 2016.

- [22] M. J. Willeminck *et al.*, "Computed tomography radiation dose reduction: Effect of different iterative reconstruction algorithms on image quality," *Journal of Computer Assisted Tomography*, vol. 00, no. 00, pp. 1-9, 2014.
- [23] S. Guariglia, G. Meliaddò, E. Zivelonghi, L. Pinali, S. Montemezzi, and C. Cavedon, "Dose reduction and image quality in CT examinations using an iterative reconstruction algorithm: a phantom study," *Biomedical Physics & Engineering Express*, vol. 1, no. 4, 2015.
- [24] E. A. Park *et al.*, "Iterative reconstruction of dual-source coronary CT angiography: assessment of image quality and radiation dose," *Int J Cardiovasc Imaging*, vol. 28, no. 7, pp. 1775-86, Oct 2012.
- [25] F. Tatsugami *et al.*, "The effect of adaptive iterative dose reduction on image quality in 320-detector row CT coronary angiography," *British Journal of Radiology*, vol. 85, no. 1016, pp. e378-e382, 2012.
- [26] R. Wang *et al.*, "CT coronary angiography: image quality with sinogram-affirmed iterative reconstruction compared with filtered back-projection," *Clin Radiol*, vol. 68, no. 3, pp. 272-8, Mar 2013.
- [27] R. E. Yoo *et al.*, "Image quality of adaptive iterative dose reduction 3D of coronary CT angiography of 640-slice CT: comparison with filtered back-projection," *Int J Cardiovasc Imaging*, vol. 29, no. 3, pp. 669-76, Mar 2013.
- [28] F. Cademartiri *et al.*, "Intravenous contrast material administration at 16-detector row helical CT coronary angiography: test bolus versus bolus-tracking technique," vol. 233, ed: Radiological Society of North America, 2004, pp. 817-823.

- [29] D. Utsunomiya, W. G. Weigold, G. Weissman, and A. J. Taylor, "Effect of hybrid iterative reconstruction technique on quantitative and qualitative image analysis at 256-slice prospective gating cardiac CT," *Eur Radiol*, vol. 22, no. 6, pp. 1287-94, Jun 2012.
- [30] P. Carrascosa, G. A. Rodriguez-Granillo, C. Capunay, and A. Deviggiano, "Low-dose CT coronary angiography using iterative reconstruction with a 256-slice CT scanner," *World J Cardiol*, vol. 5, no. 10, pp. 382-6, Oct 26 2013.
- [31] T. A. Fuchs *et al.*, "Coronary computed tomography angiography with model-based iterative reconstruction using a radiation exposure similar to chest X-ray examination," *Eur Heart J*, vol. 35, no. 17, pp. 1131-6, May 2014.
- [32] C. N. Ionita *et al.*, "Challenges and limitations of patient-specific vascular phantom fabrication using 3D Polyjet printing," *Proc SPIE Int Soc Opt Eng*, vol. 9038, p. 90380M, Mar 13 2014.

# **CHAPTER 4 An investigation of CT image quality using iterative reconstruction algorithm and a 3D-printed cardiac insert phantom**

Part of this chapter has been submitted to *Journal of Computer Assisted Tomography* and it is currently under review.



## **4.1 Bridging section**

This section aims to highlight the need to investigate the use of a 3D-printed cardiac insert phantom in the evaluation of an IR algorithm and its different strength levels for dose reduction potential in CCTA protocols.

### **4.1.1 Background**

In the previous chapter (chapter three), the development of a 3D-printed cardiac insert phantom with CT attenuation values similar to patient and Catphan® 500 phantom image datasets were described and investigated. In this chapter, the new printed phantom was used to investigate the effect of IR algorithm on CT image quality and compare the results obtained to what has been reported in the literature for dose reduction analysis. An investigation of the use of this phantom for image quality assessment and dose reduction potential is important to establish its suitability for CCTA dose optimisation studies.

Imaging phantoms are widely used as a tool for investigating the effect of IR algorithm in CT examinations [1-6]. The physical phantoms such as Catphan® (The Phantom Laboratory, Salem, NY) phantoms used in the previous studies [5, 7, 8] provide a good first-order approximation of image quality. However, due to their current shape and the complexity of IR algorithm, it is possible that such phantoms are not fully adequate to assess the clinical impact of IR algorithm because patient body habitus can influence the radiation dose during CT examination [9, 10]. An anthropomorphic phantom, such as the Lungman phantom, is designed to be very similar to patient anatomy. Therefore, a combination of this Lungman phantom with an organ-specific phantom such as the cardiac insert, built with 3D printing technology, would be an appropriate simulation of scanning

patient's heart. To date, only a few studies have used 3D-printing phantoms to evaluate the effect of IR algorithm dose reduction potential in CT examinations on image quality. Solomon et al. [11] and Leng et al. [12] used the 3D-printed of lung and liver phantoms respectively for their investigations of IR algorithm however, no study reported the application of 3D-printed cardiac insert phantoms for CCTA. Consequently, the application of a 3D-printed cardiac insert phantom associated with the Lungman phantom to evaluate the effect of IR algorithms for CCTA dose optimisation studies is a novel investigation methodology.

This chapter and the thesis are heavily focussed on the quantitative measurement of image quality. Thus, a clear working definition of image quality is needed. The ICRU report 54 [13] indicates that a utilitarian approach results in the most comprehensive and practical definition of image quality. In the report, image quality is defined as *"the effectiveness by which an image can be used for its intended task"*. This idea is commonly referred to as *"task-based"* image quality [14, 15]. Under this definition, physical characteristics of the image, such as noise, SNR, or CNR may be used to determine image quality, but are not necessarily metrics of image quality, i.e., spatial resolution. In other words, these characteristics of objective image quality is not necessarily a metric of image quality, but it is likely that any proper task-based image quality metric would be sensitive to changing properties of the imaging system, especially if the visualization or measurement is important to the clinical task in question [16]. Therefore, these characteristics of objective image quality can and shall be used to measure the image quality of this 3D-printed cardiac insert phantom especially for CCTA dose optimisation studies.

In this chapter, the findings of investigation were compared to the previous work in chapter 2 to ensure that they were within the average dose reduction range reported in the literature. The 3D-printed cardiac insert phantom, placed within the Lungman phantom, was scanned using a standard CCTA protocol using three different low-dose protocols. Then, the resulting image datasets were reconstructed with FBP and three strengths of the IR algorithm. From the systematic review, up to 40% of dose reduction was achieved using IR compared to the FBP for CCTA.

With respect to the image quality of image noise, SNR, and CNR, the results of this 3D-printed cardiac insert phantom study showed similar results to the previous literature. These findings indicate that the 3D-printed cardiac insert phantom can be used to investigate the impact of IR algorithm on image quality as compared to the FBP. CT vendors claim that the higher strength levels of IR algorithms will result in higher noise reduction and thus may improve the image quality [5, 17]. In line with that, this phantom study showed that the AIDR3D with the strong level has the highest image noise reduction and the mild level with the lowest for each of protocol. In summary, these results indicated that it may be possible to use this 3D-printed cardiac insert phantom to investigate the effect of IR algorithms with respect to the image quality and dose reduction potential. This work will be submitted to the Journal of Computer Assisted Tomography (JCAT) with the title of “An investigation of CT image quality using iterative reconstruction algorithm and a 3D-printed cardiac insert phantom”.

#### 4.1.2 References

- [1] A. K. Hara, R. G. Paden, A. C. Silva, J. L. Kujak, H. J. Lawder, and W. Pavlicek, "Iterative reconstruction technique for reducing body radiation dose at CT: feasibility study," *AJR Am J Roentgenol*, vol. 193, no. 3, pp. 764-71, Sep 2009.
- [2] S. Guariglia, G. Meliaddò, E. Zivelonghi, L. Pinali, S. Montemezzi, and C. Cavedon, "Dose reduction and image quality in CT examinations using an iterative reconstruction algorithm: a phantom study," *Biomedical Physics & Engineering Express*, vol. 1, no. 4, 2015.
- [3] K. Jensen, A. C. Martinsen, A. Tingberg, T. M. Aalokken, and E. Fosse, "Comparing five different iterative reconstruction algorithms for computed tomography in an ROC study," *Eur Radiol*, vol. 24, no. 12, pp. 2989-3002, Dec 2014.
- [4] R. M. Joemai, W. J. Veldkamp, L. J. Kroft, I. Hernandez-Giron, and J. Geleijns, "Adaptive iterative dose reduction 3D versus filtered back projection in CT: evaluation of image quality," *AJR Am J Roentgenol*, vol. 201, no. 6, pp. 1291-7, Dec 2013.
- [5] M. L. Aurumskjold, K. Ydstrom, A. Tingberg, and M. Soderberg, "Improvements to image quality using hybrid and model-based iterative reconstructions: a phantom study," *Acta Radiol*, vol. 58, no. 1, pp. 53-61, Jan 2017.
- [6] J. Cammin, G. S. K. Fung, E. K. Fishman, J. H. Siewerdsen, J. W. Stayman, and K. Taguchi, "A biological phantom for evaluation of CT image reconstruction algorithms," *Proceedings of SPIE*, vol. 9033, pp. 903307-903308, 2014.
- [7] T. Klink, V. Obmann, J. Heverhagen, A. Stork, G. Adam, and P. Begemann, "Reducing CT radiation dose with iterative reconstruction algorithms: the influence of scan and

- reconstruction parameters on image quality and CTDIvol," *Eur J Radiol*, vol. 83, no. 9, pp. 1645-54, Sep 2014.
- [8] S. Lee and H. J. Kim, "Noise properties of reconstructed images in a kilo-voltage on-board imaging system with iterative reconstruction techniques: a phantom study," *Phys Med*, vol. 30, no. 3, pp. 365-73, May 2014.
- [9] R. J. Viola, G. B. Nguyen, T. T. Yoshizumi, S. S. Stinnett, J. K. Hoang, and P. G. Kranz, "Effect of Body Habitus on Radiation Dose During CT Fluoroscopy-Guided Spine Injections," *Interventional Neuroradiology*, vol. 20, no. 5, pp. 525-532, 2014.
- [10] S. T. Schindera *et al.*, "Effect of patient size on radiation dose for abdominal MDCT with automatic tube current modulation: phantom study," *American Journal of Roentgenology*, vol. 190, no. 2, pp. W100-W105, 2008.
- [11] J. Solomon and E. Samei, "Quantum noise properties of CT images with anatomical textured backgrounds across reconstruction algorithms: FBP and SAFIRE," *Med Phys*, vol. 41, no. 9, p. 091908, Sep 2014.
- [12] S. Leng, L. Yu, T. Vrieze, J. Kuhlmann, B. Chen, and C. H. McCollough, "Construction of Realistic Liver Phantoms from Patient Images using 3D Printer and Its Application in CT Image Quality Assessment," *Proc SPIE Int Soc Opt Eng*, vol. 2015, 2015.
- [13] P. Sharp *et al.*, "Report 54," *Journal of the International Commission on Radiation Units and Measurements*, vol. 28, no. 1, pp. NP-NP, 1996.
- [14] H. H. Barrett, K. J. Myers, C. Hoeschen, M. A. Kupinski, and M. P. Little, "Task-based measures of image quality and their relation to radiation dose and patient risk," *Physics in Medicine & Biology*, vol. 60, no. 2, p. R1, 2015.

- [15] H. H. Barrett, C. K. Abbey, and E. Clarkson, "Objective assessment of image quality. III. ROC metrics, ideal observers, and likelihood-generating functions," *JOSA A*, vol. 15, no. 6, pp. 1520-1535, 1998.
- [16] E. Clarkson, M. A. Kupinski, H. H. Barrett, and L. Furenlid, "A task-based approach to adaptive and multimodality imaging," *Proceedings of the IEEE*, vol. 96, no. 3, pp. 500-511, 2008.
- [17] K. A. Abdullah, M. F. McEntee, W. Reed, and P. L. Kench, "Radiation dose and diagnostic image quality associated with iterative reconstruction in coronary CT angiography: A systematic review," *J Med Imaging Radiat Oncol*, vol. 60, no. 4, pp. 459-68, Aug 2016.

## 4.2 Manuscript

This section is written in a manuscript version as to be submitted to the *Journal of Computer Assisted Tomography (JCAT)*.

**Title:** An investigation of CT image quality using iterative reconstruction algorithm and a 3D-printed cardiac insert phantom

**Authors:** Kamarul Amin Abdullah<sup>1,2</sup>, Mark F McEntee<sup>1</sup>, Warren Reed<sup>1</sup>, Peter L Kench<sup>1</sup>

**Affiliations:** 1. Discipline of Medical Radiation Sciences, Faculty of Health Sciences, The University of Sydney, New South Wales, Australia.

2. Centre of Medical Imaging, Faculty of Health Sciences, Universiti Sultan Zainal Abidin, Terengganu, Malaysia.

### 4.2.1 Abstract

**Objective:** To investigate the use of a 3D-printed cardiac insert phantom when evaluating IR algorithms in CCTA protocols. The objective image quality was measured with respect to the different strengths of IR algorithm at multiple radiation dose levels.

**Methods:** The 3D-printed cardiac insert phantom was placed into an anthropomorphic chest phantom and scanned with a multi-detector 16-slice CT scanner. Acquisitions were performed with CCTA protocols using 120 kVp at four different tube currents; 300, 200, 100, and 50 mA (protocols A, B, C, and D respectively). The image datasets were reconstructed with FBP and different IR algorithm (*adaptive iterative dose reduction three-*

*dimensional*, AIDR3D) strengths. The image quality metrics image noise, SNR, and CNR were calculated for each protocol.

**Results:** Decreasing dose levels have significantly increased the image noise, compared to FBP of protocol A ( $p < 0.001$ ). As a result, the SNR and CNR were significantly decreased ( $p < 0.001$ ). For FBP, the highest noise with poor SNR and CNR was protocol D with  $19.0 \pm 1.6$  HU,  $18.9 \pm 2.5$ ,  $25.1 \pm 3.6$ , respectively. For IR algorithm, the AIDR3D<sub>strong</sub> yielded the lowest noise with excellent SNR and CNR. Comparing to previous literature, the percentage differences between FBP and IR algorithm for the image noise, SNR, and CNR are from 1% to 28% (mean  $\pm$  SD:  $12 \pm 9\%$ ), from 1% to 36% (mean  $\pm$  SD:  $15 \pm 13\%$ ), and from 4% to 35% (mean  $\pm$  SD:  $16 \pm 12\%$ ), respectively. Consequently, the dose reduction of using protocol B was possible.

**Conclusions:** The measurement image noise, in the 3D-printed phantom, was reduced significantly with the IR algorithm and thus, SNR and CNR was increased compared to FBP. Applying IR algorithm at various strengths has yielded a stepwise improvement of image quality allowing a dose reduction of up to 40%.

**Keywords:** reconstruction settings; coronary CTA; dose reduction; phantom; image quality

#### 4.2.2 Introduction

With the introduction of 64-slice and recently dual-source CT scanners, CCTA has emerged as a practical diagnostic imaging modality and is a less invasive assessment of CAD than invasive coronary angiography [1-4]. However, the rapid increase dose and thus the potential of radiation-induced cancer risks have prompted efforts of CCTA dose optimisation [5-8]. CCTA requires additional radiation dose with the advances in the CT



spatial and temporal resolution that allows detection of small lesions [9-11]. Reconstruction algorithms are an important way to reduce dose. Currently, FBP is the most widely used image reconstruction algorithm for CT imaging [12, 13]. FBP is a fast and robust analytic technique that performs well in most situations; however, when radiation dose is reduced or when large patients are examined, FBP results in images that are deteriorated by both electronic and quantum noise [14].

IR algorithms have been developed to provide solutions for the increasing noise at low dose protocols [15-17]. The advancement of computerisation has facilitated the application of IR algorithm in CT examinations [18, 19]. IR algorithms use statistical noise models to optimise the image quality of the final image [20, 21]. IR algorithms require multiple steps, and with every step, noise is reduced according to the specific statistical model of the IR algorithms. Hybrid IR algorithms involve the blending of IR algorithm with FBP reconstructions to keep the noise characteristics and image appearance diagnostically acceptable. [22] The amount of blending is represented by relative strengths of IR algorithm which determine the ratio between FBP and IR algorithm [23, 24]. For example, the *adaptive iterative dose reduction three-dimensional* (AIDR3D, Toshiba Medical Systems, Tochigi, Japan) has three levels of strength; mild, standard, and strong. The mild has the least iterative weighting, and the strong is the greatest. The assessment of CT image quality can be used to characterise the performance of the IR algorithm.

In our previous work [25], a 3D-printed cardiac insert phantom had been developed and the results showed that it is suitable for CCTA investigation protocols [25]. This article has further evaluated the printed phantom to measure the image noise, SNR, and CNR for the evaluation of IR algorithm on dose reduction potential. The purpose of our

investigation was to verify that image quality characteristics are the same with previous literature while noise is reduced by IR algorithm. Therefore, in this study, we used a 3D-printed cardiac insert phantom to investigate the effect of IR algorithm and its different selectable strengths on dose reduction potential while maintaining the image quality in CCTA protocols.

### **4.2.3 Materials and Methods**

The 3D-printed cardiac phantom is a similar shape and size to the cardiac insert of an anthropomorphic chest phantom (Lungman N-01, Kyoto Kagaku Co., Ltd., Kyoto, Japan) and filled with different attenuating materials (Figure 4.1a). The phantom's filling materials were composed of a jelly ( $27.24 \pm 2.67$  HU), water ( $-6.83 \pm 3.09$  HU), oil ( $-93.73 \pm 4.35$  HU), and air ( $-996.77 \pm 2.35$  HU). Cylindrical structures simulating the coronary vessels and ascending aorta were filled with contrast media ( $354.33 \pm 3.21$  HU) (Figure 4.1).

#### *4.2.3.1 Acquisition protocols*

The 3D-printed cardiac insert phantom was placed in the anthropomorphic chest phantom and scanned using a multi-detector CT scanner (Alexion, Toshiba Medical Systems Co Ltd., Otowara, Japan) (Figure 4.1, c and d). Acquisitions were based on the CCTA protocols using a 120 kVp tube voltage and tube currents (mA) of 300, 200, 100, and 50 resulting in four CT dose index volumes ( $CTDI_{vol}$ ) of 19.2 mGy (Protocol A), 11.6 mGy (Protocol B), 5.8 mGy (Protocol C), and 2.9 mGy (Protocol D). Protocol A was the reference protocol with a 100% dose level. The dose reduction rates for B, C, and D were 40%, 70%, and 85%, respectively. The detector collimation was 1 x 16 mm, the DFOV is 350 mm, and

gantry rotation time was 0.75 s. Data acquisitions of the phantom were repeated thirty times.

#### 4.2.3.2 Reconstruction settings

Protocol A was reconstructed only with the FBP, and the protocols B, C, and D with the FBP and the *adaptive iterative dose reduction three-dimensional* (AIDR3D) (Toshiba Medical Systems Co Ltd., Otowara, Japan) IR algorithm. The AIDR3D is the manufacturer’s commercial hybrid IR algorithm, which combines reconstruction in the raw data and image space [26]. The iterations are executed in image space only, where edge preservation and smoothing are performed. The corrected image is blended with the initial image from the raw data to keep the noise granularity [27]. The AIDR3D has three different strengths: mild, standard, and strong. Table 4.1 shows the imaging parameters. Note, the IR algorithm is referred to as the AIDR3D in text and figures.

Table 4.1: CT acquisition parameters and reconstruction settings. Four different protocols are used; protocols A, B, C, and D. For image reconstructions, FBP and three strengths of AIDR3D are used; mild, moderate, and strong.

<b>Parameters</b>				
Scanner type	Toshiba Alexion			
Detector collimation (mm)	16 x 1.0			
Field of view (mm)	160			
Rotation time (s)	0.75			
Scan range (mm)	125			
Tube Voltage (kV)	120			
Tube current (mA) (protocol)	300 (A)	200 (B)	100 (C)	50 (D)
CTDI <sub>vol</sub> (mGy) (protocol)	19.2 (A)	11.6 (B)	5.8 (C)	2.9 (D)
Reconstruction	FBP, AIDR3D mild, standard, and strong			

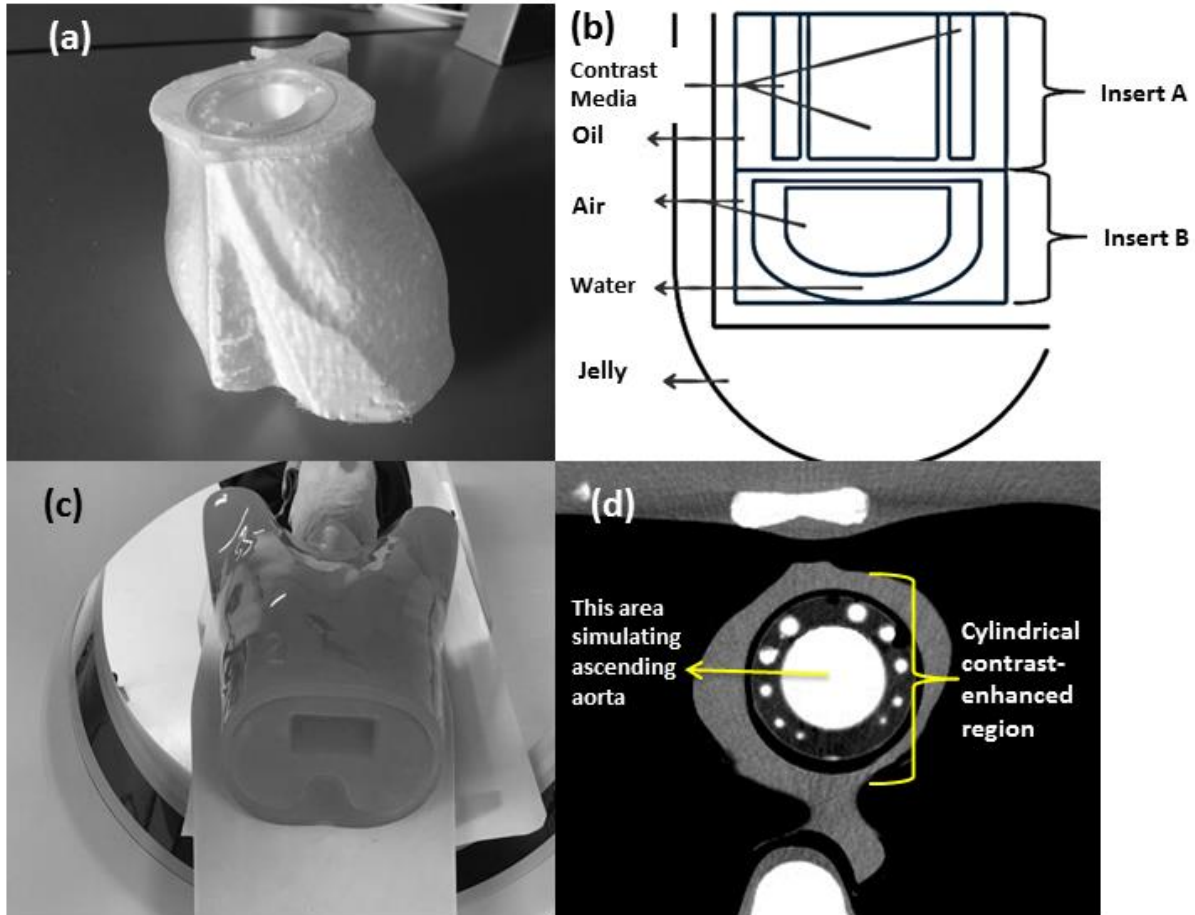


Figure 4.1: (a) The 3D-printed cardiac insert phantom. (b) A schematic diagram of the phantom with all filled materials. (c) The anthropomorphic chest phantom, containing the 3D-printed cardiac insert phantom, is placed on the scanner couch. (d) An axial CT image shows the contrast-enhanced region of the 3D-printed cardiac insert phantom; the centre simulates the contrast filled ascending aorta, and the varying size diameters of cylindrical demonstrate coronary arteries.

#### 4.2.3.3 Image quality and dose reduction

A region-of-interest (ROI) was placed in the centre of contrast-enhanced region that simulates the contrast filled ascending aorta for each slice of axial CT images. The size of ROI was adjusted to the maximum allowed area within that region. The measurements were made from 15-slices at four dose levels, resulting in  $15 \times 4 = 60$ -slices. As the acquisitions were repeated thirty-times, the total of images measured was  $60 \times 30 = 1,800$ -slices for each reconstruction. Image noise was quantified as standard deviation (SD) of attenuation values within the ROI. The signal-noise ratio (SNR) and the contrast-noise ratio

(CNR) were calculated using equations 1 and 2, respectively [28, 29]. The SNR was calculated by dividing the mean attenuation values (HU) by the corresponding SD (Equation 1).

$$SNR = \frac{HU_{mean}}{SD} \quad (\text{Eq. 1})$$

CNR was calculated as the difference between the two mean HU values (A and B) divided by the SD of the first material (A) (Equation 2). A pair of contrasts was measured (the contrast media (A) and the oil (B)) to simulate the ascending aorta and the fat.

$$CNR = \frac{HU_{mean}(A) - HU_{mean}(B)}{SD(B)} \quad (\text{Eq. 2})$$

Data analyses were carried out using Statistical Package for the Social Science (SPSS, version 21; IBM Corp., New York, NY, USA). Descriptive statistics, e.g., mean and standard deviation, were calculated. Image noise as well as SNR and CNR values were tested for normality by the Shapiro-Wilk test. Analysis of variances test examined the differences between image noise, SNR, and CNR.

In addition to that, the difference percentages of the measurement values for each image reconstructions between the low dose protocols (protocols B, C, and D) and reference protocol A were also calculated and reported. These percentages were produced to allow comparison of the results obtained with the previous literatures for dose reduction analysis. The previous literatures were selected based on our previous work [14] which investigated on the effect of using IR algorithm compared to FBP in CCTA examinations. In particular, seven databases (MEDLINE, Web of Science, EMBASE, CINAHL,

Science Direct, IEEE Xplore, and SPIE Digital Library) were searched to retrieve the selected studies, and a rigorous assessment was performed during the selection process to ensure only relevant studies were included.

## 4.2.4 Results

### 4.2.4.1 Image noise, SNR, and CNR

Image noise, SNR and CNR is shown in Table 4.2. The FBP image noise (HU values) for protocols B, C, and D was significantly higher than protocol A with the highest for protocol D ( $p < 0.001$  for all). For protocols B, C, and D, the AIDR3D<sub>strong</sub> yielded the lowest image noise ( $9.8 \pm 1.1$ ,  $12.4 \pm 0.7$ , and  $15.5 \pm 1.2$  HU, respectively) and the highest noise reduction (15%, 16%, and 18%, respectively) when compared to the FBP. In contrast, the AIDR3D<sub>mild</sub> showed the highest image noise ( $11.0 \pm 1.2$ ,  $14.1 \pm 0.9$ , and  $18.0 \pm 1.4$ , respectively) but the lowest noise reduction (<5%).

The SNR values of protocol A was the highest when compared to the other three protocols. For FBP, the SNR was significantly reduced for protocols B, C, and D, (12%-47%) when compared to the protocol A ( $p < 0.001$  for all). For protocols B, C, and D, the AIDR3D<sub>strong</sub> yielded the highest SNR while AIDR3D<sub>mild</sub> showed the lowest compared to FBP and the highest SNR percentage variation (11%, 30%, and 44%, respectively) when compared to AIDR3D<sub>standard</sub> and AIDR3D<sub>strong</sub>.

The CNR values of AIDR3D in protocols B, C, and D were significantly lower than the FBP in protocol A ( $p < 0.001$  for all). Of these, the lowest CNR was measured in the protocol D. For FBP, the highest CNR was the protocol B ( $41.3 \pm 5.7$ ) with only 12% of percentage

variation compared to the Protocol A. For IR algorithm, the higher strength of AIDR3D resulted in higher CNR. For protocols B, C, and D, the AIDR3D<sub>strong</sub> yielded the highest increase in CNR while AIDR3D<sub>mild</sub> showed the lowest increase in CNR compared to the FBP for each protocol.

Table 4.2: Results of image noise, SNR, and CNR at multiple dose levels using the 3D-printed cardiac insert phantom. Protocol A is the reference protocol, to demonstrate the dose reduction potential between other three protocols of B, C, and D between FBP and IR algorithms. Increasing the strength of IR algorithm (AIDR3D) results in more noise reduction. The strong level has the highest noise reduction while the mild has the lowest among the three IR strengths.

Image reconstructions		19.2 mGy Protocol	11.6 mGy Protocol	Diff. (%)	5.8 mGy Protocol	Diff. (%)	2.9 mGy Protocol	Diff. (%)
		A	B		C		D	
Image noise (HU)	FBP	9.5 ± 0.7	11.5 ± 1.2	21	14.7 ± 0.9	54	19.0 ± 1.6	99
	AIDR3D <sub>mild</sub>		11.0 ± 1.2	15	14.1 ± 0.9	48	18.0 ± 1.4	89
	AIDR3D <sub>standard</sub>		10.0 ± 1.1	6	13.0 ± 0.8	36	16.4 ± 1.2	72
	AIDR3D <sub>strong</sub>		9.8 ± 1.1	3	12.4 ± 0.7	30	15.5 ± 1.2	63
SNR	FBP	35.5 ± 3.4	31.2 ± 3.9	12	24.2 ± 2.8	32	18.9 ± 2.5	47
	AIDR3D <sub>mild</sub>		31.5 ± 3.6	11	24.9 ± 2.8	30	19.7 ± 2.3	44
	AIDR3D <sub>standard</sub>		33.9 ± 3.4	4	27.3 ± 3.2	23	21.5 ± 2.4	39
	AIDR3D <sub>strong</sub>		35.0 ± 4.4	1	28.0 ± 2.8	21	22.2 ± 2.1	37
CNR	FBP	46.6 ± 4.3	41.3 ± 5.7	12	32.0 ± 3.8	31	25.1 ± 3.6	46
	AIDR3D <sub>mild</sub>		41.6 ± 5.2	11	33.0 ± 3.8	29	26.1 ± 3.3	44
	AIDR3D <sub>standard</sub>		44.8 ± 4.9	4	36.0 ± 4.2	23	28.5 ± 3.3	39
	AIDR3D <sub>strong</sub>		46.2 ± 6.3	1	37.0 ± 3.8	21	29.4 ± 3.0	37

All the measurement values show a significance level of  $P < 0.001$  by ANOVA.  
Diff.: Differences

#### 4.2.4.3 Dose reduction analysis

Findings of the previous literature search based on the previous work are summarized in Table 4.3. Data was extracted into authors' name, year of published, image noise values, SNR values, CNR values, and the difference percentages. For image noise, the noise reduction between FBP and IR algorithms was from 1% to 28% (mean±SD: 12±9%). With respect to SNR and CNR, the ranges were from 1% to 36% (mean±SD: 15±13%) and from 4% to 35% (mean±SD: 16±12%), respectively. For dose reduction potential analysis (Figure 4.2), the mean difference percentages published in literature search between FBP and IR algorithms were compared to the protocols B, C, and D. From our analysis, protocol B results are below the mean values of previous literature indicating similar image quality to the reference protocol A. For protocol C and D, the image noise, SNR, and CNR results are above the mean percentage variation of the previous literature.



Table 4.3: The summary of the literature which compares the difference in image noise, signal-noise ratio (SNR), and contrast-noise ratio (CNR) between FBP and IR algorithms.

Author	Image Recons- truction	Image Noise (HU)	Diff. (%)	Signal-noise ratio (SNR)	Diff. (%)	Contrast-noise ratio (CNR)	Diff. (%)
Leipsic et al. [30]	FBP	NS	NS	NS	NS	NS	NS
	IR	6-10		-2 to -3		NS	
Shen, J. et al. [31]	FBP	35.00-35.03	NS	$11.6 \pm 2.1$	NS	NS	NS
	IR	34.99-35.02		$10.9 \pm 1.9$		NS	
Tumur, O. et al. [32]	FBP	$37.63 \pm 18.79$	6	$11.0 \pm 3.63$	5	$8.33 \pm 3.08$	5
	IR	$39.93 \pm 10.22$		$10.47 \pm 3.29$		$7.95 \pm 2.68$	
Moscariello, A. et al. [33]	FBP	$24.7 \pm 7.4$	16	NS	NS	NS	NS
	IR	$20.7 \pm 7$		NS		NS	
Wang, R. et al. [34]	FBP	$26.53 \pm 5.16$	4	$13.44 \pm 3.75$	16	$19.70 \pm 4.86$	6
	IR	$27.64 \pm 3.90$		$15.58 \pm 3.15$		$20.82 \pm 4.71$	
Yin, Wei-Hua et al. [35]	FBP	$18.7 \pm 3.8$	27	$22.5 \pm 5.4$	36	$17.5 \pm 5.5$	35
	IR	$13.7 \pm 2.7$		$30.5 \pm 7.4$		$23.7 \pm 7.5$	
Park, E.A. et al. [36]	FBP	$24.8 \pm 4.0$	11	$22.7 \pm 4.6$	14	$16.1 \pm 4.0$	14
	IR	$22.0 \pm 4.5$		$25.8 \pm 4.4$		$18.3 \pm 4.2$	
Renker M. et al. [12]	FBP	$24.9 \pm 6.0$	4	NS	NS	NS	NS
	IR	$26.0 \pm 7.5$		NS		NS	
Di Cesare, E. et al. [37]	FBP	$30.6 \pm 5.4$	10	$13.9 \pm 3.1$	27	$16.2 \pm 3.5$	27
	IR	$27.6 \pm 3.9$		$17.7 \pm 3.5$		$20.6 \pm 3.6$	
Tomizawa N. et al. [38]	FBP	$22.1 \pm 4.3$	4	$18.9 \pm 4.6$	5	$22.1 \pm 4.9$	4
	IR	$23.0 \pm 4.0$		$19.9 \pm 4.5$		$23.0 \pm 4.7$	
Williams, M. C. et al. [39]	FBP	$32 \pm NS$	28	NS	NS	$12 \pm NS$	8
	IR	$41 \pm NS$		NS		$11 \pm NS$	
Carrascosa, P. et al. [40]	FBP	$37.8 \pm 1.4$	1	$12.2 \pm 1.4$	1	NS	NS
	IR	$38.2 \pm 2.4$		$12.1 \pm 1.4$		NS	
Hou, Y. et al. [41]	FBP	$39 \pm 10$	15	NS	NS	$12 \pm 4$	25
	IR	$33 \pm 6$		NS		$15 \pm 3$	
Kordolaimi S.D. et al. [42]	FBP	NS	NS	NS	NS	NS	NS
	IR	6-10		-2 to -3		NS	

NS: Not Stated. Diff.: Differences.

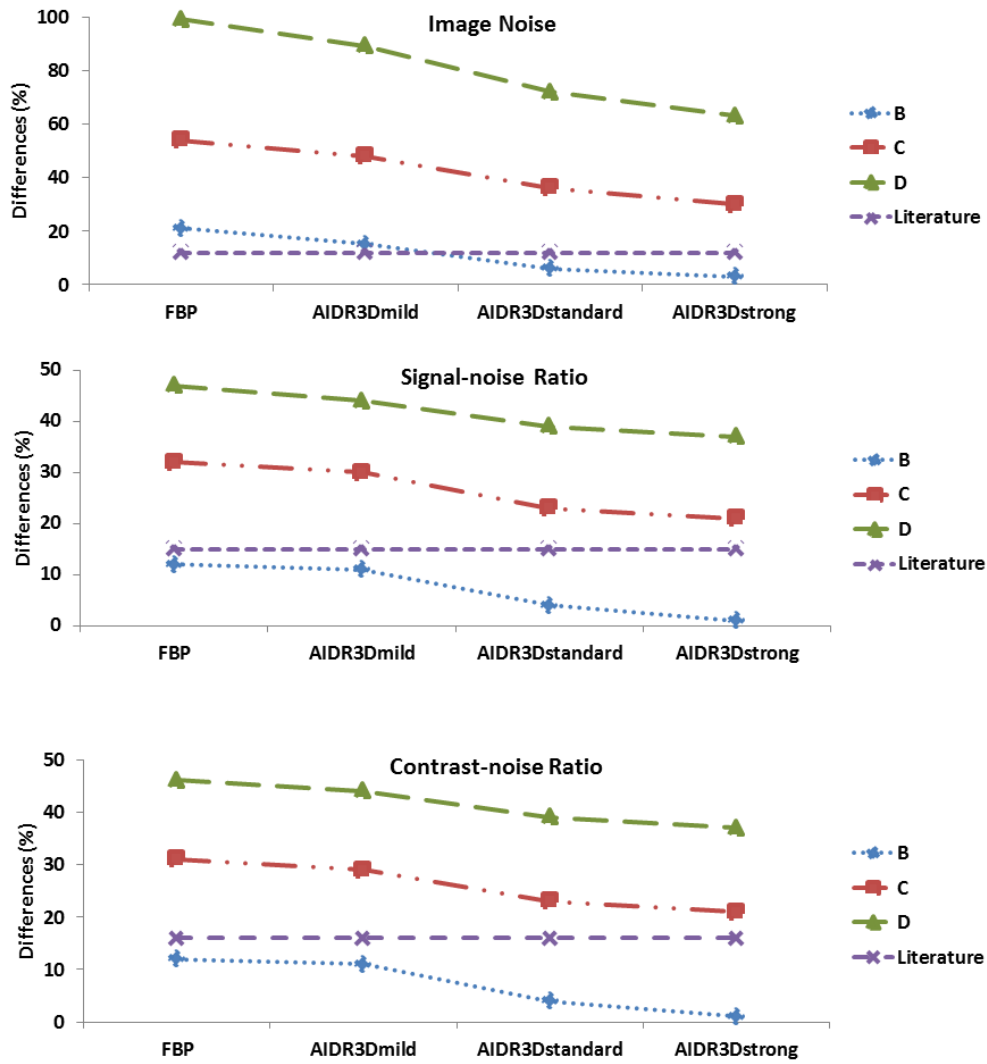


Figure 4.2: For dose reduction potential analysis, a comparison of image noise, signal-noise ratio (SNR), and contrast-noise ratio (CNR) among results were obtained with our 3D-printed cardiac insert phantom and the relevant previous literature. The literature sets the mean percentage variations published for comparison among other protocols B, C, and D. From the graph, overall protocol B results are below the mean values indicating similar image quality to reference protocol A. For protocol C and D, the image noise, SNR, and CNR results are above the mean values.

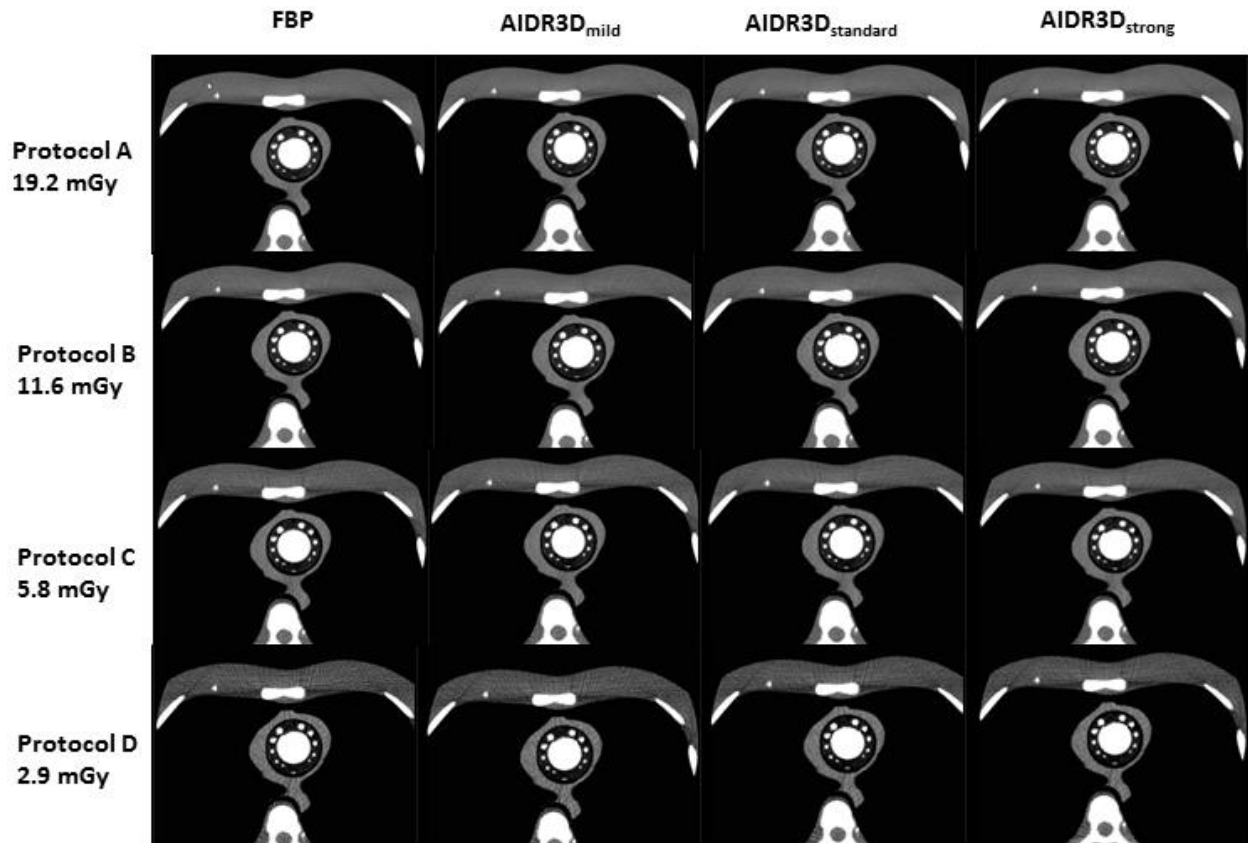


Figure 4.3: CT images of the 3D-printed cardiac insert phantom at four dose levels in columns and reconstruction methods, FBP, AIDR3D<sub>mild</sub>, AIDR3D<sub>standard</sub>, and AIDR3D<sub>strong</sub>, in rows. The insert contains contrast-material to simulate the ascending aorta and varying size of coronary arteries during cardiac CT imaging of CCTA.

#### 4.2.5 Discussion

IR algorithms claim to maintain or improve the image quality CT image quality when reducing dose by lowering the exposure factors [24, 43]. IR algorithms reduce image noise resulting from low photons flux [44]. The effect of IR algorithms on noise reduction depends on the photons flux and the selected IR strengths. This study demonstrates that using a 3D-printed cardiac insert phantom, an IR algorithm and increasing its strength have yielded a stepwise improvement in an objective measurement of image quality when compared to FBP.

The objective image quality measures of noise, SNR, and CNR are commonly used for the evaluation of IR algorithm [15, 45]. The noise characteristics of the CT image is just one metric of image quality, but it is likely that any changes made on them would affect the visualisation or measurement in a clinical task [46-48]. For example the visualisation of low contrast liver lesions are noise dependant, so reductions in noise would result in clearer visibility of the lesion. For CCTA, the image noise is usually measured in the centre of the ascending aorta as it is the area of the highest density of contrast-enhanced region [33, 49, 50]. In this study, the ROI was placed at the center of the largest diameter of the cylindrical contrast-enhanced region to simulate the ascending aorta and measure the image noise, SNR, and CNR. In line with previous studies [29, 37-39, 51-53], the IR algorithm results show significantly less image noise as compared to FBP. For the IR algorithm, increasing the strength from AIDR3D<sub>mild</sub> to the AIDR3D<sub>strong</sub> has resulted in a range of noise reduction with improved measures of SNR and CNR.

For dose reduction analysis, the mean difference percentages published in the previous literature search between FBP and IR algorithms were compared to the different percentages measured in the low dose protocols B, C, and D. In the previous literature, the results showed that CCTA with the use of IR algorithm leads to a significant reduction in radiation dose compared to the FBP. In addition, the image quality of IR algorithm at reduced dose (30–41%) is also comparable to FBP at standard dose in the diagnosis of CAD. In line with that findings, the results of our phantom and literature analysis has shown that the dose reduction was possible especially when using protocol B with up to 40% dose reduction over protocol A. On the other hand, protocol C and D were not

acceptable because the higher image noise than the reported mean difference percentages in the previous literature may result in loss of image details.

As the dose reduction potential was compared to the previous patient-based literature, the results of this study could infer the similar impact if performed in clinical settings. This is especially indicated by the image quality of IR algorithm at the reduced dose of 11.6 mGy ( $CTDI_{vol}$ ), which was similar to FBP at 19.2 mGy ( $CTDI_{vol}$ ). For a typical CCTA scan of 12-16 cm coverage in chest region [54], using this study values of 40% dose reduction, the effective dose could be reduced from 3.2-4.3 mSv for FBP reconstruction to 1.9-2.6 mSv when using IR algorithm for similar image quality assessment. In line with these findings, previous studies which also investigated on IR algorithm on adults or paediatrics have shown the similar results. In a previous study by Den Harder et al. [3], the authors reported that IR algorithm allows CCTA with an adult effective dose of 2.2 mSv while maintaining image quality. A study by Tricarico et al. [55] showed that an average dose reduction in CCTA was between 0.28-1.6 mSv for paediatrics. The lower effective dose for paediatrics, compared to adults, was not surprising, given that children has smaller size and weight. As such, the results of this 3D-printed cardiac insert phantom study would aid in development of dose optimised protocols for a department and thus, reducing the risks associated with the dose received by all types of patients. This opens up the potential of creating size specific phantoms, normal variant specific phantoms and pathology specific phantoms for optimisation. Researchers could use this 3D-printed methodology to investigate the effects on dose of rare normal variants such as situs inversus or dextra cordia.

While our results using the 3D-printed cardiac insert phantom showed good alignment to the previous literature, several limitations have been found. First, the image quality metrics were objective measures of noise only. However, in real patients, the subjective measurements, e.g. visual or perceptual, of image quality are also important for CT images with lesions. We aim to include subjective measurements in future studies using the varying size diameters of the cylindrical contrast-enhanced region to simulate lesion detectability. Second, the 3D-printed cardiac insert phantom involves no physiological motion such as breathing, heartbeat, or peristalsis. We recognised that motion contributes a significant impact on the image quality as motion during scanning can reduce the visualisation of coronary vessels [56]. Modern CTCA scanners and protocols use a large field of view, fast gantry rotation and regular heart rate to minimise the impact of physiological motion. Also, the ECG-gating method used in the recent studies [57-59] have shown that images used for reconstructed are effectively still during the acquisitions. However, in this study, the heart phantom was developed to simulate a CTCA free of motion artifacts, thus removing a constant confounding factor from all experiments. Further work plans to improve this design by introducing features to simulate the heart movement during a cardiac cycle. Third, the study was conducted using 16-slice CT scanner, an early type of CT scanner used for CCTA. Since the 3D-printed cardiac insert phantom has no cardiac motion the temporal resolution of the 16-slice is sufficient [60]. Also, this 16-slice scanner is used due to its similar ability, compared to 64-slice scanner, to visualise the smallest coronary vessels diameter of 1.5 mm in the 3D-printed cardiac insert phantom [61, 62]. However, in future studies, the 3D-printed cardiac insert phantom is planned to be acquired in other scanner models to provide more comparable results to the

current technology introduced. Last, the physical geometry of our 3D-printed cardiac insert phantom is smooth with less complexity than in the real heart. These cardiac phantom features could produce different measurements of image quality metrics when compared to the CT images of the human heart as shape and size can affect the image noise.

Using IR algorithms and increasing its strength have yielded a stepwise improvement in image quality. With the application of IR, image noise was reduced significantly and thus increased the SNR and CNR when compared to FBP. This study shows that dose reduction was achievable with up to 40%. It is possible to use a 3D-printed cardiac insert phantom to investigate the effect of IR algorithm with respect to image quality and dose reduction potential.

#### **4.2.6 References**

- [1] F. Zarb, L. Rainford, and M. F. McEntee, "Image quality assessment tools for optimization of CT images," *Radiography*, vol. 16, no. 2, pp. 147-153, 2010.
- [2] D. C. Benz *et al.*, "Minimized Radiation and Contrast Agent Exposure for Coronary Computed Tomography Angiography: First Clinical Experience on a Latest Generation 256-slice Scanner," *Acad Radiol*, vol. 23, no. 8, pp. 1008-14, Aug 2016.
- [3] A. M. Den Harder *et al.*, "Dose reduction with iterative reconstruction for coronary CT angiography: a systematic review and meta-analysis," *Br J Radiol*, vol. 89, no. 1058, p. 20150068, 2016.
- [4] D. W. Entrikin, J. A. Leipsic, and J. J. Carr, "Optimization of radiation dose reduction in cardiac computed tomographic angiography," *Cardiol Rev*, vol. 19, no. 4, pp. 163-76, Jul-Aug 2011.

- [5] S. Gordic *et al.*, "Optimizing radiation dose by using advanced modelled iterative reconstruction in high-pitch coronary CT angiography," *Eur Radiol*, vol. 26, no. 2, pp. 459-68, Feb 2016.
- [6] J. Hausleiter *et al.*, "Estimated radiation dose associated with cardiac CT angiography," *Journal of the American Medical Association*, vol. 301, pp. 500-507, 2009.
- [7] Y. Hou, J. Zheng, Y. Wang, M. Yu, M. Vembar, and Q. Guo, "Optimizing radiation dose levels in prospectively electrocardiogram-triggered coronary computed tomography angiography using iterative reconstruction techniques: a phantom and patient study," *PLoS One*, vol. 8, no. 2, p. e56295, 2013.
- [8] L. Xu and Z. Zhang, "Coronary CT angiography with low radiation dose," *Int J Cardiovasc Imaging*, vol. 26 Suppl 1, pp. 17-25, Feb 2010.
- [9] C. J.H and C. V.M, "Coronary CT angiography is a more cost-effective strategy than myocardial perfusion imaging as an initial diagnostic test in clinical practice," vol. 53, ed, 2009, pp. A274-A274.
- [10] M. Liang, M. M. Liang, D. Blair, G. Davis, and M. Menon, "The use of multi slice computed tomography coronary angiography (CTCA) as a gatekeeper to invasive coronary angiography," *Heart Lung and Circulation*, vol. 19, pp. S19-S19, 2010.
- [11] A. Aslam, U. Khokhar, M. Cortegiano, M. Poon, and S. Voros, "Adaptive Iterative Dose Reduction Is Associated with Significant Reduction in Total and Computed Tomography Coronary Angiography Radiation Exposure and Improved Image Quality, Compared to Traditional Filtered Backprojection on 320-Multidetector



- Computed Tomography," *Journal of the American College of Cardiology*, vol. 61, no. 10, 2013.
- [12] M. Renker *et al.*, "Iterative image reconstruction techniques: Applications for cardiac CT," *J Cardiovasc Comput Tomogr*, vol. 5, no. 4, pp. 225-30, Jul-Aug 2011.
- [13] J. Leipsic, B. G. Heilbron, and C. Hague, "Iterative reconstruction for coronary CT angiography: finding its way," *Int J Cardiovasc Imaging*, vol. 28, no. 3, pp. 613-20, Mar 2012.
- [14] K. A. Abdullah, M. F. McEntee, W. Reed, and P. L. Kench, "Radiation dose and diagnostic image quality associated with iterative reconstruction in coronary CT angiography: A systematic review," *J Med Imaging Radiat Oncol*, vol. 60, no. 4, pp. 459-68, Aug 2016.
- [15] M. J. Willeminck *et al.*, "Computed tomography radiation dose reduction: Effect of different iterative reconstruction algorithms on image quality," *Journal of Computer Assisted Tomography*, vol. 00, no. 00, pp. 1-9, 2014.
- [16] P. M. Almeida, "Improving iterative image reconstruction for X-ray CT," *Comput Biol Med*, vol. 43, no. 8, p. 1062, Sep 2013.
- [17] M. Beister, D. Kolditz, and W. A. Kalender, "Iterative reconstruction methods in X-ray CT," *Phys Med*, vol. 28, no. 2, pp. 94-108, Apr 2012.
- [18] D. Fleischmann and F. E. Boas, "Computed tomography--old ideas and new technology," *Eur Radiol*, vol. 21, no. 3, pp. 510-7, Mar 2011.
- [19] T. G. Flohr, C. N. De Cecco, B. Schmidt, R. Wang, U. J. Schoepf, and F. G. Meinel, "Computed tomographic assessment of coronary artery disease: state-of-the-art imaging techniques," *Radiol Clin North Am*, vol. 53, no. 2, pp. 271-85, Mar 2015.

- [20] D. Mehta, R. Thompson, T. Morton, A. Dhanantwari, and E. Shefer, "Iterative model reconstruction: simultaneously lowered computed tomography radiation dose and improved image quality," *Med Phys Int J*, vol. 2, no. 1, pp. 147-155, 2013.
- [21] A. Scibelli, "iDose4 iterative reconstruction technique," *Philips Healthcare*, pp. 1-40, 2011.
- [22] M. J. Willemink *et al.*, "Iterative reconstruction techniques for computed tomography Part 1: technical principles," *Eur Radiol*, vol. 23, no. 6, pp. 1623-31, Jun 2013.
- [23] N. Weir and M. C. Williams, "Contrast-to-Noise Ratio Improvements with AIDR 3D," *Toshiba Medical Systems Journal: Vision*, vol. 20, pp. 14-15, 2012.
- [24] L. L. Geyer *et al.*, "State of the Art: Iterative CT Reconstruction Techniques," *Radiology*, vol. 276, no. 2, pp. 338-356, 2015.
- [25] K. A. Abdullah, M. F. McEntee, W. Reed, and P. L. Kench, "Using 3D printed cardiac CT phantom for dose reduction and diagnostic image quality assessment," in *12th Annual Scientific Meeting of Medical Imaging and Radiation Therapy (ASMMIRT)*, Perth, Western Australia, 2017.
- [26] B. Roberts, "Computed Tomography Iterative Reconstruction Techniques," *Radiologic technology*, vol. 87, no. 6, pp. 649-670, 2016.
- [27] M. Kachelrieß, "Iterative Reconstruction Techniques: What do they Mean for Cardiac CT?," *Current Cardiovascular Imaging Reports*, vol. 6, no. 3, pp. 268-281, 2013.
- [28] M. J. Willemink *et al.*, "Iterative reconstruction techniques for computed tomography part 2: initial results in dose reduction and image quality," *Eur Radiol*, vol. 23, no. 6, pp. 1632-42, Jun 2013.

- [29] M. Y. Chen *et al.*, "Simulated 50 % radiation dose reduction in coronary CT angiography using adaptive iterative dose reduction in three-dimensions (AIDR3D)," *Int J Cardiovasc Imaging*, vol. 29, no. 5, pp. 1167-75, Jun 2013.
- [30] J. Leipsic *et al.*, "Estimated radiation dose reduction using adaptive statistical iterative reconstruction in coronary CT angiography: the ERASIR study," *AJR Am J Roentgenol*, vol. 195, no. 3, pp. 655-60, Sep 2010.
- [31] J. Shen *et al.*, "Prospective ECG-triggered coronary CT angiography: clinical value of noise-based tube current reduction method with iterative reconstruction," *PLoS One*, vol. 8, no. 5, p. e65025, 2013.
- [32] O. Tumur, K. Soon, F. Brown, and M. Mykytowycz, "New scanning technique using Adaptive Statistical Iterative Reconstruction (ASIR) significantly reduced the radiation dose of cardiac CT," *J Med Imaging Radiat Oncol*, vol. 57, no. 3, pp. 292-6, Jun 2013.
- [33] A. Moscariello *et al.*, "Coronary CT angiography: image quality, diagnostic accuracy, and potential for radiation dose reduction using a novel iterative image reconstruction technique-comparison with traditional filtered back projection," *Eur Radiol*, vol. 21, no. 10, pp. 2130-8, Oct 2011.
- [34] R. Wang *et al.*, "Image quality and radiation dose of low dose coronary CT angiography in obese patients: sinogram affirmed iterative reconstruction versus filtered back projection," *Eur J Radiol*, vol. 81, no. 11, pp. 3141-5, Nov 2012.
- [35] W. H. Yin *et al.*, "Effect of reduced x-ray tube voltage, low iodine concentration contrast medium, and sinogram-affirmed iterative reconstruction on image quality and radiation dose at coronary CT angiography: results of the prospective

- multicenter REALISE trial," *J Cardiovasc Comput Tomogr*, vol. 9, no. 3, pp. 215-24, May-Jun 2015.
- [36] E. A. Park *et al.*, "Iterative reconstruction of dual-source coronary CT angiography: assessment of image quality and radiation dose," *Int J Cardiovasc Imaging*, vol. 28, no. 7, pp. 1775-86, Oct 2012.
- [37] E. Di Cesare *et al.*, "Assessment of dose exposure and image quality in coronary angiography performed by 640-slice CT: a comparison between adaptive iterative and filtered back-projection algorithm by propensity analysis," *Radiol Med*, vol. 119, no. 8, pp. 642-9, Aug 2014.
- [38] N. Tomizawa, T. Nojo, M. Akahane, R. Torigoe, S. Kiryu, and K. Ohtomo, "Adaptive Iterative Dose Reduction in coronary CT angiography using 320-row CT: assessment of radiation dose reduction and image quality," *J Cardiovasc Comput Tomogr*, vol. 6, no. 5, pp. 318-24, Sep-Oct 2012.
- [39] M. C. Williams *et al.*, "Iterative reconstruction and individualized automatic tube current selection reduce radiation dose while maintaining image quality in 320-multidetector computed tomography coronary angiography," *Clin Radiol*, vol. 68, no. 11, pp. e570-7, Nov 2013.
- [40] P. Carrascosa, G. A. Rodriguez-Granillo, C. Capunay, and A. Deviggiano, "Low-dose CT coronary angiography using iterative reconstruction with a 256-slice CT scanner," *World J Cardiol*, vol. 5, no. 10, pp. 382-6, Oct 26 2013.
- [41] Y. Hou, X. Liu, S. Xu, W. Guo, and Q. Guo, "Comparisons of image quality and radiation dose between iterative reconstruction and filtered back projection reconstruction

- algorithms in 256-MDCT coronary angiography," *AJR Am J Roentgenol*, vol. 199, no. 3, pp. 588-94, Sep 2012.
- [42] S. D. Kordolaimi *et al.*, "Effect of iDose4 iterative reconstruction algorithm on image quality and radiation exposure in prospective and retrospective electrocardiographically gated coronary computed tomographic angiography," *Journal of computer assisted tomography*, vol. 38, no. 6, pp. 1-7, 2014.
- [43] P. Kroepil, A. H. Bigdeli, H. D. Nagel, G. Antoch, and M. Cohnen, "Impact of increasing levels of advanced iterative reconstruction on image quality in low-dose cardiac CT angiography," *Rofo*, vol. 186, no. 6, pp. 567-575, 2014.
- [44] J. Greffier, A. Fernandez, F. Macri, C. Freitag, L. Metge, and J. P. Beregi, "Which dose for what image? Iterative reconstruction for CT scan," *Diagn Interv Imaging*, vol. 94, no. 11, pp. 1117-21, Nov 2013.
- [45] P. Sharp *et al.*, "Report 54," *Journal of the International Commission on Radiation Units and Measurements*, vol. os28, no. 1, pp. NP-NP, 1996.
- [46] J. Solomon, A. Mileto, J. C. Ramirez-Giraldo, and E. Samei, "Diagnostic performance of an advanced modeled iterative reconstruction algorithm for low-contrast detectability with a third-generation dual-source multidetector CT scanner: potential for radiation dose reduction in a multireader study," *Radiology*, vol. 275, no. 3, pp. 735-745, 2015.
- [47] F. Verdun *et al.*, "Image quality in CT: From physical measurements to model observers," *Physica Medica: European Journal of Medical Physics*, vol. 31, no. 8, pp. 823-843, 2015.

- [48] H. H. Barrett, K. J. Myers, C. Hoeschen, M. A. Kupinski, and M. P. Little, "Task-based measures of image quality and their relation to radiation dose and patient risk," *Physics in Medicine & Biology*, vol. 60, no. 2, p. R1, 2015.
- [49] J. K. Dae *et al.*, "Saline flush effect for enhancement of aorta and coronary arteries at multidetector CT coronary angiography," vol. 246, ed: Radiological Society of North America, 2008, pp. 110-115.
- [50] M. Kidoh *et al.*, "Optimized subtraction coronary CT angiography protocol for clinical use with short breath-holding time—initial experience," *Academic radiology*, vol. 22, no. 1, pp. 117-120, 2015.
- [51] G. Sun *et al.*, "Application of low tube voltage coronary CT angiography with low-dose iodine contrast agent in patients with a BMI of 26-30 kg/m<sup>2</sup>," *Clinical radiology*, vol. 70, no. 2, pp. 138-145, 2015.
- [52] R. E. Yoo *et al.*, "Image quality of adaptive iterative dose reduction 3D of coronary CT angiography of 640-slice CT: comparison with filtered back-projection," *Int J Cardiovasc Imaging*, vol. 29, no. 3, pp. 669-76, Mar 2013.
- [53] F. Tatsugami *et al.*, "The effect of adaptive iterative dose reduction on image quality in 320-detector row CT coronary angiography," *British Journal of Radiology*, vol. 85, no. 1016, pp. e378-e382, 2012.
- [54] E. Maeda *et al.*, "Diagnostic Phase of Calcium Scoring Scan Applied as the Center of Acquisition Window of Coronary Computed Tomography Angiography Improves Image Quality in Minimal Acquisition Window Scan (Target CTA Mode) Using the Second Generation 320-Row CT," *ScientificWorldJournal*, vol. 2016, p. 1017851, 2016.

- [55] F. Tricarico *et al.*, "Cardiovascular CT angiography in neonates and children: image quality and potential for radiation dose reduction with iterative image reconstruction techniques," *Eur Radiol*, vol. 23, no. 5, pp. 1306-15, May 2013.
- [56] F. Contijoch, J. W. Stayman, and E. R. McVeigh, "The impact of small motion on the visualization of coronary vessels and lesions in cardiac CT: A simulation study," *Medical physics*, vol. 44, no. 7, pp. 3512-3524, 2017.
- [57] S. Achenbach *et al.*, "Coronary computed tomography angiography with a consistent dose below 1 mSv using prospectively electrocardiogram-triggered high-pitch spiral acquisition," *Eur Heart J*, vol. 31, no. 3, pp. 340-6, Feb 2010.
- [58] I. Armstrong, M. Trevor, and M. Widdowfield, "Maintaining image quality and reducing dose in prospectively-triggered CT coronary angiography: A systematic review of the use of iterative reconstruction," *Radiography*, vol. 22, no. 1, pp. 84-92, 2016.
- [59] J. P. Earls and E. C. Schrack, "Prospectively gated low-dose CCTA: 24 months experience in more than 2,000 clinical cases," *International Journal of Cardiovascular Imaging*, vol. 25, no. 2, pp. 177-187, 2009.
- [60] M. A. Lewis, A. Pascoal, S. F. Keevil, and C. A. Lewis, "Selecting a CT scanner for cardiac imaging: the heart of the matter," *The British Journal of Radiology*, vol. 89, no. 1065, p. 20160376, 2016.
- [61] R. Khan, S. Rawal, and M. J. Eisenberg, "Transitioning from 16-slice to 64-slice multidetector computed tomography for the assessment of coronary artery disease: Are we really making progress?," *The Canadian Journal of Cardiology*, vol. 25, no. 9, pp. 533-542, 2009.

- [62] C. Peebles, "Computed tomographic coronary angiography: how many slices do you need?," *Heart*, vol. 92, no. 5, pp. 582-584, 2006.



# **CHAPTER 5 Optimisation of iterative reconstruction strengths in a low tube voltage coronary CT angiography using a 3D-printed cardiac insert phantom**

This chapter (Paper 4) will be submitted to *Journal of Cardiovascular Computed Tomography* (2018).

## **5.1 Bridging section**

This section aims to highlight the need to evaluate the optimal IR algorithm strengths for the low tube voltage CCTA protocols using a 3D-printed cardiac insert phantom and evaluate the validity of the image quality in a group of patients.

### **5.1.1 Background**

In the previous chapter (chapter four), the study investigated the use of a 3D-printed cardiac insert phantom for IR algorithm. Increasing its strength has yielded a stepwise improvement of image quality. The study also confirmed that dose reduction was achievable of up to 40% with similar image quality. However, further evaluation of the 3D-printed cardiac insert phantom is required to investigate other aspects of image quality assessment. In this chapter, the Catphan<sup>®</sup> 500 phantom was introduced to evaluate the high spatial resolution and low contrast resolution. The combination of this Catphan<sup>®</sup> 500 phantom and the 3D-printed cardiac insert phantom is important to support the findings suggested in the previous chapter. Furthermore, the results of the 3D-printed cardiac insert phantom were then compared to the patient image datasets to test its validity against clinical studies.

As indicated in the preceding chapters (from chapter one to three), IR algorithms can reduce dose from 30-41% to the patient by allowing use of low dose protocols while maintaining image quality [1-4]. However, the previous studies [5-7] have also shown that a combination of IR algorithm to other dose optimisation strategies such as prospective ECG-gating method, high pitch acquisitions, and low tube voltage could also further reduce the dose. A previous study by Shen et al. [8], for example, reported that when IR algorithm

was combined to prospective ECG-gating method, very low dose CCTA can be achieved. Excellent image quality was found with the lowest dose of 1.8 mSv which is more than 50% dose reduction compared to FBP. Further dose reduction is also possible with the use of high pitch acquisitions. A recent study by Minwen et al. [9], who evaluated the feasibility of an IR algorithm combined with high pitch acquisitions, reported that very low dose of less than 0.1 mSv was achieved with better image quality noted when using IR algorithm compared to FBP. Thus evidence suggests that IR algorithms should be combined with other dose optimisation strategies if one to further reduce dose to the patient. The low tube voltage has been increasingly used in CCTA to reduce dose to the patient [10-12]. The continuous improvement in CT systems (e.g., faster gantry rotation, more detectors, and dual-energy tube) has resulted in various low tube voltages used in CCTA such as 70, 80, and 100 kVp [6, 13]. However, the very low tube voltages of 70-80 kVp protocols are still under investigation and limited to patients with low to normal BMI, which is not representative of the CAD population [14, 15]. In this chapter, the CT dose optimisation study were carried out using a 64-slice CT scanner where the current CCTA protocols used in the centre, is 120 kVp of the tube voltage. Therefore, the IR algorithm was suggested to combine with the low tube voltage CCTA of 100 kVp to further reduce radiation dose.

In addition to that, the IR algorithm strength levels were also modified in order to find the balance between the image quality and dose reduction potential. Based on the findings in the previous chapter (chapter four), it was postulated that IR algorithm with higher strength levels may allow the use of low tube voltage of 100 kVp and thus reducing dose to the patient. As a result, the higher IR algorithm strength levels will then improve the detection of small object size; allowing more noise reduction than the standard levels.

Therefore, the modification of IR strength levels could be an important clinical benefit for detecting small diameter of lesions and coronary vessels.

This phantom-based study demonstrated that radiation dose could be substantially reduced up to 57% with the use of 100 kVp and ASIR 60%. This combination yielded a comparable image quality to the current local CCTA protocols using 120 kVp of ASIR 40%. Consequently, further dose reduction has been achieved with 16% higher than the average range (30-41%) which was found in the previous chapters. The comparison of the image noise, SNR, and CNR values between the 3D-printed cardiac insert phantom and the 27 series of patient image datasets using the Bland-Altman plots indicated small mean differences of the measurement of agreements. Therefore, the phantom-based methodology using 3D printing technology can be used for CCTA dose optimisation studies and may be comparable to the findings of a clinical study of dose optimisation. This is important because dose optimisations studies using phantoms are faster, cheaper, and can be carried out by people that are not licenced to do CT on humans, but can use phantoms. In Australia, for example, those with IA9 licence could carry out this optimisation studies and find results similar to a clinical study.

### **5.1.2 References**

- [1] K. A. Abdullah, M. F. McEntee, W. Reed, and P. L. Kench, "Radiation dose and diagnostic image quality associated with iterative reconstruction in coronary CT angiography: A systematic review," *J Med Imaging Radiat Oncol*, vol. 60, no. 4, pp. 459-68, Aug 2016.

- [2] M. Beister, D. Kolditz, and W. A. Kalender, "Iterative reconstruction methods in X-ray CT," *Phys Med*, vol. 28, no. 2, pp. 94-108, Apr 2012.
- [3] B. Chen, J. C. Ramirez Giraldo, J. Solomon, and E. Samei, "Evaluating iterative reconstruction performance in computed tomography," *Med Phys*, vol. 41, no. 12, p. 121913, Dec 2014.
- [4] L. L. Geyer *et al.*, "State of the Art: Iterative CT Reconstruction Techniques," *Radiology*, vol. 276, no. 2, pp. 338-356, 2015.
- [5] W. H. Sommer *et al.*, "Saving Dose in Triple-Rule-Out Computed Tomography Examination Using a High-Pitch Dual Spiral Technique," *Investigative Radiology*, vol. 45, no. 2, pp. 64-71, 2010.
- [6] Z. Sun, G. H. Choo, and K. H. Ng, "Coronary CT angiography: Current status and continuing challenges," *British Journal of Radiology*, vol. 85, no. 1013, pp. 495-510, 2012.
- [7] G. Vorobiof, S. Achenbach, and J. Narula, "Minimizing radiation dose for coronary CT angiography," *Cardiol Clin*, vol. 30, no. 1, pp. 9-17, Feb 2012.
- [8] J. Shen *et al.*, "Prospective ECG-triggered coronary CT angiography: clinical value of noise-based tube current reduction method with iterative reconstruction," *PLoS One*, vol. 8, no. 5, p. e65025, 2013.
- [9] M. Zheng, H. Zhao, J. Xu, Y. Wu, and J. Li, "Image quality of ultra-low-dose dual-source CT angiography using high-pitch spiral acquisition and iterative reconstruction in young children with congenital heart disease," *Journal of cardiovascular computed tomography*, vol. 7, no. 6, p. 376, 2013.

- [10] B. Bischoff *et al.*, "Impact of a reduced tube voltage on CT angiography and radiation dose: results of the PROTECTION I study," *JACC: Cardiovascular Imaging*, vol. 2, no. 8, pp. 940-946, 2009.
- [11] G. M. Feuchtner *et al.*, "Radiation dose reduction by using 100-kV tube voltage in cardiac 64-slice computed tomography: a comparative study," *European journal of radiology*, vol. 75, no. 1, pp. e51-e56, 2010.
- [12] G. Sun *et al.*, "Application of low tube voltage coronary CT angiography with low-dose iodine contrast agent in patients with a BMI of 26–30 kg/m<sup>2</sup>," *Clinical radiology*, vol. 70, no. 2, pp. 138-145, 2015.
- [13] I. Danad, B. Ó Hartaigh, and J. K. Min, "Dual-energy computed tomography for detection of coronary artery disease," *Expert review of cardiovascular therapy*, vol. 13, no. 12, pp. 1345-1356, 2015.
- [14] B. R. Jun, H. S. Yong, E. Y. Kang, O. H. Woo, and E. J. Choi, "64-slice coronary computed tomography angiography using low tube voltage of 80 kV in subjects with normal body mass indices: comparative study using 120 kV," (in eng), *Acta Radiol*, vol. 53, no. 10, pp. 1099-106, 2012.
- [15] F. Zhang *et al.*, "Feasibility study of low tube voltage (80 kVp) coronary CT angiography combined with contrast medium reduction using iterative model reconstruction (IMR) on standard BMI patients," (in eng), *Br J Radiol*, vol. 89, no. 1058, p. 20150766, 2016.

## 5.2 Manuscript

This section is written in a manuscript version as to be submitted to *Journal of Cardiovascular Computed Tomography (JCCT)*.

**Title:** Optimisation of iterative reconstruction strengths in a low tube voltage coronary CT angiography using a 3D-printed cardiac insert phantom

**Authors:** Kamarul Amin Abdullah<sup>1,2</sup>, Mark F McEntee<sup>1</sup>, Warren Reed<sup>1</sup>, Peter L Kench<sup>1</sup>

**Affiliations:** 1. Discipline of Medical Radiation Sciences, Faculty of Health Sciences, The University of Sydney, New South Wales, Australia.

2. Centre of Medical Imaging, Faculty of Health Sciences, Universiti Sultan Zainal Abidin, Terengganu, Malaysia.

### 5.2.1 Abstract

**Objective:** The purpose of this study was to investigate the optimal IR algorithm strength for low tube voltage CCTA protocols using a phantom-based methodology and validate the image quality characteristics with retrospective patient CCTA datasets.

**Methods:** A 3D-printed cardiac insert that was placed in the Lungman phantom and Catphan<sup>®</sup> 500 phantom were scanned using CCTA protocols at 120 kVp and 100 kVp tube voltages. All image datasets were reconstructed with FBP and ASIR algorithm at 40% and 60%. HU values, image noise, SNR, CNR, high spatial resolution, and low contrast resolution were reported and analysed. A total of 27 series of patient image datasets were retrospectively retrieved from a local database of the same CT workstation. The

measurement of agreement of the image quality characteristics between patient and phantom datasets were compared.

**Results:** There was a significant interaction between the effects of low tube voltage and IR algorithm strengths on image noise, SNR, and CNR (all  $p < 0.001$ ) but not HU values. Image noise of the image datasets of the 120 kVp FBP versus 100 kVp ASIR 60% ( $16.6 \pm 3.8$  vs  $16.7 \pm 4.8$ ), SNR of 120 kVp ASIR 40% versus 100 kVp ASIR 60% ( $27.3 \pm 5.4$  vs  $26.4 \pm 4.8$ ), and CNR of 120 kVp FBP versus 100 kVp ASIR 40% ( $31.3 \pm 3.9$  vs  $30.1 \pm 4.3$ ) were not significantly different (all  $P > 0.05$ ). For the modulation transfer function (MTF), there was a minimal change of image quality ( $< 10\%$ ) for each tube voltage but increases ( $> 10\%$ ) when higher strengths of ASIR were used. For low contrast detectability, the highest was seen at ASIR 60% at 120 kVp. The mean differences of image quality characteristics were small between the patient datasets and the 3D-printed cardiac insert phantom.

**Conclusion:** This phantom-based methodology study incorporating a novel 3D-printed cardiac insert demonstrated that the radiation dose could be substantially reduced up to 57% with the use of 100 kVp and ASIR 60% in CCTA examinations. This combination yielded comparable image quality noise characteristics to the standard CCTA protocols using 120 kVp of ASIR 40%.

**Keywords:** CT image reconstruction, 3D printing, phantom, dose reduction, image quality

## 5.2.2 Introduction

CCTA has emerged as a powerful diagnostic tool for diagnosing CAD [1-3]. With the increasing number of MSCT scanners worldwide, the volume of CCTA scans performed is likely to increase. CCTA contributes to the overall burden of medical radiation exposure,



although the radiation-induced cancer risks are relatively small versus the benefits of its diagnostic information [4, 5]. In a previous multi-centre study [6], the authors reported an average effective dose of 12 mSv associated with CCTA and demonstrated a wide variation (5-30 mSv) among participating centres. Accordingly, strategies to obtain diagnostic CCTA images with as low as reasonably achievable (ALARA) radiation dose need to be developed. The current strategy that has become a particular interest among many researchers is the use of a low tube voltage.

CCTA is usually performed with a tube voltage of 120 kVp [7-9]. Scanning acquisitions at a low tube voltage of 100 kVp has been suggested as an effective way to reduce radiation dose in non-obese patients while maintaining the image quality [10, 11]. The low tube voltage helps to enhance coronary vessels as a result of the increased attenuation of iodinated contrast material [12, 13]. However, the low tube voltage can also deteriorate the image quality by increasing noise and beam hardening artifacts [14]. The tube current settings can compensate the increment of noise, [12] but this method produces additional radiation dose to the patients. Consequently, IR algorithms are used.

An IR algorithm is an effective method of reducing radiation exposure while maintaining the image quality [15, 16]. Currently, FBP has been widely used but contains inherent limitations of increasing image noise and producing artifacts at reduced exposure factors [17]. IR algorithms provide noise reduction when the exposure factors are reduced [18]. They also offer a wide selection of strength levels that represents the power of noise reduction [19, 20]. Depending on the type of the IR algorithms, increasing strengths of the IR algorithm may also result in “blooming” artifacts that typically affect the visualisation of small structures [21]. As a result, the process of increasing the IR algorithm strengths must

be carefully considered to balance with the impact on the image quality. We previously have described the use of our 3D-printed cardiac insert phantom for evaluating the effect of IR algorithm and increasing its strength levels on image quality and as dose reduction potential [22]. Therefore, the purpose of this study was to investigate the optimal IR algorithm strengths for a low tube voltage of 100 kVp at CCTA protocols using a phantom-based methodology, incorporating a 3D-printed cardiac insert phantom, and validate the resultant noise image quality characteristics with relevant patient datasets.

### **5.2.3 Materials and Methods**

#### *5.2.3.1 Phantoms*

Two phantoms were used in this present study; (i) 3D-printed cardiac insert phantom, and a (ii) Catphan<sup>®</sup> 500 (The Phantom Laboratory, Greenwich, NY, USA) phantom (see Figure 5.1). The 3D-printed cardiac insert phantom, simulating the contrast-enhanced region of the ascending aorta and coronary vessels in CCTA, was constructed using 3D printing technology and placed within an anthropomorphic chest phantom (Lungman N-01, Kyoto Kagaku Co., Ltd., Kyoto, Japan). We previously have described the development of the 3D-printed cardiac insert phantom [22]. The contrast medium used was Ultravist 370 (Schering Health Care Ltd, Burgess Hill, UK). For the Catphan<sup>®</sup> 500 phantom, two modules of CTP528 and CTP515 were included. The modules were used to assess the axial spatial resolution and the performance of low contrast detectability.

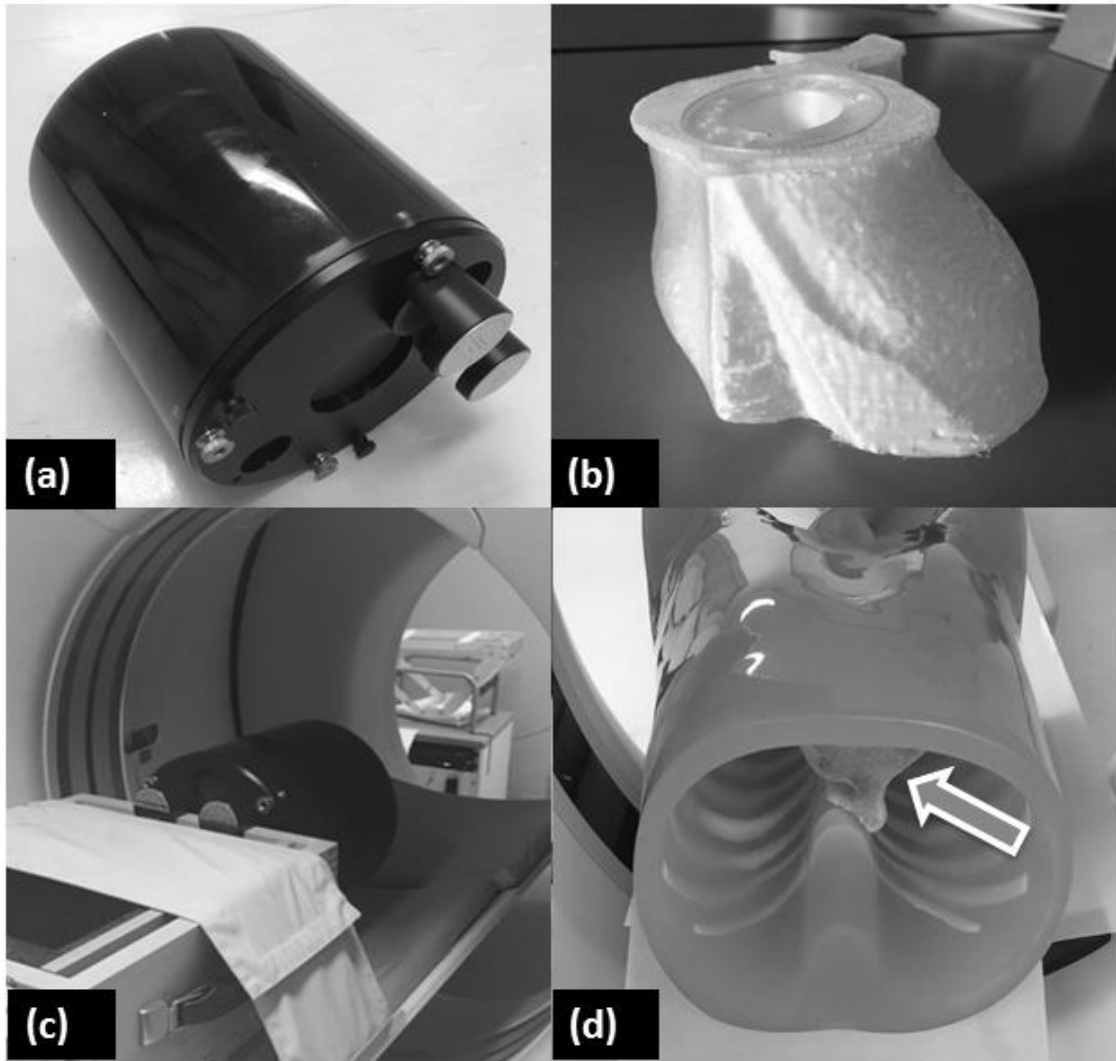


Figure 5.1: (a) The Catphan® 500 phantom (The Phantom Laboratory, Greenwich, NY, USA); (b) The 3D-printed cardiac insert phantom; (c) The Catphan® 500 phantom was positioned on the scanner table; and (d) The anthropomorphic chest phantom (Lungman N-01, Kyoto Kagaku, Japan), with the 3D-printed cardiac insert phantom positioned within (arrow), was placed on the scanner table.

### 5.2.3.2 Acquisition and reconstruction

The 3D-printed cardiac insert phantom was positioned within the Lungman phantom. The Lungman and the Catphan® 500 phantoms were scanned using 64-slice SPECT/CT scanner (Discovery 570c, GE Healthcare, Milwaukee, WI, USA). Both phantoms were scanned at 120 kVp and 100 kVp tube voltages with auto mA settings resulting two

CT dose indices volume (CTDI<sub>vol</sub>) of 4.27 mGy and 1.82 mGy, respectively. For the IR algorithm, the adaptive statistical iterative reconstruction (ASIR) (GE Healthcare, Milwaukee, WI, USA) was used. Three different strengths were investigated: ASIR 0% (FBP), ASIR 40%, and ASIR 60%. The 120 kVp with the ASIR 40% is the standard tube voltage and IR strength level used in the current local CCTA protocols. Table 5.1 shows the summary of CT parameters and reconstruction settings used in this present study.

Table 5.1: Summary of CT parameters and reconstruction settings.

<b>Parameters</b>	
Collimation (mm)	64 x 0.625
Tube current (mA)	Auto
Tube voltage (kVp) (CTDI <sub>vol</sub> (mGy))	120 (4.27), 100 (1.82)
Reconstruction settings	FBP, ASIR 40%, ASIR 60%

### 5.2.3.3 Image quality assessment

For the 3D-printed cardiac insert phantom, image quality was determined using ImageJ software (v1.46r, National Institutes of Health, Bethesda, MD, USA, <http://imagej.nih.gov/ij/>), while for the Catphan® 500 phantom, the AutoQA Lite™ program (v3.1.5.7, Iris QA, LLC, Maryland, USA) was used.

The attenuation values (Hounsfield Units, HU) and the image noise were measured by placing a region of interest (ROI) within the contrast-enhanced region simulating the ascending aorta included in the 3D-printed cardiac insert phantom (Figure 5.2(a)). The signal-noise ratio (SNR) and the contrast-noise ratio (CNR) were calculated according to equations (1) and (2) respectively. The CNR was obtained by using the HU values and

image noise of the contrast material (CM) and the oil to simulate the myocardial fat in the equation (2) (Figure 5.2(b)).

$$\text{SNR} = \frac{\text{HU}_{\text{cm}}}{\sigma_{\text{cm}}} \quad (\text{Eq. 1})$$

$$\text{CNR} = \frac{\text{HU}_{\text{cm}} - \text{HU}_{\text{oil}}}{(\sigma_{\text{cm}} + \sigma_{\text{oil}})/2} \quad (\text{Eq. 2})$$

The axial spatial resolution was measured using the images obtained from the CTP528 module of Catphan® 500 phantom. First, the point spread function (PSF) was calculated from the scan of a small tungsten carbide bead (approximately 250 microns in diameter) (Figure 5.2(c)). Next, the line spread functions (LSF) were determined by integrating the PSF along vertical and horizontal directions. Last, the modulation transfer function (MTF) was calculated from the discrete Fourier Transform of the LSF datasets. The MTF values were automatically calculated by the AutoQA Lite™ program with the output measures of MTF<sub>50%</sub>, MTF<sub>10%</sub>, and MTF<sub>2%</sub>.

The axial spatial resolution was measured using the images obtained from the CTP528 module of Catphan® 500 phantom. First, the point spread function (PSF) was calculated from the scan of a small tungsten carbide bead (approximately 250 microns in diameter) (Figure 5.2(c)). Next, the line spread functions (LSF) were determined by integrating the PSF along vertical and horizontal directions. Last, the modulation transfer function (MTF) was calculated from the discrete Fourier Transform of the LSF datasets. The MTF values were automatically calculated by the AutoQA Lite™ program with the output measures of MTF<sub>50%</sub>, MTF<sub>10%</sub>, and MTF<sub>2%</sub>.

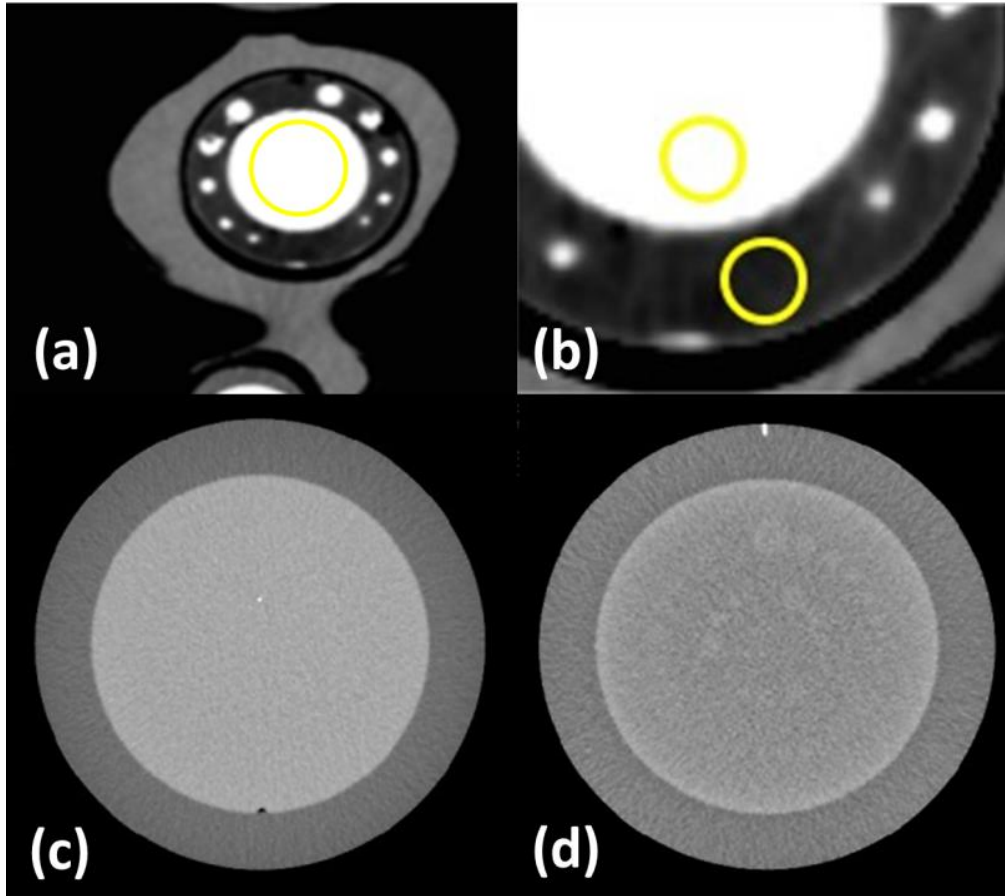


Figure 5.2: (a) To measure noise an ROI was placed within the contrast-enhanced region of the 3D-printed cardiac insert phantom simulating the ascending aorta. (b) Two similar sizes of ROIs were placed to measure CNR between the contrast material (the ascending aorta) and the oil (fat). (c) The CTP528 module of Catphan® 500 phantom was used for the evaluation of MTF (axial spatial resolution). (d) The CTP515 module of Catphan® 500 phantom was used for the evaluation of low contrast resolution.

#### 5.2.3.4 Patient datasets

The local ethics committee approved the study in July 2017 (Appendix 2). Nine patients with suspected or known CAD who had CCTA imaging in August 2017 were randomly selected. The CCTA patient image datasets were retrieved from the same CT systems used to perform acquisitions of the two previously described phantom acquisitions. Three male and six female patients with a mean age of  $61 \pm 7$  years old were included in the CCTA image dataset. The datasets were then exported to the 3D

reconstruction settings. All image datasets retrieved were scanned using CCTA protocols with tube voltage of 120 kVp.

The image datasets were reconstructed using three different strengths of IR algorithm; 0% (FBP), ASIR 40%, and ASIR 60%. The image noise, defined as the standard deviation, was measured by placing the ROI within the ascending aorta. The SNR and CNR were measured by using the same equations that were described previously. Results were compared to the analysis of the 3D-printed cardiac insert phantom image datasets using CCTA protocols with tube voltage of 120 kVp.

Data analyses were carried out using Statistical Package for the Social Science (SPSS, version 21; IBM Corp., New York, NY, USA). Descriptive statistics, e.g., mean and standard deviation, were calculated. Image noise, SNR and CNR values were tested for normality by the Shapiro-Wilk test. The Analysis of variances test was used to examine the differences between image noise, SNR, and CNR.

## **5.2.4 Results**

### *5.2.4.1 Image noise, SNR, CNR and resolution*

There were a significant differences between the measures of image noise, SNR, and CNR (all  $P < 0.001$ ) for IR strengths and the tube voltage, but not for HU (Table 5.2). The simple main effect analysis showed that SNR and CNR of the image datasets of ASIR 40% and ASIR 60% were significantly higher than FBP, regardless of the tube voltage. The image noise was significantly lower for the image datasets of 120 kVp tube voltage as compared to the 100 kVp, whereas the SNR and CNR were significantly higher (all  $P < 0.001$ , Table 5.2). The image datasets of ASIR 60% with 120 kVp resulted in the lowest image noise and

the highest SNR and CNR ( $P < 0.05$ ), whereas the FBP with 100 kVp protocol showed the highest image noise and the lowest SNR and CNR. There was no significant difference in HU values between the image datasets of the 120 kVp and 100 kVp. Image noise of the image datasets of the 120 kVp FBP versus 100 kVp ASIR 60% ( $16.6 \pm 3.8$  vs  $16.7 \pm 4.8$ ), SNR of 120 kVp ASIR 40% versus 100 kVp ASIR 60% ( $27.3 \pm 5.4$  vs  $26.4 \pm 4.8$ ), and CNR of 120 kVp FBP versus 100 kVp ASIR 40% ( $31.3 \pm 3.9$  vs  $30.1 \pm 4.3$ ) were not significantly different (all  $P > 0.05$ , Figure 5.3).

Table 5.2: Results of HU, image noise, SNR, and CNR of the 3D-printed cardiac insert phantom between 120 kVp and 100 kVp.

Parameter	120 kVp				100 kVp			
	FBP	ASIR 40%	ASIR 60%	<i>P</i> - value	FBP	ASIR 40%	ASIR 60%	<i>P</i> - value
	mean $\pm$ SD	mean $\pm$ SD	mean $\pm$ SD		mean $\pm$ SD	mean $\pm$ SD	mean $\pm$ SD	
CT number (HU)	407.9 $\pm$ 6.4	408.0 $\pm$ 6.5	408.0 $\pm$ 6.5	NS	421.0 $\pm$ 5.6	421.0 $\pm$ 5.6	421.0 $\pm$ 5.6	NS
Image noise	16.6 $\pm$ 3.8	13.5 $\pm$ 4.2	12.1 $\pm$ 4.3	<0.001	23.7 $\pm$ 4.1	18.9 $\pm$ 4.6	16.7 $\pm$ 4.8	<0.001
Signal-noise ratio	21.7 $\pm$ 3.5	27.3 $\pm$ 5.4	30.9 $\pm$ 6.8	<0.001	18.1 $\pm$ 2.3	23.1 $\pm$ 3.7	26.4 $\pm$ 4.8	<0.001
Contrast-noise ratio	31.3 $\pm$ 3.9	38.9 $\pm$ 5.7	43.8 $\pm$ 7.1	<0.001	23.9 $\pm$ 2.8	30.1 $\pm$ 4.3	34.3 $\pm$ 5.4	<0.001

FBP, filtered back projection; HU, Hounsfield unit; IR, iterative reconstruction; SD, standard deviation



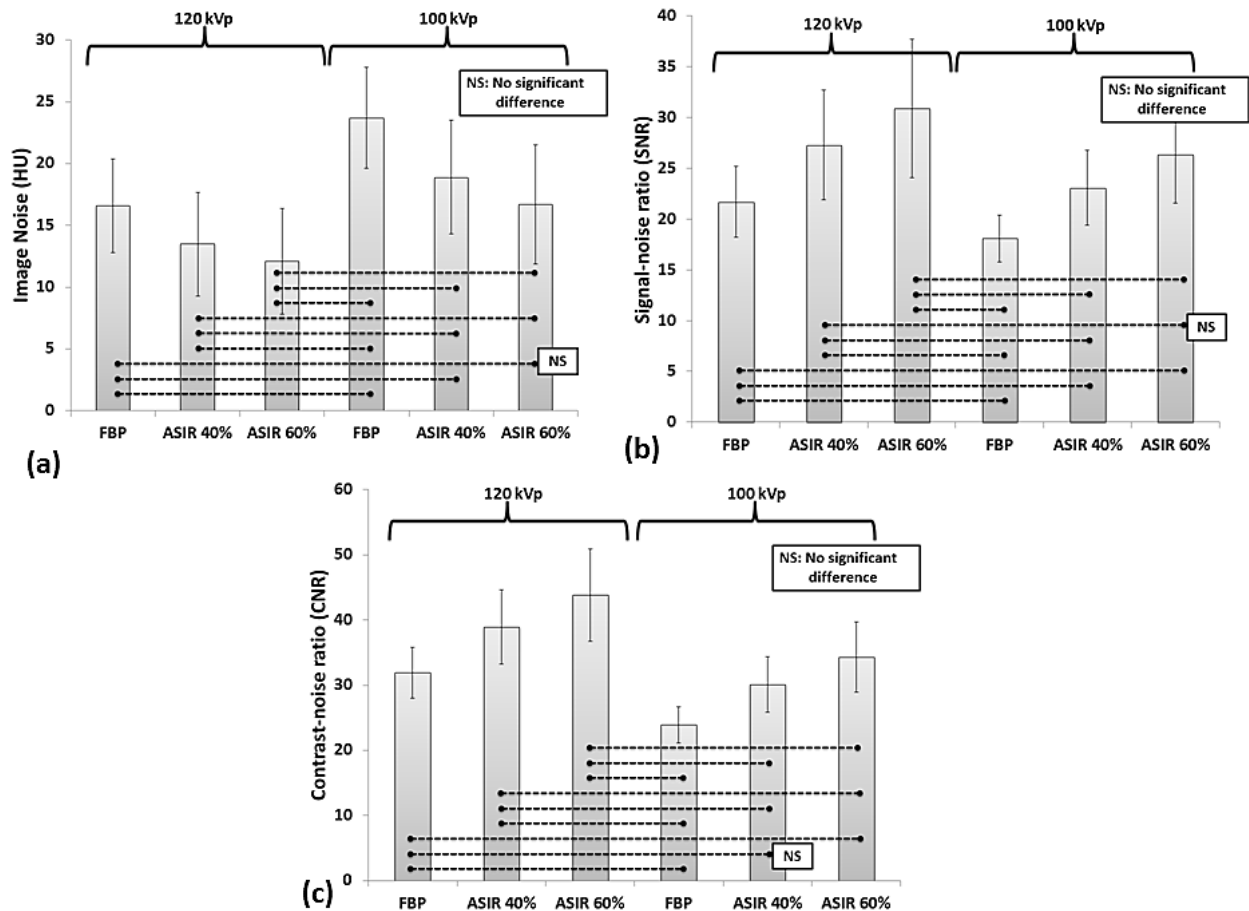


Figure 5.3: Bar graphs demonstrate significant differences in image noise (a), SNR (b), and CNR (c) (all  $P < 0.05$ ) between the 120-kVp and the 100-kVp. No significant differences of 120 kVp FBP versus 100 kVp ASIR 60% for image noise, 120 kVp ASIR 40% versus 100 kVp ASIR 60% for SNR, and 120 kVp FBP versus 100 kVp ASIR 40% for CNR. The 120-kVp series reconstructed with ASIR 60% provided the lowest image noise and highest SNR and CNR ( $P < 0.05$ ), whereas 100-kVp series reconstructed with FBP showed the highest image noise and lowest SNR and CNR.

Table 5.3 shows the results of MTF obtained with the Catphan® 500 phantom when the strengths of IR algorithm were increased. For both tube voltages, the spatial frequency of MTF was mildly affected by the reconstruction levels (variation  $< 10\%$ ). As a result, there was a minimal change in the image quality. However, between 120 kVp and 100 kVp protocols, the spatial frequency of MTF was strongly affected (variation  $> 10\%$ ), indicating changes in the image quality.

Table 5.3: Results of *modulation transfer function*, MTF at 120 kVp and 100 kVp.

Tube voltage (kVp)	Reconstruction settings	MTF 50% (lp mm-1)	MTF 10% (lp mm-1)	MTF 2% (lp mm-1)
120	FBP	0.416	0.659	0.806
	ASIR 40%	0.411	0.699	0.850
	ASIR 60%	0.414	0.720	0.888
100	FBP	0.370	0.702	0.804
	ASIR 40%	0.307	0.693	0.817
	ASIR 60%	0.297	0.686	0.840

Figure 5.4 illustrates the behaviour of low contrast resolution for different strengths of IR algorithm at 120 kVp and 100 kVp. The low contrast object diameter range was 3 to 15 mm for both tube voltages and at all reconstruction settings. From the graph, the image datasets reconstructed with FBP at 100 kVp required the highest contrast to detect the smallest size of object diameter of 3 mm and decreases as the object size diameter increases, i.e. the FBP at 100 kVp has the lowest contrast resolution among the others. The ASIR 60% at 100 kVp has a higher contrast resolution for the small object diameter than the FBP at 120 kVp. The highest contrast resolution was the ASIR 60% at 120 kVp.

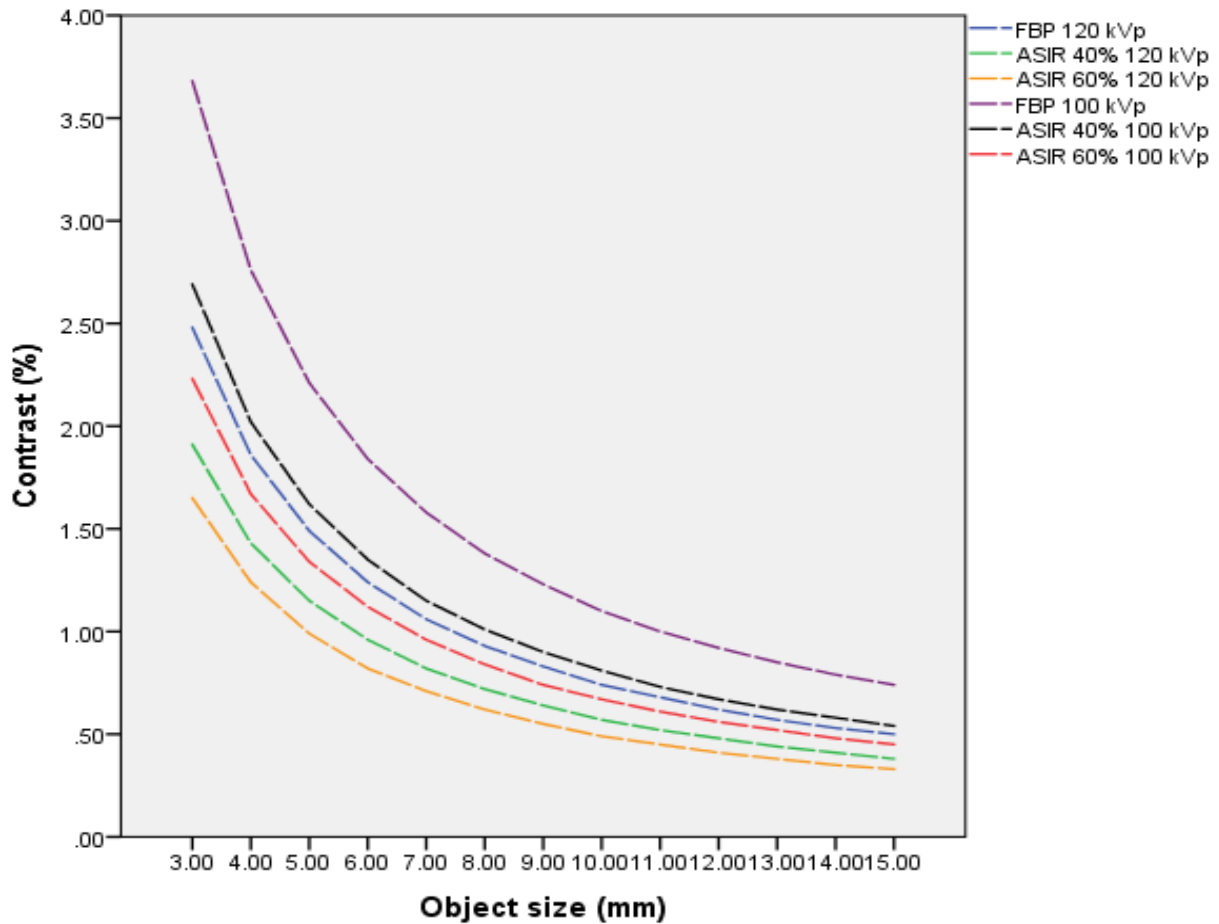


Figure 5.4: Results of low contrast resolution using CTP515 module of Catphan® 500.

#### 5.2.4.2 Measurement of agreement

The mean differences in the measured image noise, SNR, and CNR, which are an estimate of agreement, were small between the 3D-printed cardiac insert phantom and patient (image noise: difference,  $11.9 \pm 3.8$  HU; 95% CI, 10.4 to 13.4 HU; limits of agreement, 4.7 and 19.1 HU, signal-noise ratio (SNR): difference,  $-9.6 \pm 5.0$ ; 95% CI, -11.6 to -7.6; limits of agreement, -19.5 and 0.2, and contrast-noise ratio (CNR): difference,  $-16.7 \pm 6.3$ ; 95% CI, -19.2 to -14.2; limits of agreement, -29.2 and -4.2)(see Figure 5.5).

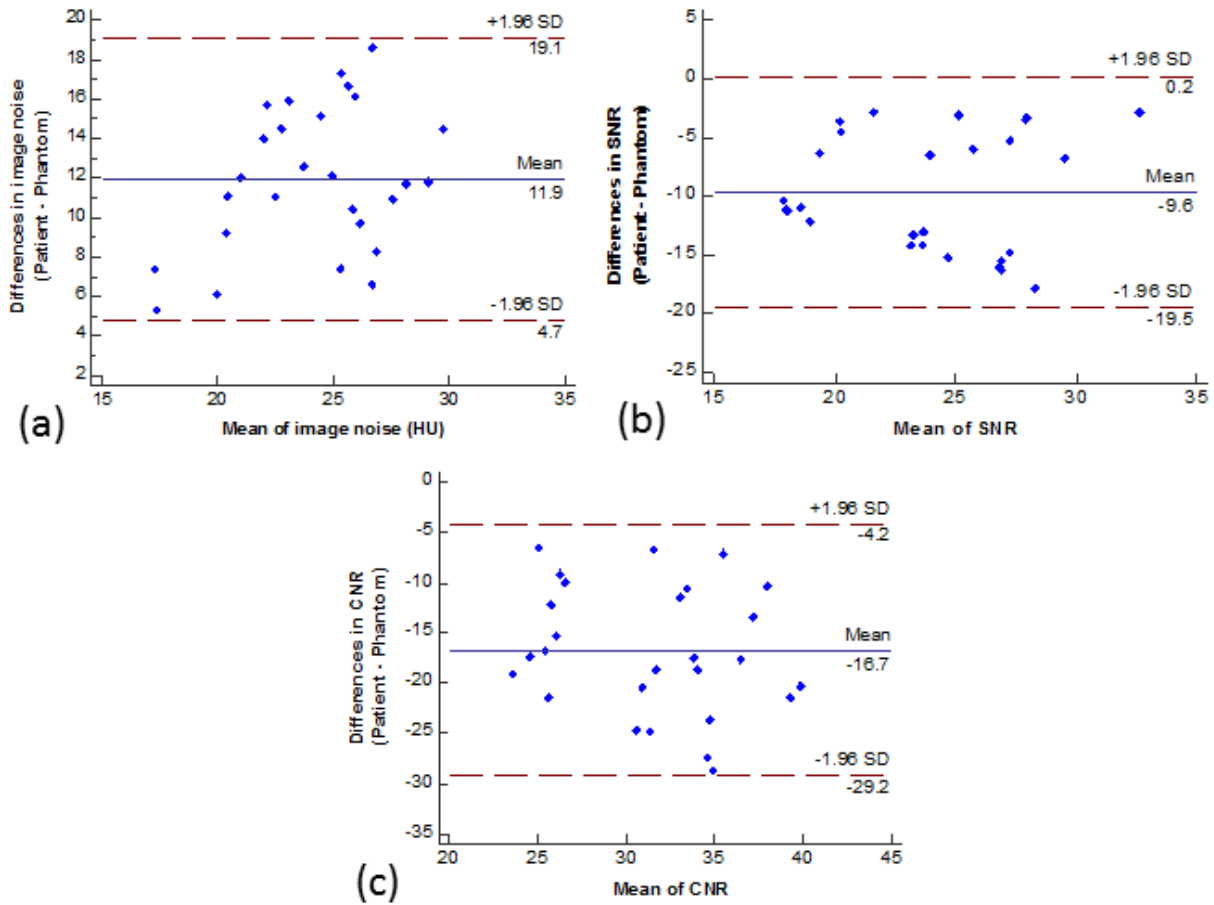


Figure 5.5: Bland-Altman plot. Differences in measured a) image noise, b) signal-noise ratio (SNR), and c) contrast-noise ratio (CNR) between the 3D-printed cardiac insert phantom and patient. Dotted lines delineate limits of agreement between two datasets.

## 5.2.5 Discussion

The results of this phantom-based methodology, incorporating the 3D-printed cardiac insert phantom, showed that the ASIR 60% with a low tube voltage of 100 kVp has produced comparable image quality noise characteristics to the current local CCTA protocols of 120 kVp and ASIR 40%. Consequently, the radiation dose has been reduced by more than half. In a previous systematic review by Abdullah et al. [23], the authors concluded that using an IR algorithm allows up to 41% dose reduction as compared to FBP while maintaining similar image quality. However, our study showed that a 57% dose

reduction was achieved when combined with the lower tube voltage. Our findings revealed that although the IR algorithm is already a powerful tool to reduce dose, the higher IR strengths at a lower tube voltage of 100 kVp has resulted in further dose reduction.

The IR algorithm is claimed to maintain, or in some cases improve, CT image quality while allowing reduced dose to the patient [24, 25]. The IR algorithm works by reducing image noise when using lower CT exposure factors. The power of noise reduction is strongly related to the IR algorithm strengths used during image reconstruction [26-28]. The higher strengths usually produce better image quality noise characteristics. However, overly increasing the strengths may also degrade the image quality characteristics. For example, a previous study by Kroepil et al. [27] reported that compared to FBP, CT images reconstructed using the highest IR strength may appear more 'blotchy' with loss of granular image appearances mainly due to a smoothing effect. Therefore, the appropriate IR algorithm strengths have to be carefully considered to prevent poor image quality and lower diagnostic value. Our study has shown that the ASIR 60% at 100 kVp was comparable the image quality compared to the current protocols of ASIR40% at 120 kVp and thus, resulting in a dose reduction to the patient. Demonstrating again, that image optimisation result acquired from this type of bespoke phantom are comparable to those reported in the literature. This opens up a new field of phantom design, allow the researcher to design a phantom for a specific research question without having to rely only on commercially available phantoms.

Our study adds to existing data by investigating the combination of higher IR algorithms strengths and low tube voltage at CCTA using two phantoms; 3D-printed cardiac insert and Catphan® 500 phantoms. These phantoms allow us to adequately

evaluate all possible image quality noise characteristics such as image noise, SNR, CNR, high spatial resolution, and low contrast resolution. The results derived from the acquisitions with phantoms were similar to those in the patient datasets where the mean differences to estimate agreement were small. Consequently, the 3D-printed cardiac phantom in conjunction with Catphan® 500 phantom can be used as a tool for dose optimisation in clinical CCTA studies.

Several limitations of our study merit consideration. First, this investigation was conducted at a single centre using a 64-slice CT scanner and thus, the results may not be applicable to other institutions where different types of CT scanners (e.g., 128 or 320-slice), protocols, and IR algorithms settings are used. However, the results could provide an opportunity for other researchers to implement similar studies at their centre to assess optimum protocols. Second, all scans were performed on the phantoms without cardiac motion. Cardiac motion is an important factor in CCTA examination that could produce artifacts and deteriorate the image quality. Therefore, we are planning to develop a heart-beating cardiac insert phantom in the future that may better simulate CCTA images. Third, the subjective image quality was not assessed by the clinical observers which would support the findings. Last, a small number of patients were included in this study. Therefore, in future studies, a larger cohort may be required to improve the accuracy of results.

In conclusion, this phantom-based study demonstrated that radiation dose could be substantially reduced with the use of ASIR 60% at 100 kVp of low tube voltage. This combination yielded a comparable noise image quality characteristics with a 57% reduction in  $CTDI_{vol}$  compared with the current local protocol using 120 kVp of ASIR 40%.

Therefore, the optimisation of IR algorithm settings in low tube voltage CCTA protocols using this phantom-based methodology is possible and a 3D-printed cardiac insert phantom can be used as part of CCTA protocol dose optimisations strategy.

## 5.2.6 References

- [1] T. F. Jakobs *et al.*, "Multislice helical CT of the heart with retrospective ECG gating: reduction of radiation exposure by ECG-controlled tube current modulation," *Eur Radiol*, vol. 12, no. 5, pp. 1081-6, May 2002.
- [2] S. Achenbach, C. M. Kramer, W. A. Zoghbi, and V. Dilsizian, "The year in coronary artery disease," *JACC Cardiovasc Imaging*, vol. 3, no. 10, pp. 1065-77, Oct 2010.
- [3] A. M. Ajlan, B. G. Heilbron, and J. Leipsic, "Coronary computed tomography angiography for stable angina: past, present, and future," *Can J Cardiol*, vol. 29, no. 3, pp. 266-74, Mar 2013.
- [4] M. Dewey, E. Zimmermann, M. Laule, W. Rutsch, and B. Hamm, "Three-vessel coronary artery disease examined with 320-slice computed tomography coronary angiography," *Eur Heart J*, vol. 29, no. 13, p. 1669, Jul 2008.
- [5] F. J. Rybicki *et al.*, "Initial evaluation of coronary images from 320-detector row computed tomography," *The International Journal of Cardiovascular Imaging*, vol. 24, no. 5, pp. 535-546, 2008.
- [6] J. Hausleiter *et al.*, "Estimated radiation dose associated with cardiac CT angiography," *Journal of the American Medical Association*, vol. 301, pp. 500-507, 2009.

- [7] J. Ripsweden *et al.*, "Impact on image quality and radiation exposure in coronary CT angiography: 100 kVp versus 120 kVp," *Acta Radiologica*, vol. 51, no. 8, pp. 903-909, 2010.
- [8] E.-A. Park, W. Lee, J.-H. Kang, Y. H. Yin, J. W. Chung, and J. H. Park, "The image quality and radiation dose of 100-kVp versus 120-kVp ECG-gated 16-slice CT coronary angiography," *Korean journal of radiology*, vol. 10, no. 3, pp. 235-243, 2009.
- [9] K. Matsumoto, M. Jinzaki, Y. Tanami, A. Ueno, M. Yamada, and S. Kuribayashi, "Virtual monochromatic spectral imaging with fast kilovoltage switching: improved image quality as compared with that obtained with conventional 120-kVp CT," *Radiology*, vol. 259, no. 1, pp. 257-262, 2011.
- [10] C. H. Park, J. Lee, C. Oh, K. H. Han, and T. H. Kim, "The feasibility of sub-millisievert coronary CT angiography with low tube voltage, prospective ECG gating, and a knowledge-based iterative model reconstruction algorithm," *Int J Cardiovasc Imaging*, vol. 31 Suppl 2, pp. 197-203, Dec 2015.
- [11] G. Sun *et al.*, "Application of low tube voltage coronary CT angiography with low-dose iodine contrast agent in patients with a BMI of 26-30 kg/m<sup>2</sup>," *Clinical radiology*, vol. 70, no. 2, pp. 138-145, 2015.
- [12] T. Nakaura *et al.*, "Abdominal Dynamic CT in Patients with Renal Dysfunction: Contrast Agent Dose Reduction with Low Tube Voltage and High Tube Current-Time Product Settings at 256-Detector Row CT," *Radiology*, vol. 261, no. 2, pp. 467-476, 2011.
- [13] K. T. Bae, "Intravenous Contrast Medium Administration and Scan Timing at CT: Considerations and Approaches," *Radiology*, vol. 256, no. 1, pp. 32-61, 2010.



- [14] A. R. Seyal, A. Arslanoglu, S. F. Abboud, A. Sahin, J. M. Horowitz, and V. Yaghmai, "CT of the Abdomen with Reduced Tube Voltage in Adults: A Practical Approach," *RadioGraphics*, vol. 35, no. 7, pp. 1-17, 2015.
- [15] C. H. McCollough, A. N. Primak, N. Braun, J. Kofler, L. F. Yu, and J. Christner, "Strategies for Reducing Radiation Dose in CT," *Radiologic Clinics of North America*, vol. 47, no. 1, pp. 27-+, 2009.
- [16] A. Ploussi *et al.*, "Evaluation of Radiation Exposure Reduction using Hybrid Iterative Reconstruction Algorithm in Chest-Abdomen-Pelvis CT," *Journal of Radiology and Diagnostic Imaging*, vol. 1, no. 2, pp. 40-44, 2013.
- [17] M. Q. Hu, M. Li, Z. Y. Liu, M. P. Huang, H. Liu, and C. H. Liang, "Image quality evaluation of iterative model reconstruction on low tube voltage (80 kVp) coronary CT angiography in an animal study," *Acta Radiol*, vol. 57, no. 2, pp. 170-7, Feb 2016.
- [18] J. B. Thibault, K. D. Sauer, C. A. Bouman, and J. Hsieh, "A three-dimensional statistical approach to improved image quality for multislice helical CT," *Med Phys*, vol. 34, no. 11, pp. 4526-44, Nov 2007.
- [19] A. D. Hardie, R. M. Nelson, R. Egbert, W. J. Rieter, and S. V. Tipnis, "What is the preferred strength setting of the sinogram-affirmed iterative reconstruction algorithm in abdominal CT imaging?," *Radiol Phys Technol*, vol. 8, no. 1, pp. 60-3, Jan 2015.
- [20] S. Gordic *et al.*, "Optimizing radiation dose by using advanced modelled iterative reconstruction in high-pitch coronary CT angiography," *Eur Radiol*, vol. 26, no. 2, pp. 459-68, Feb 2016.

- [21] L. Liu, "Model-based Iterative Reconstruction: A Promising Algorithm for Today's Computed Tomography Imaging," *Journal of Medical Imaging and Radiation Sciences*, vol. 45, no. 2, pp. 131-136, 2014.
- [22] K. A. Abdullah, M. F. McEntee, W. Reed, and P. L. Kench, "Using 3D printed cardiac CT phantom for dose reduction and diagnostic image quality assessment," in *12th Annual Scientific Meeting of Medical Imaging and Radiation Therapy (ASMMIRT)*, Perth, Western Australia, 2017.
- [23] K. A. Abdullah, M. F. McEntee, W. Reed, and P. L. Kench, "Radiation dose and diagnostic image quality associated with iterative reconstruction in coronary CT angiography: A systematic review," *J Med Imaging Radiat Oncol*, vol. 60, no. 4, pp. 459-68, Aug 2016.
- [24] M. L. Aurumskjold, K. Ydstrom, A. Tingberg, and M. Soderberg, "Improvements to image quality using hybrid and model-based iterative reconstructions: a phantom study," *Acta Radiol*, vol. 58, no. 1, pp. 53-61, Jan 2017.
- [25] M. S. Bittencourt *et al.*, "Iterative reconstruction in image space (IRIS) in cardiac computed tomography: initial experience," *Int J Cardiovasc Imaging*, vol. 27, no. 7, pp. 1081-7, Oct 2011.
- [26] C. Ghetti, F. Palleri, G. Serreli, O. Ortenzia, and L. Ruffini, "Physical characterization of a new ct iterative reconstruction method operating in sinogram space," *Journal of Applied Clinical Medical Physics*, vol. 14, no. 4, pp. 263-271, 2013.
- [27] P. Kroepil, A. H. Bigdeli, H. D. Nagel, G. Antoch, and M. Cohnen, "Impact of increasing levels of advanced iterative reconstruction on image quality in low-dose cardiac CT angiography," *Rofo*, vol. 186, no. 6, pp. 567-575, 2014.

- [28] D. Utsunomiya, W. G. Weigold, G. Weissman, and A. J. Taylor, "Effect of hybrid iterative reconstruction technique on quantitative and qualitative image analysis at 256-slice prospective gating cardiac CT," *Eur Radiol*, vol. 22, no. 6, pp. 1287-94, Jun 2012.

## **CHAPTER 6 Discussion, limitations, future investigations, and conclusions**

## 6.1 Discussion

From this research, a novel design cardiac insert phantom was developed using 3D printing technology and its application for optimising CCTA protocols investigated. In this section, a summary of the findings and their clinical implications are discussed in the light of the role of a 3D-printed cardiac insert phantom in CCTA dose optimisation studies using an IR algorithm as the dose optimisation strategy. This work is discussed with regards to the three research aims of the experimental studies outlined in chapters three, four, and five of this thesis.

The first study, in chapter three, of the thesis is outlined development and initial assessment of a novel design of 3D-printed cardiac insert phantom for an anthropomorphic chest phantom or Lungman, including the associated 3D printing methodology. Presently, the most widely used phantoms in CCTA dose optimisation studies are quality assurance phantoms such as the Catphan<sup>®</sup> phantoms (The Phantom Laboratory) [1-3] and ACR phantom (American College of Radiology) [4, 5]. These phantoms are comprehensive and serve well for CT image quality assessment. However, their shape could be improved to produce relevant CCTA images to include the surrounding structures such as bone, soft tissue, and muscles. These structures and their locations can inherently affect the image quality due to beam hardening effects [6, 7]. Therefore, in this study, the anthropomorphic chest phantom was used. The anthropomorphic chest phantom or Lungman is also widely used in many CT dose optimisation studies [8, 9] but in CCTA, this phantom is lacking due to insufficient heart features to resemble CCTA images. The design of the new cardiac insert phantom for the Lungman and the ability of 3D printing to duplicate the heart size with relevant features make it more suitable for CCTA dose optimisation studies.

Although 3D printing is able to produce a high quality printed phantom in a rapid manner, but the initial stage of getting the appropriate settings is cumbersome. Many previous studies have indicated that numerous trials were taken to produce high quality printed objects despite the printer settings have been pre-set by the suppliers [10, 11]. With respect to the fused deposition modelling 3D printer that was used in this study, many factors had to be considered, i.e. the printing platform temperature, the cooling fan speed, the nozzle size opening, the printer speed, the printing resolution and the thickness of layers. In addition,, the process of improving the models, e.g. minimising the surface errors, using the computer-aided design software added more time and effort to 3D printing process. However, in this study, the details of the print settings used have been shared in Table 3.1 and the softcopy link of the model is embedded in the appendix 3. Other researchers who wish to perform similar investigations can download the cardiac 3D model and test the printer settings on their 3D printer. The printer settings would need to adjust as different printers may have different impact on the output but providing an existing model and initial settings reduce could reduce the development time for other investigators.

Another issue when developing the phantom is the cost required. Although the expense of commercial phantoms is justified due to their longevity and reusability, their high cost of may be a barrier for some researchers. In this study, a rigorous cost analysis was not performed, but the total of phantom production can be considered as cost-effective. The 3D printer and the printing materials are the largest cost contributed during the production. It is estimated that the cost of the fused deposition modelling 3D printer is less than USD5,000 [12, 13]. The amount is considered appropriate since the printer can be

used numerous times and could last a long time if well-maintained. The printing materials are consumable products. There are various types of printing materials available such as PLA, ABS, and lay bricks. The cost for these types of materials can vary from USD10 to USD160 per kilogram [14]. As indicated in the chapter three, in total, the cost for printing materials and internal materials was USD70. If the phantom lasts for 6 months, and a new phantom is to be developed every 6 months, the total for a year will be \$140 for a year.

3D printing technology is also commonly used to produce phantoms in clinical nuclear medicine [15-17]. The phantoms have been manufactured in a shell or empty space similar to our phantom development technique but they have been filled with water and radionuclide. A study by Gear et al. [18], for example, investigated a 3D-printed shell of liver, spleen and kidney then filled both with the water and radionuclides (Tc-99m SPECT and F-18 PET). The results show the phantom is able to display the anatomy of interest and suitable for their investigations as a validation tool for dose optimisation studies in post-selective internal radiation therapy. In this study of thesis, the phantom has been developed for CT dose optimisation studies also using a 3D printed shell with different fill materials of different electron densities inserted to produce background anatomy to represent the heart. Although the internal design does not represent the real features of human cardiac anatomy the attenuation properties for investigations for CCTA dose optimisation studies are comparable to the patient and the Catphan® 500 images.

The 3D-printed cardiac insert phantom's design allows CCTA dose optimisation investigations, in particular, the quantitative measurement of noise image quality characteristics, similar to patient data. This new phantom contains a contrast-enhanced region to allow measurement of noise image quality for the purpose of optimisation in

CCTA protocols. The contrast-enhanced region has been designed in a cylindrical shape with a similar diameter to the average ascending aorta (~30mm). In the literature, the measurement of image noise is usually taken by placing the ROI in the contrast-enhanced region of aorta to measure the image noise which is represented by the standard deviation values [19-22]. Therefore, the phantom has been designed to have the contrast-enhanced region simulating the aorta to allow the measurement. Measurements of noise image quality in the 3D printed phantom contrast enhanced region were comparable to patient datasets and the quality assurance phantom of Catphan® 500.

The second study of the thesis investigated the application of the 3D-printed cardiac insert phantom for CCTA dose optimisation studies by comparing the IR algorithm and FBP reconstruction methods at different tube current levels. This study assessed whether the phantom is able to measure the image quality characteristics such as the image noise, SNR, and CNR in the centre on the contrast-enhanced region of aorta for CCTA dose optimisation studies. The ROI measurement provided the attenuation values and standard deviation values which can be used to calculate SNR and CNR. The original cardiac insert of the Lungman also did not have the contrast-enhanced features which thus the ROI measurement for CCTA image quality measurement could not be performed. For phantom studies such as the Catphan® phantom, the ROI measurement is placed within the inserts of the CTP401/404 modules that used to represent the contrast-enhanced of the CT images [3, 23-25]. However, the results may inappropriate due to CCTA requires greater HU values of contrast-enhanced region than other CT examinations to enable visualisation of the small diameters of coronary vessels.



The results also show that using low dose levels has produced more image noise than the reference protocols and increasing the strengths of the IR algorithm resulted in more noise reduction. In the literature, many phantoms studies [25-27] have reported the results of using various IR algorithms compared to FBP but only a few [28, 29] have shown the results between FBP and different IR algorithm strength levels. This 3D-printed phantom study has investigated the use of FBP and different IR algorithm strength levels. The investigations of IR algorithm and its strength level could provide better results to represent the impact of using the IR algorithm in CCTA dose optimisation studies.

In clinical settings, the amount of dose reduction is important to reduce the radiation-induced cancer risks [30-32]. Therefore, in this study, the dose reduction analysis was performed by comparing the image quality measurements obtained to the previous literature. The method was chosen due to these previous literature represents the actual results in patients using the IR algorithm. The mean difference percentages of image quality measurements outlined between the FBP and IR algorithm among the selected studies is relevant to indicate the appropriate ranges or values. Therefore, the results can determine the minimum dose level that can be used for dose reduction on patient studies. The results of this study have indicated that the dose could be reduced up to 40% which is also below the range reported in the systematic review of the chapter two. Consequently, this phantom could be used to determine the dose reduction potential with respect to the use of IR algorithm and its different strength levels.

The final study has demonstrated that the phantom-based methodology allowed the assessment of IR algorithm strengths for the noise reduction when a low tube voltage is used. The use of 3D-printed cardiac insert phantom, which incorporated to the Lungman

phantom, in this study has provided evidence that it can be used for CCTA dose optimisation studies. The phantom can be used to modify the IR algorithm strength levels especially when a lower exposure factors has been proposed. As a result, the impact can be assessed before commencing the patient studies.

The results have shown that the dose can be reduced when the higher strength level of IR algorithm was chosen. The IR algorithm strength level has been increased due to the increasing image noise at the low tube voltage of 100 kVp. Previous studies [24, 29] have reported that IR strength level should be increased when the low exposure factors were used but did not determine by how much, especially for CCTA protocols. They only suggested the importance of the increase IR strength level to produce the optimum image quality. Therefore, in this final study of thesis, the IR algorithm strength level has been increased from 40% to 60% to allow for more noise reduction as well as significant changes to the image quality. Consequently, the SNR and CNR were also affected.

## **6.2 Limitations**

This phantom-based methodology has suffered several limitations. First, the shape and size of the cardiac insert has been replicated from the Lungman phantom. This insert has no coronary vessels and subsequently does not precisely replicate the human heart. As a result, the effect of changes the IR algorithm strength levels on the ability to evaluate the CAD in the vessels was unable to be investigated.

Second, the phantom does not provide representation of surrounding lung tissues that would normally present in CCTA images. The lung tissues have also been removed during the phantom scanning as they are attached to the original cardiac insert phantom.

The removal of lung tissues causes the beam directly penetrating the phantom that could have impact on the image quality noise characteristics.

Third, the methodological approach adopted provided quantitative assessment rather than qualitative. Consequently, it did not consider clinical decision making or radiologists' perception of image quality or diagnostic confidence.

Fourth, the assessment of the 3D-printed cardiac insert phantom associated with the Lungman phantom for the performance of dose optimisation studies was only performed on a single scanner. It is important to compare various types of CT scanner to provide more information and validate its impact on dose reduction and image quality.

Fifth, the phantom is static and does not represent cardiac motion during scanning. The cardiac motion is an important factor CCTA protocols due to the motion artifacts during the scanning. However, for the investigation of the impact of IR algorithm on noise image quality, a static phantom can be used as motion-free images are reconstructed.

Sixth, only CT tube current and voltage were investigated. Further research is required to determine how the 3D-printed cardiac insert phantom performs at the assessment of dose optimisation for other CT parameters, such as slice thickness, filters, high-pitch, etc.

Last, only two types of IR algorithm have been investigated in this research. More types of IR algorithm should be described and measured since they work differently and are exclusive to each CT vendors.

### **6.3 Future investigations**

This study has identified a number of potential future investigations including producing a dynamic 3D-printed cardiac insert phantom. This investigation using dynamic 3D-printed heart will provide better simulate CCTA images in which the heart that moves, in a motion similar to a heartbeat, during the scanning. This will also provide opportunities to investigate other dose optimisation strategies used during the CCTA scanning such as the prospective ECG-gating and high pitch acquisitions.

The qualitative assessment of the image quality is an important for the detection coronary lesions in the coronary segments. The detectability of the small diameters structures usually can be evaluated using the qualitative scores with the inclusion of other criteria such as the image artifacts.

Further, the new fully IR algorithms, such as the *Forward-projected-model-based Iterative Reconstruction SoluTion* or FIRST (Toshiba Medical Systems, Tokyo, Japan) which, in theory, has greater potential to provide improved noise reduction and therefore dose reduction than the hybrid IR algorithms studied in this thesis. Consequently, this would benefit from further investigations using the 3D-printed cardiac insert phantom.

### **6.4 Conclusions**

This thesis has investigated the application of a novel 3D-printed cardiac insert phantom for CCTA dose optimisation studies using IR algorithm. Findings demonstrate the developed 3D-printed cardiac insert phantom is able to represent CCTA images for dose optimisation studies. Analysis has shown that this phantom is suitable to investigate the effect of IR algorithm on dose reduction while maintaining noise image quality. A new

phantom-based methodology for CCTA dose optimisation studies has been proposed that contains anatomical structures with equivalent electron densities and improved surrounding attenuation. Evidence provided should also provide new horizons to researchers for novel 3D-printed phantoms and facilitate better CT optimisation process regarding their clinical implementation.

## 6.5 References

- [1] M. L. Aurumskjold, K. Ydstrom, A. Tingberg, and M. Soderberg, "Improvements to image quality using hybrid and model-based iterative reconstructions: a phantom study," *Acta Radiol*, vol. 58, no. 1, pp. 53-61, Jan 2017.
- [2] K. Gulliksrud, C. Stokke, and A. C. Martinsen, "How to measure CT image quality: variations in CT-numbers, uniformity and low contrast resolution for a CT quality assurance phantom," *Phys Med*, vol. 30, no. 4, pp. 521-6, Jun 2014.
- [3] E. P. S. Sande, A. C. T. Martinsen, E. O. Hole, and H. M. Olerud, "Interphantom and interscanner variations for Hounsfield units—establishment of reference values for HU in a commercial QA phantom," *Physics in Medicine & Biology*, vol. 55, no. 17, p. 5123, 2010.
- [4] S. N. Friedman, G. S. Fung, J. H. Siewerdsen, and B. M. Tsui, "A simple approach to measure computed tomography (CT) modulation transfer function (MTF) and noise-power spectrum (NPS) using the American College of Radiology (ACR) accreditation phantom," *Medical physics*, vol. 40, no. 5, 2013.

- [5] R. J. Cropp, P. Seslija, D. Tso, and Y. Thakur, "Scanner and kVp dependence of measured CT numbers in the ACR CT phantom," *Journal of applied clinical medical physics*, vol. 14, no. 6, pp. 338-349, 2013.
- [6] J. F. Barrett and N. Keat, "Artifacts in CT: recognition and avoidance," *Radiographics*, vol. 24, no. 6, pp. 1679-1691, 2004.
- [7] K. Kitagawa, R. T. George, A. Arbab-Zadeh, J. A. Lima, and A. C. Lardo, "Characterization and correction of beam-hardening artifacts during dynamic volume CT assessment of myocardial perfusion," *Radiology*, vol. 256, no. 1, pp. 111-118, 2010.
- [8] L. M. Hurwitz *et al.*, "Radiation dose savings for adult pulmonary embolus 64-MDCT using bismuth breast shields, lower peak kilovoltage, and automatic tube current modulation," *American Journal of Roentgenology*, vol. 192, no. 1, pp. 244-253, 2009.
- [9] S. Abadi, H. Mehrez, A. Ursani, M. Parker, and N. Paul, "Direct quantification of breast dose during coronary CT angiography and evaluation of dose reduction strategies," *American Journal of Roentgenology*, vol. 196, no. 2, pp. W152-W158, 2011.
- [10] P. Tack, J. Victor, P. Gemmel, and L. Annemans, "3D-printing techniques in a medical setting: a systematic literature review," *Biomedical engineering online*, vol. 15, no. 1, p. 115, 2016.
- [11] J. Solomon and E. Samei, "Quantum noise properties of CT images with anatomical textured backgrounds across reconstruction algorithms: FBP and SAFIRE," *Med Phys*, vol. 41, no. 9, p. 091908, Sep 2014.

- [12] S. J. Leigh, R. J. Bradley, C. P. Pursell, D. R. Billson, and D. A. Hutchins, "A simple, low-cost conductive composite material for 3D printing of electronic sensors," *PloS one*, vol. 7, no. 11, p. e49365, 2012.
- [13] R. Baguley. (2018, 13 March). *Best 3D printers 2018*. Available: <https://www.tomsguide.com/us/best-3d-printers.review-2236.html>
- [14] 3ders.org. (2018). *Price compare of 3D printing materials: Filament*. Available: <https://www.3ders.org/pricecompare/>
- [15] F. Rengier *et al.*, "3D printing based on imaging data: review of medical applications," *Int J Comput Assist Radiol Surg*, vol. 5, no. 4, pp. 335-41, Jul 2010.
- [16] J. Madamesila, P. McGeachy, J. E. Villarreal Barajas, and R. Khan, "Characterizing 3D printing in the fabrication of variable density phantoms for quality assurance of radiotherapy," in *Physica Medica*, ed, 2015.
- [17] A. P. Robinson *et al.*, "Organ-specific SPECT activity calibration using 3D printed phantoms for molecular radiotherapy dosimetry," *EJNMMI Phys*, vol. 3, no. 1, p. 12, Dec 2016.
- [18] J. I. Gear, C. Long, D. Rushforth, S. J. Chittenden, C. Cummings, and G. D. Flux, "Development of patient-specific molecular imaging phantoms using a 3D printer," *Med Phys*, vol. 41, no. 8, p. 082502, Aug 2014.
- [19] E. A. Park *et al.*, "Iterative reconstruction of dual-source coronary CT angiography: assessment of image quality and radiation dose," *Int J Cardiovasc Imaging*, vol. 28, no. 7, pp. 1775-86, Oct 2012.

- [20] F. Tatsugami *et al.*, "The effect of adaptive iterative dose reduction on image quality in 320-detector row CT coronary angiography," *British Journal of Radiology*, vol. 85, no. 1016, pp. e378-e382, 2012.
- [21] R. Wang *et al.*, "CT coronary angiography: image quality with sinogram-affirmed iterative reconstruction compared with filtered back-projection," *Clin Radiol*, vol. 68, no. 3, pp. 272-8, Mar 2013.
- [22] F. Cademartiri *et al.*, "Intravenous contrast material administration at 16-detector row helical CT coronary angiography: test bolus versus bolus-tracking technique," vol. 233, ed: Radiological Society of North America, 2004, pp. 817-823.
- [23] K. Gulliksrud, C. Stokke, and A. C. T. Martinsen, "How to measure CT image quality: variations in CT-numbers, uniformity and low contrast resolution for a CT quality assurance phantom," *Physica Medica: European Journal of Medical Physics*, vol. 30, no. 4, pp. 521-526, 2014.
- [24] T. Klink, V. Obmann, J. Heverhagen, A. Stork, G. Adam, and P. Begemann, "Reducing CT radiation dose with iterative reconstruction algorithms: the influence of scan and reconstruction parameters on image quality and CTDIvol," *Eur J Radiol*, vol. 83, no. 9, pp. 1645-54, Sep 2014.
- [25] C. Ghetti, O. Ortenzia, and G. Serreli, "CT iterative reconstruction in image space: a phantom study," *Phys Med*, vol. 28, no. 2, pp. 161-5, Apr 2012.
- [26] M. J. Willeminck *et al.*, "Computed tomography radiation dose reduction: Effect of different iterative reconstruction algorithms on image quality," *Journal of Computer Assisted Tomography*, vol. 00, no. 00, pp. 1-9, 2014.



- [27] K. Jensen, A. C. Martinsen, A. Tingberg, T. M. Aalokken, and E. Fosse, "Comparing five different iterative reconstruction algorithms for computed tomography in an ROC study," *Eur Radiol*, vol. 24, no. 12, pp. 2989-3002, Dec 2014.
- [28] S. D. Kordolaimi, I. Saradeas, A. Ploussi, I. Pantos, S. Argentos, and E. P. Efstathopoulos, "Introduction of an effective method for the optimization of CT protocols using iterative reconstruction algorithms: comparison with patient data," *AJR Am J Roentgenol*, vol. 203, no. 4, pp. W434-9, Oct 2014.
- [29] O. Rampado, L. Bossi, D. Garabello, O. Davini, and R. Ropolo, "Characterization of a computed tomography iterative reconstruction algorithm by image quality evaluations with an anthropomorphic phantom," *Eur J Radiol*, vol. 81, no. 11, pp. 3172-7, Nov 2012.
- [30] J. M. Albert, "Radiation risk from CT: implications for cancer screening," *AJR Am J Roentgenol*, vol. 201, no. 1, pp. W81-7, Jul 2013.
- [31] K. E. Applegate and N. G. Cost, "Image Gently: a campaign to reduce children's and adolescents' risk for cancer during adulthood," *J Adolesc Health*, vol. 52, no. 5 Suppl, pp. S93-7, May 2013.
- [32] A. J. Einstein *et al.*, "Radiation dose and cancer risk estimates in 16-slice computed tomography coronary angiography," *J Nucl Cardiol*, vol. 15, no. 2, pp. 232-40, Mar-Apr 2008.

# Appendices

# Appendix 1: Ethics approval letter.



**Health**  
South Western Sydney  
Local Health District

**Research and Ethics Office**  
Leadership · Quality · Governance  
Locked Bag 7103, LIVERPOOL BC, NSW, 1871  
Phone: 02 8738 8304  
Facsimile: 02 8738 8310  
<http://www.sswahs.nsw.gov.au/swslhd/ethics/default.html>

South Western Sydney Local Health District acknowledges the traditional owners of this land.

23 July 2017

Mr Kamarul Abdullah  
Medical Radiation Sciences Faculty of Health Sciences  
The University of Sydney

Dear Mr Abdullah,

**\*\*\*THIS LETTER CONSTITUTES ETHICAL APPROVAL ONLY. THIS RESEARCH PROJECT MUST NOT COMMENCE AT A SITE UNTIL SEPARATE AUTHORISATION FROM THE CHIEF EXECUTIVE OR DELEGATE OF THAT SITE HAS BEEN OBTAINED.\*\*\***

**Project Title:** Phantom validation and dose reduction potential for coronary CT angiography  
**HREC Reference:** LNR/17/LPOOL/209  
**SSA Reference:** LNRSSA/17/LPOOL/210  
**Local Project Number:** HE17/112

Thank you for your response dated 19 July 2017 to our request for further information dated 19 June 2017. This Human Research Ethics Committee is constituted and operates in accordance with the National Health and Medical Research Council's *National Statement on Ethical Conduct in Research Involving Humans* and the *CPMP/ICH Note for Guidance on Good Clinical Practice*.

I am pleased to advise that the Committee has granted ethical approval of the above project.

The following documentation has been reviewed and approved:

Document	Version	Date
Low and Negligible Risk Form	AU/6/76CD212	11.05.2017
Protocol	2.0	18.07.2017

**Please ensure for all future documents submitted for review include a document version number, document date and page numbering.**

Monitoring Requirements:  
(*National Statement Chapters 2.1 and 5.5*)

- The Committee has classified this project as:

**Low Risk**

- Monitoring required for this study will be:
  - Submission of Annual Progress Reports with the first report due **23 July 2018 and annually thereafter for the duration of the approval period**

Approval is valid for the following site only:

- Bankstown-Lidcombe Hospital

Please note the following conditions of approval:

- The Principal Investigator will immediately report anything which might warrant review of ethical approval of the project in the specified format, including:
  - any serious or unexpected adverse events; and
  - unforeseen events that might affect continued ethical acceptability of the project.

Page 1 of 2

2. The Principal Investigator will report proposed changes to the research protocol, conduct of the research, or length of HREC approval to the HREC in the specified format, for review. For multi-centre studies, the Chief Investigator should submit to the Lead HREC and then send the amendment approval letter to the investigators at each sites so that they can notify their Research Governance Officer.
3. The Principal Investigator will inform the HREC, giving reasons, if the project is discontinued before the expected date of completion.
4. The Principal Investigator will provide an annual report to the HREC and at completion of the study in the specified format.
5. The Principal Investigator must reassure participants about confidentiality of the data.
6. Proposed changes to the personnel involved in the study are submitted to the HREC accompanied by a CV where applicable.
7. The Principal Investigator is responsible for ensuring the research project is conducted in line with relevant NSW Health, South Western Sydney Local Health District and Hospital policies available from: <http://www.sswahs.nsw.gov.au/swslhd/ethics/policies.html>

HREC approval is valid for (5) years. If the study is ongoing at the conclusion of the five year approval period, a full resubmission may be required. Ethics approval will continue during the re-approval process.

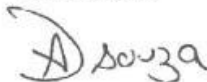
**The South Western Sydney Local Health District Human Research Ethics Committee has been accredited by the NSW Ministry of Health to provide single ethical and scientific review of research proposals conducted within the NSW public health system and Victorian and Queensland Public Health Organisations participating in the Mutual Acceptance Scheme.**

**You are reminded that this letter constitutes ethical approval only. This research project must not commence at a site until separate authorisation from the Chief Executive or delegate of that site has been obtained. It is your responsibility to forward a copy of this letter together with any approved documents as enumerated above, to all site investigators for submission to the site's Research Governance Officer.**

Should you have any queries about your project please contact **Annamarie D'Souza** on the telephone number listed above. The HREC Terms of Reference, Standard Operating Procedures, membership and standard forms are available from the SWSLHD website: <http://www.sswahs.nsw.gov.au/swslhd/ethics/default.html>

Please quote the Local HREC reference **HE17/112** in all correspondence. The HREC wishes you every success in your research

Yours faithfully



**Annamarie D'Souza**  
*on behalf of*  
**Professor Jeremy Wilson**  
Chairperson, SWSLHD Human Research Ethics Committee

This HREC is constituted and operates in accordance with the National Health and Medical Research Council's (NHMRC) *National Statement on Ethical Conduct in Human Research (2007)*. The processes used by this HREC to review multi-centre research proposals have been certified by the National Health and Medical Research Council.

## Appendix 2: Site specific authorisation letter.



**Health**  
South Western Sydney  
Local Health District

**Research and Ethics Office**  
Leadership · Quality · Governance  
Locked Bag 7103, LIVERPOOL BC, NSW, 1871  
Phone: 02 8738 8304  
Facsimile: 02 8738 8310  
<http://www.sswahs.nsw.gov.au/swslhd/ethics/default.html>

South Western Sydney Local Health District acknowledges the traditional owners of this land.

7 August 2017

Mr Kamarul Abdullah  
Medical Radiation Sciences Facility of Health Sciences  
The University of Sydney

Dear Mr Abdullah,

**Project Title:** Phantom validation and dose reduction potential for coronary CT angiography  
**HREC Reference:** LNR/17/LPOOL/209  
**SSA Reference:** LNRSSA/17/LPOOL/210  
**Local Project Number:** HE17/112

### \*\*\*SITE SPECIFIC AUTHORISATION\*\*\*

Thank you for your correspondence received 3 August 2017 in response to our request for further information dated 24 July 2017.

I am pleased to inform you that the Chief Executive has granted authorisation for this study to take place at the following site(s):

- Bankstown-Lidcombe Hospital

The following conditions apply to this research project. These are additional to those conditions imposed by the Human Research Ethics Committee that granted ethical approval:

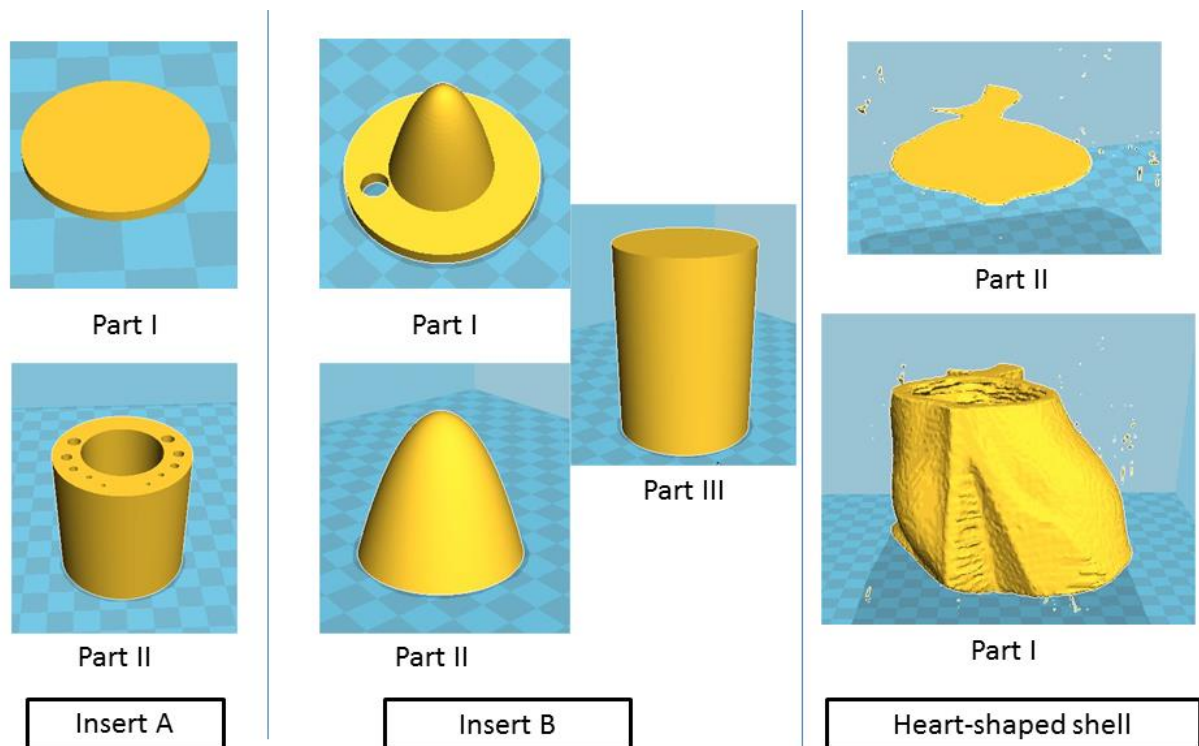
1. Proposed amendments to the research protocol or conduct of the research which may affect the ethical acceptability of the project, and which are submitted to the lead HREC for review, are copied to this office.
2. Proposed amendments to the research protocol or conduct of the research which may affect the ongoing site acceptability of the project, are to be submitted to this office.
3. Please note that you are responsible for making the necessary arrangements (e.g. identity pass and vaccine compliance as per NSW Health Policy Directive PD2011\_005) for any researcher who is not employed by the South Western Sydney Local Health District and is conducting the research on-site.
4. The Principal Investigator is responsible for ensuring the research project is conducted in line with relevant NSW Health, South Western Sydney Local Health District and Hospital policies available from: <http://www.sswahs.nsw.gov.au/swslhd/ethics/policies.html>
5. Proposed changes to the personnel involved in the study at South Western Sydney Local Health District sites are submitted to the South Western Sydney Local Health District Research and Ethics Office accompanied by the required supporting documents. A list of the documentation required to add an Investigator to a study is located on the South Western Sydney Local Health District Research and Ethics Office website: <http://www.swslhd.nsw.gov.au/ethics/forms.html>

Yours sincerely,

**Annamarie D'Souza**  
Manager, Research and Ethics Office  
South Western Sydney Local Health District (SWSLHD)

Page 1 of 1

### Appendix 3: 3D-printed models and the softcopy link of the models.



#### a) Insert A

Part I (Link: <https://goo.gl/1xYeme>)

Part II (Link: <https://goo.gl/MfyijW>)

#### b) Insert B

Part I (Link: <https://goo.gl/E3JLg9>)

Part II (Link: <https://goo.gl/ARHko6>)

Part III (Link: <https://goo.gl/CH5ih9>)

#### c) Heart-shaped shell

Part I (Link: <https://goo.gl/Fmxg4s>)

Part II (Link: <https://goo.gl/jsoG8e>)